Phases of QCD

Lattice Thermodynamics and Quasiparticle Approaches

Michael A. Thaler

Technische Universität München
Physik-Department
Institut für Theoretische Physik T39
Univ.-Prof. Dr. W. Weise

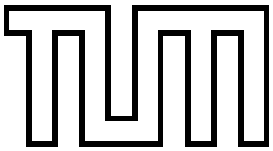

Phases of QCD: Lattice Thermodynamics and Quasiparticle Approaches

Dipl.-Phys. (Univ.) Michael Thaler

Vollständiger Abdruck der von der Fakultät für Physik der Technischen Universität München zur Erlangung des akademischen Grades eines

Doktors der Naturwissenschaften (Dr. rer. nat.)

genehmigten Dissertation.

Vorsitzender: Univ.-Prof. Dr. Stephan Paul

Prüfer der Dissertation:

1. Univ.-Prof. Dr. Wolfram Weise
2. Univ.-Prof. Dr. Manfred Lindner

Die Dissertation wurde am 5.12.2005 bei der Technischen Universität München eingereicht und durch die Fakultät für Physik am 11.1.2006 angenommen.

Summary

The main goal of this work is a comprehensive description of lattice QCD thermodynamics at finite quark chemical potential. As a first step a phenomenologically successful quasiparticle model that describes lattice results of the equation of state for the deconfined phase of QCD for $T_c \leq T \lesssim 4\,T_c$ is extended to finite quark chemical potential μ. The phase diagram and finite density corrections to the equation of state are calculated and compared to lattice QCD results. Subsequently, an improved model based on two fundamental features of QCD, *confinement* and *chiral symmetry* and its spontaneous breaking at low temperatures, is developed. In this generalized Nambu–Jona-Lasinio model quarks couple simultaneously to the chiral condensate and to a background temporal gauge field representing Polyakov loop dynamics. The chiral condensate and the Polyakov loop as functions of temperature and quark chemical potential are calculated by minimizing the thermodynamic potential of the system. The resulting equation of state, (scaled) pressure difference and quark number density at finite quark chemical potential are then confronted with corresponding lattice QCD data. Finally this model is extended to the physically relevant three-flavor case.

Zusammenfassung

Das Hauptziel dieser Arbeit liegt in einer umfassenden Beschreibung der Gitter-QCD Thermodynamik bei endlichem chemischen Potential. Zuerst wird ein phänomenologisch erfolgreiches Quasiteilchenmodell, daß Gitter-QCD Ergebnisse für die Zustandsgleichung des Quark-Gluon-Plasmas im Bereich $T_c \leq T \lesssim 4\,T_c$ erfolgreich beschreibt, auf endliches chemisches Potential der Quarks erweitert. Das Phasendiagramm und Korrekturen zur Zustandsgleichung bei endlicher Quarkdichte werden berechnet. Als nächstes wird ein neues Modell entwickelt, daß auf zwei der grundlegenden Eigenschaften der QCD, *Confinement* und *chiraler Symmetriebrechung*, basiert. In diesem verallgemeinerten Nambu–Jona-Lasinio Modell koppeln Quarks gleichzeitig an das chirale Kondensat und ein zeitartiges Hintergrund-Eichfeld, daß die Dynamik des Polyakov Loop repräsentiert. Das chirale Kondensat und der Polyakov Loop werden als Funktion der Temperatur und des chemischen Potentials der Quarks durch Minimieren des thermodynamischen Potentials berechnet. Die resultierende Zustandsgleichung, die (skalierte) Druckdifferenz und die Quarkdichte bei endlichem chemischen Potential der Quarks werden dann mit entsprechenden Gitter-QCD Daten verglichen. Schließlich wird das Modell noch auf den physikalisch relevanten 3-Flavor-Fall erweitert.

Contents

Introduction

It is an everyday experience that a solid piece of matter will first turn into a liquid and then into a gas if it is heated. The most familiar example, of course, is water which is frozen into ice below 273.15 K at normal pressure. If it is heated, ice will turn into liquid water above 273.15 K and liquid water will turn into steam above 373.15 K. If the temperature is increased further to a few thousand degrees, the atoms that make up matter start colliding so violently that they may lose one or more of their electrons in these collisions. A new state of matter emerges, which is called a plasma. It is a mixture of free electrons with negative charges and positively charged ions which can move freely. But what happens if matter is heated even more? To answer this question, physicists undertake major efforts to create extreme conditions in earth-bound experiments. Temperatures up to 10^8 K can be achieved using plasma fusion reactors. Above this temperature, conventional heating mechanisms become inefficient and more importantly, there is no way to confine the plasma. However, even higher temperatures can be achieved in heavy-ion collisions, i. e. high energy collisions between nuclei such as sulfur, lead and gold [Won94, Hei01]. In such collisions, some of the kinetic energy of the projectiles is converted into thermal energy. When a temperature of about 10^{10} K is reached, nuclei dissolve and a liquid of protons and neutrons is formed with a boiling point of about 10^{11} K, above which they evaporate and form a hadron gas. Hadrons are not fundamental particles themselves and at even higher temperatures, their substructure, quarks and gluons, becomes relevant.

The behavior of matter in this regime is described by quantum chromodynamics (QCD), the fundamental theory of quarks, gluons and their interactions. QCD is a consistent quantum field theory with a simple and elegant underlying Lagrangian, based entirely on the invariance under non-Abelian local gauge transformations. What makes QCD unusual are two remarkable properties: *asymptotic freedom*, which means that at very high energies quarks and gluons interact only weakly and turn into quasifree particles [Pol73, GW73] and *confinement*, which connotes that at low energies the force between quarks increases as the distance between them is increased, so that quarks are always bound into hadrons and cannot be removed individually. We can now understand what happens to matter if a system is heated more and more: eventually all energy scales become small compared to the temperature, which will in turn become the only relevant scale. Thus, at very high temperatures, the interaction between quarks and gluons becomes weak and a new state of matter is formed, where quarks and gluons are no longer confined into individual hadrons, but can travel over larger distances. This (locally)

deconfined phase is called Quark-Gluon Plasma (QGP). We can estimate the temperature where this transition happens. The thermal number density of a gas of massless pions is given by

$$n_\pi(T,\mu) = 3\int \frac{\mathrm{d}^3p}{(2\pi)^3}\frac{1}{\exp[(p-\mu)/T]-1} \simeq 0.3\,T^3 \quad \text{for} \quad \mu = 0. \tag{0.1}$$

The factor of three in front of the integral counts the number of pionic states, $\pi^\pm$ and π^0. We now assume that the transition to the QGP happens if the hadrons fill up all available space and thus $n_\pi(T_c) \simeq V_\pi^{-1}$. Accepting that the volume occupied by a single pion is $V_\pi = (4\pi/3)r_\pi^3$, we obtain $T_c \simeq 1/r_\pi$. With a typical hadronic scale, $r_\pi \simeq 0.7$ fm, we find that the transition to this new form of matter happens at a temperature of about 10^{12} K, a temperature which is about 100.000 times hotter than the temperature in the center of the sun.

The most fundamental theoretical approach to compute thermodynamic properties of matter at finite temperatures is lattice QCD [Wil74, Cre83]. In these calculations, the grand canonical partition function, which is the central quantity for matter in thermal equilibrium, is evaluated on a discrete space-time lattice. Improvements of the original algorithms and the availability of high-performance supercomputers permit fairly accurate and reliable simulations. Lattice QCD calculations have numerically established the existence of a transition from a hadronic phase to a quark-gluon plasma phase at a temperature of about 170 MeV. A rapid rise in the pressure and the energy density is observed close to this temperature due to the increase in number of degrees of freedom: Below T_c the relevant degrees of freedom are heavy hadrons, there is not much thermal motion and the pressure and the energy density are low. The number of available states in the QGP is much larger because quarks and gluons carry color. In addition, these states are (almost) massless. Lattice QCD also predicts a second transition from a state where chiral symmetry is spontaneously broken to one where it is restored. A broken chiral symmetry implies the existence of (almost) massless Goldstone bosons. This has important consequences for the observed hadron spectrum: pions, which constitute the Goldstone bosons of the broken chiral symmetry, are much lighter than the next heavier states. This phase transition occurs at almost the same temperature as the confinement-deconfinement transition.

QCD at finite quark chemical potential plays a role in two rather different regimes: Small quark chemical potentials are relevant for heavy ion collisions, where the initial state has a small non-zero baryon number. On the other hand, the core of neutron stars is composed of cold and very dense nuclear matter. Lattice simulations at finite quark chemical potential are exceedingly difficult because of the so-called "sign-problem" that prevents standard Monte-Carlo methods from being applicable. However, recently new methods have been proposed [FK02b, A$^+$02, dFP02] that allow lattice simulations for small quark chemical potentials and the phase boundary line has been determined in this region. A sketch of the expected phase diagram of QCD is shown in figure 0.1. Depending on the temperature T and the baryon chemical potential μ, strongly interacting

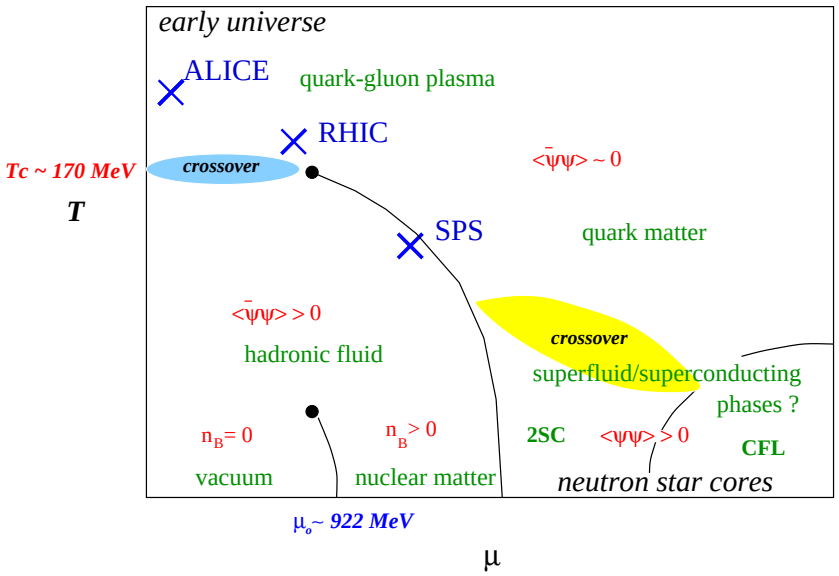

Figure 0.1: Sketch of the phase diagram of QCD in the $T-\mu$ plane [Han01]. At finite temperature and vanishing quark chemical potential, where most of today's lattice QCD simulations are performed, the transition from the hadronic phase to the QGP is presumably a crossover. This smooth crossover is expected to turn into a first order transition at a critical point (T_c, μ_c). At very large quark chemical potentials and small temperature, quark matter supposedly becomes a color-superconductor. For further explanations, see text.

matter may occur in different phases: the hadronic phase, the QGP phase and (several) color-superconducting phases. The $(T, \mu = 0)$ axis is reasonably well understood from lattice QCD calculations. Below a critical temperature of order $T \sim 170$ MeV strongly interacting matter is in the hadronic phase and there is a smooth crossover to a deconfined QGP phase if the temperature is increased. This smooth crossover persists at small quark chemical potentials and turns into a first order transition at a critical point $(T_c, \mu_c) = (160 \pm 4, 242 \pm 12)$ MeV [FK02a]. At the critical point the transition is second order. At large quark chemical potentials and small temperature, quark matter presumably becomes a color-superconductor. There can be several color-superconducting phases, depending on the symmetries of the order parameter for the condensation of quark Cooper pairs.

The early universe evolved close to the temperature axis in the phase diagram of strongly interacting matter. Matter in the core of compact stellar objects, like neutron stars, is close to the quark chemical potential axis, at values of μ around 400 – 500 MeV. Nuclear collisions at bombarding energies around $E_{\mathrm{Lab}} \sim 1$ AGeV explore a region of temperatures and quark chemical potentials around $(T, \mu) \sim (70, 250)$ MeV. Collisions at current RHIC energies of $\sqrt{s} = 200$ AGeV are expected to excite matter in a region around and above $(T, \mu) \sim (170, 10)$ MeV. Collision energies in between these two extremes cover the intermediate region and, in particular, may probe the critical endpoint.

At very high temperatures, the strong coupling constant g_s becomes small and one may suspect that the equation of state of the QGP can be calculated perturbatively. Unfortunately, however, this is not the case because of collective excitations in the plasma. The energy of individual particles is of order T and the average distance between two neighboring particles is $\bar{r} \sim 1/T$. The energy scale $g_s T$ is associated with the collective motion of the particles, which takes place over distances $d \sim 1/(g_s T)$. The decay rate of the quasiparticles is of order $g_s^2 T$. These different scales make a naive perturbative treatment of the plasma impossible. In order to overcome this problem, resummation schemes have been proposed, based for example on the Hard Thermal Loop (HTL) approach [BP92, FT92, BI94, ABS99, ABPS02, BIR99a, BIR99b, BIR01] or on dimensionally reduced screened perturbation theory [KLRS03, BIR03, IRV04]. However, these approaches still give reliable results only for temperatures $T \gtrsim 2.5\,T_c$, far above the critical temperature $T_c \sim 0.2$ GeV. At these high temperatures, the HTL approach motivates and justifies a picture of weakly interacting quasiparticles, as determined by the HTL propagators. In order to extend such descriptions to lower temperatures closer to T_c, various models have been proposed. Early attempts were based on the MIT bag model [EKS82]. More sophisticated approaches became necessary when more precise lattice data appeared. Various aspects of QCD thermodynamics have been investigated in terms of quasiparticle models based on perturbative calculations carried out in the HTL scheme [PKPS96, LH98, PKS00, ST03, BKS05], in terms of a condensate of Z_3 Wilson lines [Pis00], by refined quasiparticle models based on the HTL-resummed entropy and extensions thereof [RR03], by an improved version with a temperature-dependent number of active degrees of freedom [SW01], by an evaporation model of the gluon condensate [DGR04], and by quasiparticle models formulated in dynamical terms [IST05] (for a recent review see [Ris04]).

In the first part of this work, we will extend the improved quasiparticle model with a temperature-dependent number of active degrees of freedom to finite quark chemical potential. Such an extension is important for a number of reasons: First, for current heavy ion collision experiments at SPS and RHIC the chemical freeze-out occurs at $\mu_{f.o.} \simeq 100$ MeV, (baryon chemical potential $\mu_B \simeq 300$ MeV) [BMHS99] and $\mu_{f.o.} \simeq 15$ MeV, ($\mu_B \simeq 45$ MeV) [BMMRS01], respectively. Thus, a finite quark chemical potential should be introduced to describe deconfined quark matter created in these experiments. Second, first lattice QCD simulations at finite quark chemical potential are now available and it is of great theoretical interest to interpret these results. Third, the introduction of an additional external control parameter helps to test the reliability of the quasiparticle approach. In the second part of this thesis, we will turn to a more microscopic description of the QGP. The deconfinement phase transition is well defined in the heavy-quark limit, where the Polyakov loop serves as an order parameter. This phase transition is characterized by the spontaneous breaking of the $Z(3)$ center symmetry of QCD. In principle an effective theory for the Polyakov loop can be constructed by integrating out the gluon fields. The thermodynamic potential can then be deduced from this effective theory. The chiral phase transition, on the other hand, has a well-defined order parameter in the chiral limit of massless quarks: the chiral (or quark) condensate $\langle \bar{q}q \rangle$. This con-

densate, and its dynamical generation, is described by the Nambu–Jona-Lasinio (NJL) model. It is an effective Lagrangian of relativistic fermions interacting through local fermion-fermion couplings. In principle, this Lagrangian can be obtained from QCD by "integrating out" the gluonic degrees of freedom, replacing them by a local four-point color-current interaction. Neither the heavy quark limit, nor the chiral limit are realized in nature. However, both the Polyakov loop and the quark condensate can still serve as an indicator for a rapid crossover towards deconfinement and chiral symmetry restoration. Our investigations will be based on a synthesis of a two-flavor NJL model and the non-linear dynamics involving the Polyakov loop. Various lattice data are used to set up the model and test its predictions. Finally, this model will be extended to three quark flavors.

* * *

This work is organized as follows:

The basics of finite temperature QCD are introduced in the first chapter. We set in with a summary of important aspects of vacuum QCD, where our main focus will be on chiral symmetry and its spontaneous breaking. Then we briefly review thermal field theory, the appropriate framework in which to calculate the thermodynamics of hot QCD. In the final section of this chapter, an up-to-date overview of the thermodynamics of QCD, referring mainly to latest lattice data, is presented. The critical temperatures for the phase transition from the hadronic phase to the QGP phase from various lattice QCD simulations with different numbers of flavors are listed and thermodynamical quantities from recent finite-temperature simulations of full QCD including dynamical quarks are discussed. Finally, some methods to obtain expectation values of observables at finite quark chemical potential are reviewed and results for thermodynamic observables and the phase boundary line are presented. These results will be extensively referred to in subsequent chapters.

The aim of the second chapter is to explain what we have learned about QCD thermodynamics from lattice QCD simulations using a very simple, concrete model. To this end, we introduce the MIT bag model, a phenomenological model that implements two key properties of QCD, *asymptotic freedom* and *confinement*. Because of its simple analytic form the MIT bag model is the most widely used equation of state to study the properties of deconfined matter at high temperatures and large densities. This model is then tested with results from lattice QCD simulations, both at finite temperature and finite quark chemical potential. The primary purpose of this chapter is to qualitatively explain some of the key features of the lattice QCD phase diagram in terms of a clear and intuitive physical model and to set the stage for the more refined models which will be discussed in subsequent chapters.

The third chapter is devoted to the quasiparticle description of hot QCD. Lattice QCD

thermodynamical quantities have been successfully described by a gas of non-interacting quark-gluon quasiparticles with temperature dependent quasiparticle masses. At high temperatures, such a description is motivated by HTL perturbation theory. For $T \lesssim 3\,T_c$, non-perturbative confinement physics not amenable in an expansion in g_s starts to become important. Since confinement simply reduces the number of thermally active degrees of freedom in a statistical sense, confinement can be schematically incorporated in a quasiparticle model by a modification of the particle distribution functions [SW01]. This model successfully describes and predicts a variety of lattice data including the Debye screening mass, which is not correctly estimated by other quasiparticle models. In this chapter we study the extension of this model to finite quark chemical potential μ. The phase boundary line $T_c(\mu)$ and thermodynamical quantities at finite μ are calculated and tested with recent lattice QCD results.

The 'classic' two-flavor NJL model, which incorporates the chiral symmetry of QCD and its spontaneous breakdown at $T < T_c$, is discussed in chapter 4. It is an effective Lagrangian of relativistic fermions interacting through local fermion-fermion couplings. In principle it can be obtained from QCD by "integrating out" the gluonic degrees of freedom, replacing them by a four-point color-current interaction. Starting from this QCD motivated interaction, we investigate the vacuum properties of the theory and outline how the NJL model can be employed to study quark and meson properties at finite temperature and density. As an application we then calculate the constituent quark mass, the pion mass, and the sigma mass as functions of temperature and quark chemical potential/density. We then derive the thermodynamic potential. The chapter is concluded with a brief comparison of the NJL model and the MIT bag model.

In chapter 5 we study the color-octet sector of the NJL model in detail. One of the key properties of QCD is color confinement, which requires that quarks have to be part of bound color-singlet states. One of the shortcomings of the NJL model is that it does not confine quarks and thus allows for colored quark-antiquark excitations. We will calculate the masses of the lowest-lying color-octet bound states and show that such excitations are only possible at energies far above the cutoff of the theory and that they are thus insignificant for the low-energy spectrum. Finally we show that this also holds at finite temperature and finite quark chemical potential.

A generalized NJL model which includes features of both chiral symmetry restoration and confinement is investigated in chapter 6. We first present a detailed review of the Polyakov loop as an order parameter of deconfinement in the heavy quark limit. Subsequently, an effective theory for the Polyakov loop is constructed and its thermodynamic properties are studied and compared to continuum extrapolated $SU(3)$ lattice QCD results. We then introduce a generalized two-flavor NJL Lagrangian, in which quarks couple to a (spatially constant) temporal background $SU(3)$ gauge field representing Polyakov loop dynamics. This Polyakov-loop-extended NJL model (the PNJL model) incorporates the chiral symmetry of QCD and its spontaneous breakdown at $T < T_c$, while at the same time it also includes features of confinement. We derive its thermody-

namic potential and study the thermodynamic properties. The predictions of the model are then tested with lattice data available for full QCD thermodynamics at zero and finite quark chemical potential. The chapter is completed with a discussion of the quark mass dependence of the PNJL model.

In chapter 7 the PNJL model is extended to three flavors. The main difference between the two flavor case and the three flavor case is that the strange quark mass is different from the masses of non-strange quarks. This means that we have to deal with an explicitly broken $SU(3)$ flavor symmetry, and thus $\langle \bar{s}s \rangle \neq \langle \bar{u}u \rangle$, even for equal chemical potentials. We study how the quark condensate depends on the current quark masses and how chiral restoration occurs at finite temperature and finite quark chemical potential if an explicit symmetry breaking exists. We also explore how the subtle interplay between the chiral condensate and the Polyakov loop dynamics is affected by the larger strange quark mass. As an application, various thermodynamical quantities are calculated and confronted with recent lattice QCD results.

To conclude, we summarize our results and present an outlook regarding future work. Several short appendices serve to complete the material presented in the main body of the text.

* * *

A short note on *conventions*: We use natural units $\hbar = c = k_B = 1$ throughout this work. Indices which appear twice in a formula are summed over. Temperature is denoted by T and sometimes by $\beta = 1/T$. Thermal averages are always $\langle \dots \rangle_\beta$, unless otherwise stated. The word 'vacuum' refers to the situation of zero temperature and no baryon density. Finally, Lorentz 4-vectors are denoted by x, p and so on, whereas 3-vectors $\boldsymbol{x}, \boldsymbol{p}$ are printed in bold font.

Chapter 1

Basics of QCD Thermodynamics

In this first chapter we briefly summarize Quantum Chromodynamics (QCD) as the fundamental theory of strong interactions. We will discuss the chiral symmetry of QCD and its spontaneous breaking, which will play an important role in later parts of this work, in detail. Subsequently, thermal field theory, the appropriate tool to study QCD at finite temperature and finite chemical potential, is introduced. Finally we gather what is known about the QCD equation of state (EoS) and the QCD phase transition and its dependence on the external parameters temperature and quark chemical potential, mainly referring to current lattice QCD results. We discuss up-to-date results from lattice simulations of full QCD including dynamical quarks at finite temperature and vanishing quark chemical potential. We then outline some of the approaches that are used to circumvent the so-called "sign problem" at finite densities, at least for small quark chemical potentials. This problem prohibits the straight-forward application of the Monte-Carlo methods used at vanishing quark chemical potential and makes calculations exceedingly more costly. The results of this chapter will be extensively referred to in subsequent chapters.

1.1 Vacuum properties of QCD

QCD, the non-Abelian gauge field theory that describes the dynamics and interactions of colored quarks, is one of the components of the $SU(3) \times SU(2) \times U(1)$ Standard Model. The fundamental degrees of freedom of this theory are spin-1 gauge bosons, the gluons A^a_μ, and massive spin-$\frac{1}{2}$ fermions, the quarks ψ. Gluons are characterized by their color index a ($a = 1 \ldots 8$) and transform as the adjoint representation of the gauge group, while quarks belong to its fundamental complex representation. A quark of specific flavor (such as a strange quark) comes in three colors, whereas there are eight different gluons and thus the gauge group of QCD is $SU(3)$. QCD is defined as a field theory by its Lagrangian density,

$$\mathcal{L}_{\mathrm{QCD}} = -\frac{1}{2}\mathrm{Tr}(G_{\mu\nu}G^{\mu\nu}) + \bar{\psi}(\mathrm{i}\gamma^\mu D_\mu - \hat{m})\psi, \tag{1.1}$$

with the gluonic field strength tensor

$$G_{\mu\nu} \equiv (\partial_\mu A^a_\nu - \partial_\nu A^a_\mu + g_s f^{abc} A^b_\mu A^c_\nu)t^a, \tag{1.2}$$

and the gauge covariant derivative

$$D_\mu = \partial_\mu + ig_s t^a A^a_\mu. \tag{1.3}$$

g_s is the QCD coupling constant and the matrices t^a denote the eight Gell-Mann matrices, which are the generators of $SU(3)$. They satisfy the commutation relations $[t^a, t^b] = if^{abc}t^c$ where the f^{abc} are the group structure constants of $SU(3)$. Among the $N_f = 6$ quark flavors with $m_u, m_d, m_s \approx 4, 7, 150$ MeV and $m_c, m_b, m_t \approx 1.5, 4.5, 170$ GeV, there is a natural separation in sectors of 'light' and 'heavy' quarks. Only light quarks are considered in this work: As we work within a temperature range $T \ll m_c$, the influence of heavy quarks on thermodynamics is negligible. With $N_f = 3$ we have

$$\psi(x) = \begin{pmatrix} u_\alpha(x) \\ d_\alpha(x) \\ s_\alpha(x) \end{pmatrix}, \tag{1.4}$$

where $\alpha = 1 \ldots 3$ is a color index. The current quark mass matrix in $\mathcal{L}_{\mathrm{QCD}}$ becomes

$$\hat{m} = \begin{pmatrix} m_u & & \\ & m_d & \\ & & m_s \end{pmatrix}. \tag{1.5}$$

Since QCD is renormalizable, its bare parameters g_s and m_q depend on the energy scale μ at which the theory is probed. The renormalization group equation for the running coupling $\alpha_s(\mu) = g_s^2(\mu)/4\pi$ reads

$$\mu \frac{d}{d\mu}\alpha_s(\mu) = \beta(\alpha_s) = -\frac{\beta_0}{6\pi}\alpha_s^2 - \frac{\beta_1}{24\pi^2}\alpha_s^3 - \mathcal{O}(\alpha_s^4), \tag{1.6}$$

where

$$\beta_0 = 33 - 2N_f \quad \text{and} \quad \beta_1 = 306 - 38N_f. \tag{1.7}$$

In solving this differential equation for α_s, a constant of integration is introduced. This constant is the single fundamental parameter of QCD that must be determined from experiment. The solution of (1.6) can be written as an expansion in inverse powers of $\ln(\mu^2/\Lambda^2_{\mathrm{QCD}})$:

$$\alpha_s(\mu) = \frac{12\pi}{\beta_0 \log(\mu^2/\Lambda^2_{\mathrm{QCD}})} - \frac{36\pi\beta_1 \log(\log(\mu^2/\Lambda^2_{\mathrm{QCD}}))}{\beta_0^3 \log^2(\mu^2/\Lambda^2_{\mathrm{QCD}})} + \mathcal{O}\left(\frac{\log^2(\log(\mu^2/\Lambda^2_{\mathrm{QCD}}))}{\log^3(\mu^2/\Lambda^2_{\mathrm{QCD}})}\right), \tag{1.8}$$

with $\Lambda_{\mathrm{QCD}} \simeq 0.2 - 0.3$ GeV denoting the constant of integration. This solution illustrates the property of *asymptotic freedom*. Since $N_f < 16$, the coupling constant becomes small at high energies (e.g. $\alpha_s(m_\tau = 1.77\ \mathrm{GeV}) = 0.35$ and $\alpha_s(m_Z = 91\ \mathrm{GeV}) = 0.117$ [E$^+$04]), thus allowing a perturbative treatment of the interactions between quarks and gluons. On the other hand, this equation has a Landau pole in the infrared. Consequently, the coupling becomes large at low energies and a perturbative expansion in terms of quarks

and gluons as degrees of freedom is no longer feasible. In nature, only bound states of quarks and gluons which form color-singlets are observed at low energies. From the point of view of group theory this means that in constructing the baryon state out of three quarks, we have to pick out the singlet representation in the decomposition of the product of three triplets into irreducible representations:

$$\mathbf{3} \otimes \mathbf{3} \otimes \mathbf{3} = \mathbf{1} \oplus \mathbf{8} \oplus \mathbf{8} \oplus \mathbf{10}. \tag{1.9}$$

Mesons, which are made of quark-antiquark pairs, correspond to the singlet of the irreducible representations in $\mathbf{3} \otimes \mathbf{3}^*$:

$$\mathbf{3} \otimes \mathbf{3}^* = \mathbf{1} \oplus \mathbf{8}. \tag{1.10}$$

The requirement that quarks at low energies have to be part of a bound color-singlet state is called *color confinement*. This property has significant impact on the ground state of the theory: the empty Fock space cannot be the ground state, otherwise it would be possible to excite a single quark as asymptotic state. This hints to the presence of condensates in the QCD vacuum.

1.2 Chiral symmetry and condensates

Besides the local $SU(3)$ gauge symmetry, the QCD Lagrangian (1.1) also possesses a global $U(1)$ symmetry, i. e. the Lagrangian is invariant under global phase transformations $\psi \to e^{i\theta}\psi$. By applying Noether's theorem, this symmetry yields the conservation of baryon number,

$$\mathcal{B} = \frac{1}{3}\int \mathrm{d}^3x \psi^\dagger \psi. \tag{1.11}$$

In the limit of vanishing quark masses, the QCD Lagrangian (1.1) has an extra symmetry related to the conserved left- or right-handedness (chirality) of zero mass spin-1/2 particles. This limiting case is important as the masses of the light quarks are small compared to typical hadronic mass scales such as the nucleon mass $M_N \sim 1$ GeV. Consider

$$\mathcal{L}_{\mathrm{QCD}} \equiv \mathcal{L}^{(0)}_{\mathrm{QCD}} + \delta\mathcal{L}, \tag{1.12}$$

where $\mathcal{L}^{(0)}_{\mathrm{QCD}}$ refers to the limit $\hat{m} = 0$ and $\delta\mathcal{L} = -\bar{\psi}\hat{m}\psi$. $\mathcal{L}^{(0)}_{\mathrm{QCD}}$ is invariant under the group

$$U(3)_L \otimes U(3)_R \equiv SU(3)_L \otimes SU(3)_R \otimes U(1)_V \otimes U(1)_A. \tag{1.13}$$

The chiral flavor group $SU(3)_L \otimes SU(3)_R$ transforms the left- and right-handed quark fields $\psi_{L,R} \equiv \frac{1}{2}(1 \mp \gamma_5)\psi$ according to

$$\psi_L \to e^{i\frac{\lambda^a}{2}\theta^a_L}\psi_L \qquad \text{and} \qquad \psi_R \to e^{i\frac{\lambda^a}{2}\theta^a_R}\psi_R, \tag{1.14}$$

where λ^a are the Gell-Mann matrices in flavor space and $a = 1 \ldots 8$. Applying Noether's theorem yields the conserved currents,

$$J^{\mu a}_L = \bar{\psi}_L \gamma^\mu \frac{\lambda^a}{2}\psi_L \quad \text{and} \quad J^{\mu a}_R = \bar{\psi}_R \gamma^\mu \frac{\lambda^a}{2}\psi_R, \tag{1.15}$$

with $\partial_\mu J_L^{\mu a} = \partial_\mu J_R^{\mu a} = 0$. Instead of left- and right-handed currents, it is common to introduce vector and axial-vector currents

$$J_V^{\mu a} \equiv J_R^{\mu a} + J_L^{\mu a} = \bar{\psi}\gamma^\mu \frac{\lambda^a}{2}\psi \quad \text{and} \quad J_A^{\mu a} \equiv J_R^{\mu a} - J_L^{\mu a} = \bar{\psi}\gamma^\mu\gamma_5 \frac{\lambda^a}{2}\psi, \tag{1.16}$$

with $\partial_\mu J_V^{\mu a} = \partial_\mu J_A^{\mu a} = 0$. Chiral $SU(3)_L \otimes SU(3)_R$ symmetry is therefore equivalent to invariance under the group $SU(3)_V \otimes SU(3)_A$ with transformations

$$\psi \to e^{i\frac{\lambda^a}{2}\theta_V^a}\psi \qquad \text{and} \qquad \psi \to e^{i\gamma_5\frac{\lambda^a}{2}\theta_A^a}\psi. \tag{1.17}$$

The axial $U(1)_A$ symmetry, i. e. invariance under

$$\psi \to e^{i\gamma_5\theta_A}\psi \tag{1.18}$$

is known to be broken in nature and probably broken in QCD by instanton effects [tH76, Shu88]. This gives rise to the unnaturally large η' mass.

There is strong empirical evidence that the $SU(3)_A$ symmetry is spontaneously broken in the physical vacuum: For massless fermions helicity eigenstates are also parity eigenstates. If the $SU(3)_A$ symmetry remains unbroken, one would observe degenerate hadronic multiplets of opposite parity (so-called parity doublets) in the meson and baryon spectrum. However, such doublets are not observed in nature. For example, the ρ meson mass $m_\rho = 770$ MeV is much smaller than the mass of its axial partner, the a_1 meson, which is $m_{a_1} = 1260$ MeV. The spontaneously broken $SU(3)_A$ symmetry leads to the appearance of eight *Goldstone* bosons, which are identified as the pions, kaons, antikaons and the η meson. In nature, the Goldstone bosons are not exactly massless because chiral symmetry is explicitly broken by the small but finite current quark masses. However, their masses of $140 - 500$ MeV are small compared to typical hadronic masses of 1 GeV.

Spontaneous chiral symmetry breaking goes in parallel with a qualitative re-arrangement of the vacuum, an entirely non-perturbative phenomen. The ground state is now populated by scalar quark-antiquark pairs. The corresponding ground state expectation value

$$\langle\bar{\psi}\psi\rangle \equiv \langle 0|\bar{\psi}\psi|0\rangle = \langle 0|\bar{\psi}_L\psi_R + \bar{\psi}_R\psi_L|0\rangle = -\operatorname{Tr}\lim_{y\to x_+}\langle 0|\mathcal{T}\psi(x)\bar{\psi}(y)|0\rangle \tag{1.19}$$

is called the chiral (or quark) condensate. Here, $\mathcal{T}$ is the time ordering operator. The chiral condensate can be related to the pion decay constant $f_\pi = 92.4$ MeV via the Gell-Mann, Oakes, Renner (GOR) relation [GMOR68]

$$m_\pi^2 f_\pi^2 = -\frac{1}{2}(m_u + m_d)\langle\bar{u}u + \bar{d}d\rangle + \mathcal{O}(m_{u,d}^2). \tag{1.20}$$

Taking $m_u = 5$ MeV and $m_d = 7$ MeV yields a value for the chiral condensate, $\langle\bar{u}u\rangle = \langle\bar{d}d\rangle \simeq -(250\text{ MeV})^3$.

Chiral symmetry breaking is also observed in lattice QCD calculations. The chiral condensate $\langle\bar{\psi}\psi\rangle_\beta$ at finite temperature is derived starting from the pressure by taking the derivative with respect to the quark mass:

$$\langle\bar{\psi}\psi\rangle_\beta \sim \frac{\partial p(T,V)}{\partial m_q}. \tag{1.21}$$

Lattice QCD results for $\langle\bar{\psi}\psi\rangle_\beta$ are shown in Fig. 1.1. Above a critical temperature T_c the finite expectation value of the chiral condensate melts away, resulting in a system, where chiral symmetry is not spontaneously broken anymore.

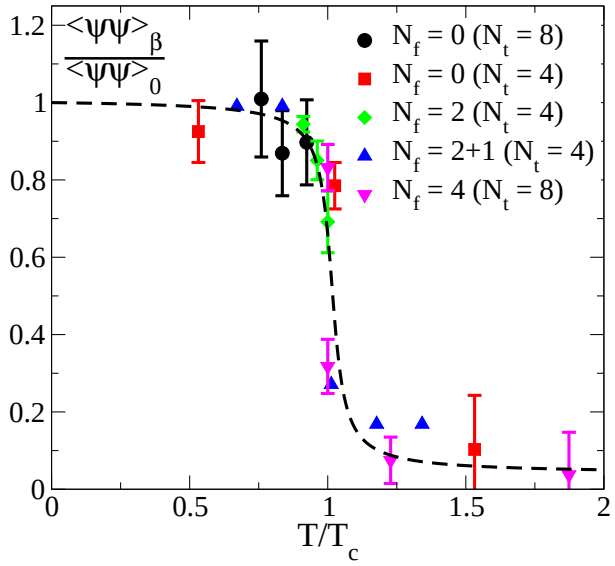

Figure 1.1: Temperature dependence of the chiral condensate from lattice QCD [B+95b].

1.3 Thermal field theory

Our aim in this work is to study QCD at finite temperature and finite quark chemical potential. The appropriate tool to calculate the properties of a hot system of quarks and gluons is thermal field theory (TFT). In the following, we introduce the main concepts and techniques of TFT which will be of importance for the discussion of the physics of the QGP in subsequent chapters. We mostly follow [Kap89] and [Bel96] here.

In a relativistic quantum system where particles can be created and destroyed, it is most straightforward to compute observables in the grand canonical ensemble. In this ensemble, the volume V, the temperature T, and the chemical potential μ are fixed variables. The grand canonical partition function is

$$\mathcal{Z}(V,T,\mu) = \mathrm{Tr}\, e^{-\beta(\mathcal{H}-\mu\mathcal{N})}. \tag{1.22}$$

Here, $\beta = 1/T$ is the inverse temperature, $\mathcal{H}$ is the Hamiltonian of the system and $\mathcal{N}$ is the particle number operator. For simplicity we will assume $\mu = 0$ in the rest of this section. The statistical average of an operator $\mathcal{A}$ is obtained using

$$\langle \mathcal{A} \rangle_\beta = \frac{1}{\mathcal{Z}} \mathrm{Tr} \left[\mathcal{A} e^{-\beta \mathcal{H}} \right] . \tag{1.23}$$

Consider the propagation of spinless neutral particles, represented by a scalar field $\phi(x)$, in a heat bath. This involves the thermal average of the Green's function

$$\langle G(x,x') \rangle_\beta \equiv \langle \mathcal{T} \phi(x) \phi(x') \rangle_\beta = \sum_n \langle n | G(x,x') | n \rangle . \tag{1.24}$$

Here, $\mathcal{T}$ denotes the time ordered product of the fields. Next we make use of the operator identity

$$\mathcal{T} \phi(x) \phi(x') = \langle 0 | \mathcal{T} \phi(x) \phi(x') | 0 \rangle + : \phi(x) \phi(x') : , \tag{1.25}$$

where $: \phi(x) \phi(x') :$ denotes the normal-ordered product of $\phi(x)$ and $\phi(x')$. Contrary to the vacuum case, the normal-ordered product of two fields does not vanish in the presence of a heat bath because of the term $\sum_n \langle n | \ldots | n \rangle$ in (1.24). Decomposing the field ϕ in creation and annihilation operators $a_p^\dagger$ and a_p, the new term is given by

$$2 \int \frac{\mathrm{d}^3 p}{(2\pi)^3} \frac{1}{2E_p} e^{i(x-x')} \langle a_p^\dagger a_p \rangle_\beta = 2 \int \frac{\mathrm{d}^3 p}{(2\pi)^3} \frac{1}{2E_p} e^{i(x-x')} f_B(E_p), \tag{1.26}$$

where $f_B(E_p) = (\exp(\beta E_p) - 1)^{-1}$ is the Bose-Einstein distribution function. It describes the propagation of "on-shell" particles from the heat bath with the statistical probability of having the appropriate momentum. Adding the usual vacuum part, we find the thermal propagator in momentum space:

$$D_F(p) = \frac{i}{p^2 - m^2 + i\epsilon} + 2\pi \delta(p^2 - m^2) f_B(|p_0|). \tag{1.27}$$

The calculation for the free fermion field is similar and results in the thermal propagator

$$S_F(p) = (\not{p} + m) \cdot \left(\frac{i}{p^2 - m^2 + i\epsilon} - 2\pi \delta(p^2 - m^2) f_D(|p_0|) \right) , \tag{1.28}$$

where $f_D(p_0) = (\exp(\beta p_0) + 1)^{-1}$ is the Fermi-Dirac distribution function.

1.3.1 Perturbative techniques

So far we have only discussed free particles. We will now consider the case of an interacting field theory. If the interaction is a small correction to the free Hamiltonian, then a perturbative expansion in powers of the coupling constant can be performed. Our starting point is the observation that the statistical density operator $\rho = \exp(-\beta \mathcal{H})$ can be regarded as a time evolution operator in imaginary time $\tau = it$ over the interval $[0, \beta]$.

Therefore, the partition function can be expressed in terms of an Euclidean path integral. In the case of a scalar field, it reads

$$\mathcal{Z}(T,V) = \oint \mathcal{D}\phi \exp\left(-\int_0^\beta \mathrm{d}\tau \int_V \mathrm{d}^3x\, \mathcal{L}_E[\phi(\boldsymbol{x},\tau)]\right), \tag{1.29}$$

where the field ϕ has to obey periodic boundary conditions, $\phi(\boldsymbol{x},0) = \phi(\boldsymbol{x},\tau)$. Due to their spinor nature, fermionic fields obey anti-periodic boundary conditions. Field theory at finite temperature is then equivalent to a Euclidean field theory in a four-dimensional space-time with the time component compactified on a ring with circumference $\beta = 1/T$. The thermal expectation value of an operator $\mathcal{A}[\phi]$ in contact with a heat bath is then given by

$$\langle \mathcal{A} \rangle_\beta = \frac{1}{\mathcal{Z}} \oint \mathcal{D}\phi\ \mathcal{A}[\phi] \exp\left(-\int_0^\beta \mathrm{d}\tau \int_V \mathrm{d}^3x\, \mathcal{L}_E[\phi(\boldsymbol{x},\tau)]\right). \tag{1.30}$$

The formal similarity of (1.29) with the generating functional $Z[J]$ for vanishing external sources J at zero temperature makes both perturbative (Feynman diagram) and lattice techniques easily adaptable tools to evaluate $\langle \mathcal{A} \rangle_\beta$. The corresponding expression of (1.29) for QCD follows as

$$\mathcal{Z}(T,V,\mu) = \oint \mathcal{D}A_\mu \mathcal{D}\bar{\psi}\mathcal{D}\psi \exp\left(-\int_0^\beta \mathrm{d}\tau \int_V \mathrm{d}^3x\, \{\mathcal{L}^E_{\mathrm{QCD}} - \mu_q \psi^\dagger \psi\}\right), \tag{1.31}$$

where $\mathcal{L}^E_{\mathrm{QCD}}$ is the Euclidean versions of (1.1), and we have introduced an explicit dependence on the quark chemical potential μ_q.

1.3.2 The imaginary time formalism

Various choices for the time path in Eqn. (1.31) are possible, which lead to different calculational frameworks. The simple choice of the direct path results in the so-called *imaginary time formalism*, which we will utilize in this work. Its major advantage is that in the Fourier language the Feynman rules are very similar to those of the vacuum theory, except that the energies in the propagators are discrete and imaginary. The loop integrals are replaced by

$$\int \frac{\mathrm{d}^4p}{(2\pi)^4} \ \rightarrow\ iT \sum_{n=-\infty}^{+\infty} \int \frac{\mathrm{d}^3p}{(2\pi)^3}, \tag{1.32}$$

where the sum is understood to be taken over the discrete set of Matsubara frequencies ω_n. Energy-momentum conserving delta functions become

$$(2\pi)^4 \delta^{(4)}(p) \ \rightarrow\ \frac{(2\pi)^3}{iT} \delta_{n,0} \delta^{(3)}(\boldsymbol{p}). \tag{1.33}$$

The Matsubara frequencies appear as

$$p_0 \;\rightarrow\; \omega_n = \frac{2\pi i}{\beta}(n+\zeta), \quad n \;\in\; \mathbb{Z} \text{ and } \zeta = \begin{cases} 0 & \text{for bosons,} \\ \\ \frac{1}{2} & \text{for fermions.} \end{cases} \tag{1.34}$$

In Appendix D we show in detail how one and two fermion line integrals, which are used frequently in this work, can be calculated using the imaginary time formalism.

1.4 The QCD phase diagram

Thermodynamical information is often presented in the form of a phase diagram, in which different manifestations or phases of a substance occupy different regions of a plot whose axis are calibrated in terms of external conditions or control parameters. For QCD, the relevant control parameters are the current quark masses m_i, the temperature T and the quark chemical potentials μ_i, $i = u, d, s$. If we only consider two flavors of quarks with identical masses $m_u = m_d \equiv m_q$ and a common quark chemical potential $\mu_u = \mu_d \equiv \mu_q$, the phase boundaries are two dimensional surfaces in the three-dimensional parameter space $\{T, \mu_q, m_q\}$. If the quark mass m_q is also fixed, the phase boundaries are lines in the two-dimensional parameter space $\{T, \mu_q\}$. This case is referred to in the following.

The QCD phase transition happens at a temperature where the coupling is not small and QCD is strongly interacting. The only way to perform calculations in this regime is to simulate QCD on a lattice, i. e. to evaluate Eqn. (1.31) numerically at discrete space-time points using Monte-Carlo techniques. This is possible since one is dealing with an Euclidean path integral where large fluctuations are exponentially damped, unlike in Minkowski space, where the dominant contribution to the path integral emerges from the interference pattern of oscillating amplitudes. Furthermore, the introduction of a lattice spacing a introduces a cut-off $1/a$ in momentum space that regularizes the continuum-inherent ultraviolet divergences.

1.4.1 The critical temperature

The QCD phase transition at finite temperature and vanishing quark chemical potential has been successfully studied on the lattice in the case of pure $SU(3)$ gauge theory and also for QCD with dynamical quarks. In Table 1.1 the transition temperatures extrapolated to the chiral limit, found in lattice simulations with various improved actions, are summarized. For pure $SU(3)$ gauge theory, the transition temperature is $T_c \sim \Lambda_{\mathrm{QCD}}$. If quarks are added, T_c is lowered because the critical energy density that triggers the phase transition can be reached earlier if more thermally active degrees of freedom are present.

action	N_f	N_t	T_c[MeV]	Ref.
plaquette	0	∞	268	[BKLP99, EHK98]
Symanzik	0	∞	269	[BKLP99]
RG	0	∞	276	[O$^+$99]
RG+clover	2	4	171(4)	[AK$^+$01b]
Symanzik+p4	2	4	173(8)	[KLP$^+$01b]
Symanzik+p4	3	4	154(8)	[KLP$^+$01b]

Table 1.1: The transition temperature T_c in the chiral limit. The scale is fixed by $\sqrt{\sigma} \simeq 425$ MeV for pure $SU(3)$ gauge theory and $m_V = 770$ MeV for $N_f = 2$ and $N_f = 3$ QCD. N_t denotes the number of temporal lattice sites used for the simulations. $N_t = \infty$ means that the lattice results have been continuum extrapolated.

For two light and one heavy quark flavor, the transition temperature remains close to the two-flavor value, indicating that the quark mass dependence of T_c is small [Sch02]. A fit to several lattice calculations of T_c at different quark mass values suggests a linear behavior of the form [KLP01a]

$$T_c(m_\pi) = T_c(0) + 0.039(4)m_\pi, \tag{1.35}$$

where m_π stands for the mass of the pseudo-scalar Goldstone particle. The weak m_π-dependence indicates that the transition is not 'pion'-dominated, but rather 'resonance'-driven.

1.4.2 The equation of state

The EoS is one of the most important quantities in a phenomenological study of hot QCD and different lattice collaborations have investigated this issue recently. The CP-PACS collaboration carried out a systematic calculation of the EoS of full QCD for two flavors of Wilson-type quarks. The simulations were performed on $16^3 \times 4$ and $16^3 \times 6$ lattices with a RG-improved action for the gluon sector and a meanfield-improved clover action for the quark sector [AK$^+$01a]. The pressure was calculated using the integral method [EFK$^+$90]. This method is based on the equation $p = -f$ ($f = (-T/V) \ln \mathcal{Z}$ is the free energy density), which is valid for large homogeneous systems. Since the derivatives of the partition function can be expressed by expectation values of operators, which can be computed by a Monte-Carlo simulation, the pressure can be obtained by integrating these expectation values in parameter space. The energy density ϵ is acquired by combining the results for the pressure and the interaction measure $\epsilon - 3p$, which can be accurately computed in lattice QCD simulations. The scaled pressure p/T^4 and the scaled energy density ϵ/T^4 are shown in Fig. 1.2.

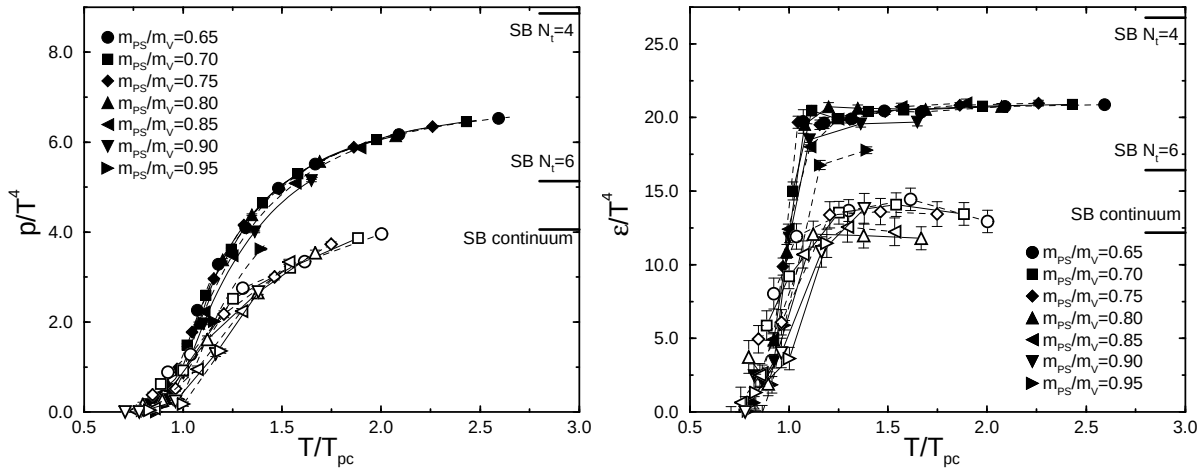

Figure 1.2: The scaled pressure p/T^4 (left panel) and the scaled energy density ϵ/T^4 (right panel) calculated with RG-improved gauge and meanfield-improved clover quark actions on $16^3 \times 4$ (filled symbols) and $16^3 \times 6$ (open symbols) lattices as a function of T/T_c [AK$^+$01a].

Filled symbols denote results from simulations performed on lattices with $N_t = 4$ temporal lattice sites, while open symbols denote results from calculations with $N_t = 6$. Different shapes of the symbols correspond to different values of $m_{\rm PS}/m_{\rm V}$, i. e. to different quark masses. The short lines on the right axis indicate the Stefan-Boltzmann ideal gas values for $N_t = 4$, $N_t = 6$ and the continuum limit. The dependence of both, pressure and energy density on the quark masses appears to be rather weak over a wide range of values. On the other hand, the N_t-dependence is sizeable for large temperatures: there is a big difference in both, pressure and energy density calculated on $N_t = 4$ and $N_t = 6$ lattices for $T \gtrsim 1.2\,T_c$. However, the cutoff effects due to the small values of N_t are not important close to T_c and that the magnitude and the temperature dependence of the EoS on $N_t = 6$ lattices are quite similar for improved Wilson and staggered quarks. The lattice simulations do not indicate that the pressure and the energy density approach their respective Stefan-Boltzmann ideal gas values in the high temperature limit. The deviations are too big to be reproduced in ordinary high temperature perturbation theory. However, they are accounted for in quasiparticle models [PKS00, SW01] and resummed perturbative approaches [BI02]. Similar observations have been made with staggered quarks. The difference in both, pressure and energy density from simulations with quark masses $m_q/T = 0.075$ and $m_q/T = 0.15$ is small within errors [B$^+$97]. The pressure and the energy density also do not approach their respective Stefan-Boltzmann ideal gas values even at temperatures as large as $T = 4\,T_c$. A clear deviation of the pressure and the energy density from their respective Stefan-Boltzmann limits at finite N_t has also been observed in a quenched study of the EoS with the RG-improved action [O$^+$99].

The Bielefeld group has calculated the EoS for $N_f = 2$, 3 and 2+1 on a $16^3 \times 4$ lattice, using the p4-improved staggered quark action with the Symanzik improved gauge

action [KLP00]. For this action the N_t-dependence is known in the Stefan-Boltzmann limit. The EoS has been computed at $m_q/T = 0.4$ for $N_f = 2$ and $N_f = 3$, and at $m_{u,d}/T = 0.4$ and $m_s/T = 1.0$ for $N_f = 2 + 1$. The results are shown in Fig. 1.3.

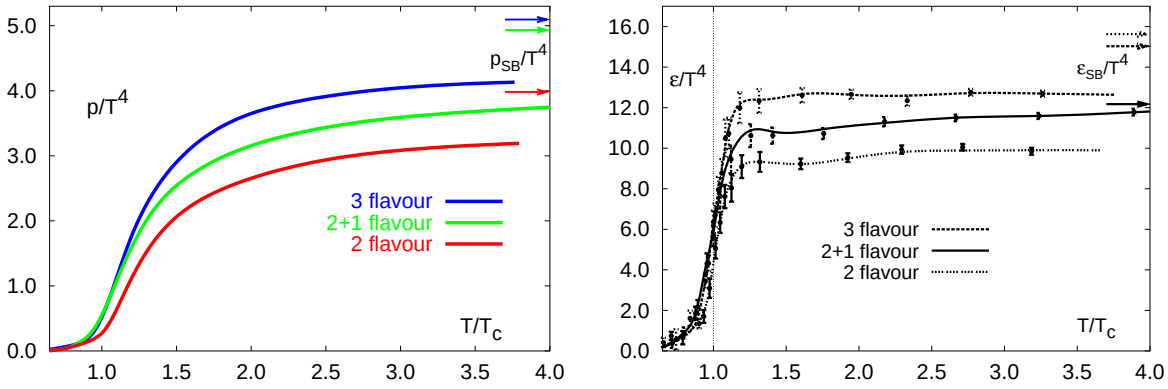

Figure 1.3: The scaled pressure p/T^4 (left panel) and the scaled energy density ϵ/T^4 (right panel) from the p4-improved staggered action on a $16^3 \times 4$ lattice as a function of T/T_c [KLP00].

A clear N_f-dependence is visible for both, pressure and energy density. They become larger when the number of degrees of freedom increases. As in the case of Wilson-type quarks, pressure and energy density deviate substantially from the ideal gas limit indicated by the arrows on the right axis of the figures.

1.4.3 Finite density

Lattice QCD simulations at finite density are exceedingly difficult because of the so-called "sign-problem". The fermion determinant obtained by integrating out the fermion fields in Eqn. (1.31) is real for vanishing quark chemical potential, but becomes complex as soon as $\mu_q \neq 0$. Therefore, the application of importance-sampling methods is no longer feasible, increasing the numerical efforts by several orders of magnitude. In the following we summarize some recent approaches to circumvent the sign problem at least for small chemical potentials. For further details, the reader is referred to e. g. Refs. [LP03, MNNT03].

Glasgow method

The key idea of this method is to expand the partition function Eqn. (1.31) in the fugacity variable $e^{\mu_q/T}$. The partition function is then given by

$$\mathcal{Z} = \int \mathcal{D}U \, \frac{\det M(\mu_q)}{\det M(0)} \det M(0) e^{-\beta_0 S_g[U]} = \left\langle \frac{\det M(\mu_q)}{\det M(0)} \right\rangle_{\mu_q=0}, \tag{1.36}$$

where $M(\mu_q)$ is the fermion determinant, obtained by integrating out the fermion fields in (1.31), $\beta_0 = 1/(2g_s)$ is the gauge coupling, S_g is the gauge part of the action and U is

the link variable on the lattice that is associated with the gauge field. The determinant ratio is now treated like an observable, while the integration measure is defined at $\mu_q = 0$. Thus it is positive and the sign problem does not appear. However, two problems arise: The reweighting factor corresponds to a ratio of two partition functions with different actions. Thus it decays exponentially with the difference between their free energies $e^{-\Delta F/T} \propto e^{-cV}$, where c is a constant. In the thermodynamic limit where $V \to \infty$, this difference tends to zero and consequently the reweighting factor becomes zero. Hence, extrapolations to this limit are extremely difficult. Furthermore, the overlap between the reweighted ensemble and the full ensemble deteriorates with increasing μ_q, making importance-sampling methods untrustworthy.

Multiparameter reweighting

The ensemble overlap can be significantly improved by a multidimensional generalization [FK02b] of the Glasgow method. The essential idea is to reweight in the lattice gauge coupling β in addition to μ_q,

$$\mathcal{Z} = \int \mathcal{D}U \, \frac{\det M(\mu_q)}{\det M(0)} e^{-(\beta-\beta_0)S_g[U]} \det M(0) e^{-\beta_0 S_g[U]} = \left\langle \frac{e^{-\beta S_g} \det M(\mu_q)}{e^{-\beta_0 S_g} \det M(0)} \right\rangle_{\mu_q=0,\beta_0}, \tag{1.37}$$

and choose β_0 so that

$$\left| \frac{\det M(\mu_q)}{\det M(0)} \right| e^{-(\beta-\beta_0)S_g[U]} \tag{1.38}$$

becomes as large as possible. At imaginary chemical potential, the predictions of this method are in agreement with direct simulations, while the Glasgow method fails to reproduce them due to the overlap problem [FK02b]. A first estimate of the QCD phase diagram for $2+1$ flavors [FK02a] is shown in Fig. 1.4. This simulation was carried out using staggered fermions on a 4×8^3 lattice with a pion mass at least twice as large as the physical value. The calculation finds a critical point $(T_c, \mu_c) = (160 \pm 4 \text{ MeV}, 242 \pm 12 \text{ MeV})$ where the first-order transition that separates the hadronic and the QGP phase ends. For smaller T and μ_q, the transition becomes a crossover.

Taylor expansion

A different attempt to explore the phase diagram at least for small μ_q exploits the fact that derivatives of an observable with respect to μ_q can be calculated with standard methods at $\mu_q = 0$. Hence, the phase transition line close to $\mu_q = 0$ is obtained by Taylor expanding [A$^+$02]:

$$T_c(\mu_q) = T_c(0) + \mu_q \frac{dT_c}{d\mu_q}\bigg|_{\mu_q=0} + \frac{\mu_q^2}{2} \frac{d^2T_c}{d\mu_q^2}\bigg|_{\mu_q=0} + \dots \tag{1.39}$$

Derivatives with odd powers of μ_q vanish because of the realness of the partition function, so it is sufficient to calculate only $d^2T_c/d\mu_q^2(\mu_q = 0)$ on the lattice. Truncation errors

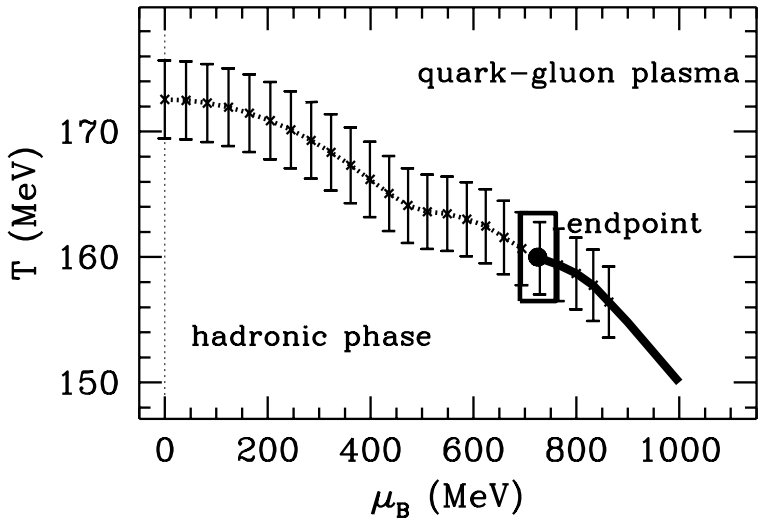

Figure 1.4: The $T - \mu_B$ diagram from the lattice calculation of [FK02a]. Note that $\mu_B \equiv 3\mu_q$. The critical endpoint is located at $T_c = 160 \pm 4$ MeV and $\mu_c = 242 \pm 12$ MeV. The solid line denotes a first order transition, the dashed line a crossover. $T_c(\mu_B = 0)$ is determined within the same calculation as 172 ± 3 MeV.

accordingly enter at $\mathcal{O}(\mu_q^4)$. Assuming that the transition line remains parabolic, a sketch of the phase diagram for $N_f = 2$ staggered fermions can be drawn, see figure 1.5. This method can also be applied to study thermodynamic quantities at finite quark chemical potential. In [A$^+$03] derivatives of the thermodynamic potential with respect to the quark chemical potential μ_q up to fourth order were calculated, enabling estimates of the pressure and the quark number density as a function of μ_q. These simulations were carried out on a $16^3 \times 4$ lattice with two continuum flavors of p4-improved staggered quarks with masses $m/T = 0.4$. Results for the scaled pressure difference $\Delta p(T, \mu_q)/T^4 = (p(T, \mu_q) - p(T, 0))/T^4$ and the scaled total quark number density $n_q(T, \mu_q)/T^3 = (\partial p/\partial \mu_q)/T^3$ are shown in Fig. 1.6.

Imaginary chemical potential

Another line of attack is, to perform lattice QCD simulations at imaginary chemical potential, where the fermion determinant is positive and thus standard methods as in the case of $\mu_q = 0$ can be used. For small μ_q/T an analytic continuation to real μ_q can be performed. This technique was employed in [dFP02] to calculate the transition line on a $8^3 \times 4$ lattice with two flavors of staggered quarks. It was found that the transition line is well represented by the equation

$$\frac{T_c(\mu_B)}{T_c(0)} = 1 - 0.00563(38) \left(\frac{\mu_B}{T}\right)^2, \tag{1.40}$$

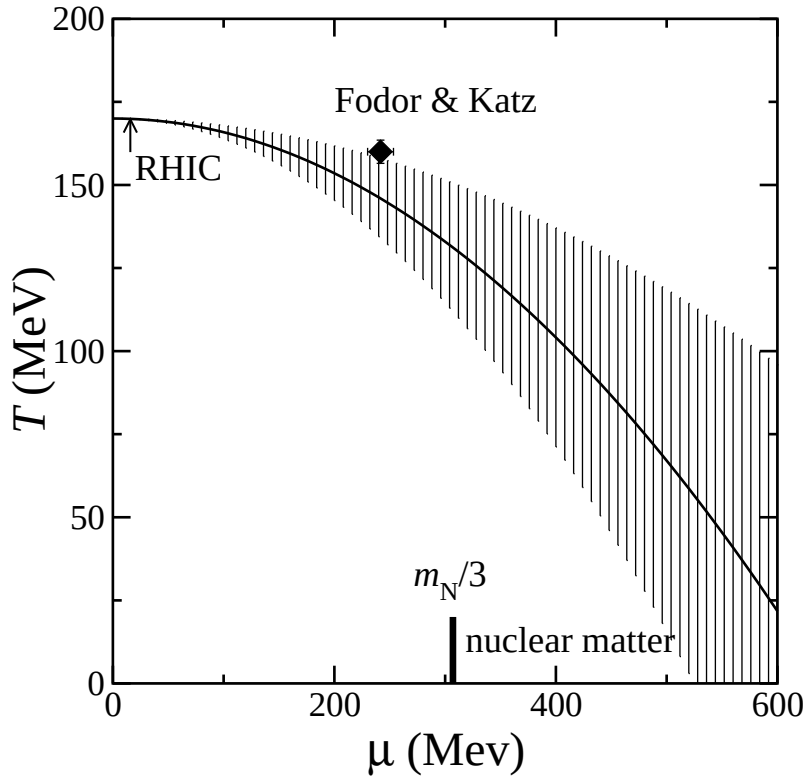

Figure 1.5: Sketch of the phase diagram for $N_f = 2$ using the value for $d^2T_c/d\mu_q^2(\mu_q = 0)$ [A$^+$02], calculated on a 4×16^3 lattice with rotationally improved staggered fermions. The diamond shows the end point of the first order phase transition from Fig. 1.4. The arrow marks the chemical freeze-out point at RHIC Au+Au collisions at $\sqrt{s} = 130$ AGeV [BMMRS01].

while the next-order term $\mathcal{O}((\mu_B/T)^4)$ is statistically insignificant up to $\mu_B \sim 500$ MeV. In a subsequent work [dFP03], the transition line was also determined for three degenerate quark flavors. The results are presented in Fig. 1.7.

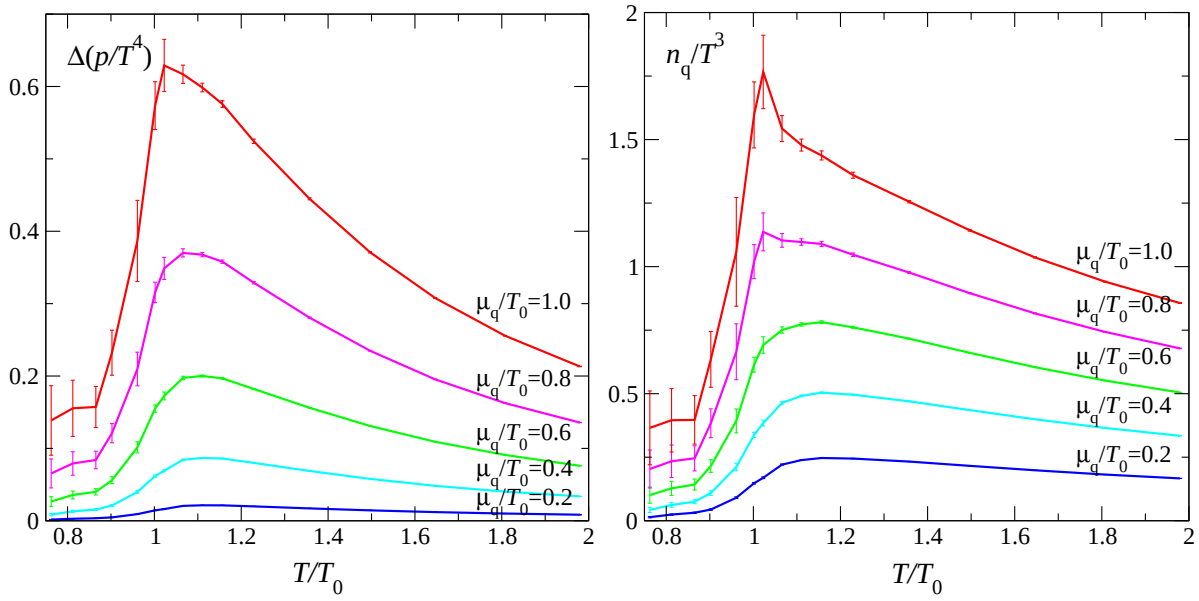

Figure 1.6: The scaled pressure difference $\Delta p(T, \mu_q)/T^4$ and the scaled quark number density $n_q(T, \mu_q)/T^3$ as a function of the temperature for different values of the quark chemical potential [A+03].

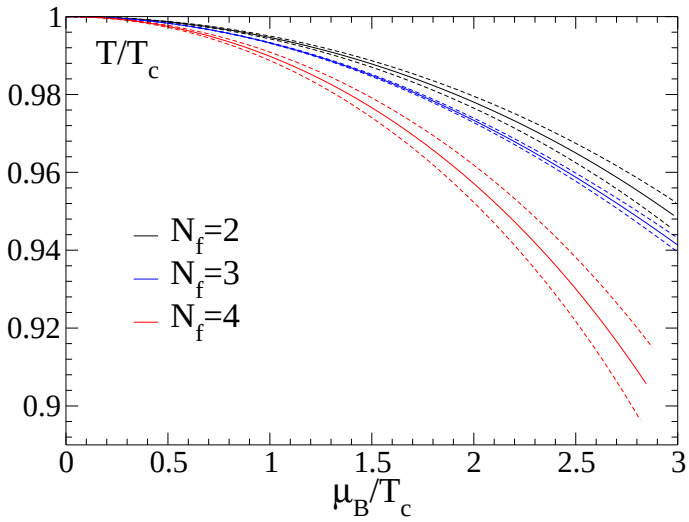

Figure 1.7: One sigma error bands on $T_c(\mu_B)$ for different values of N_f [DL03, dFP02, dFP03]. Only the $N_f = 3$ calculation is accurate enough to include a quartic term.

Chapter 2

A Simple Model

In this chapter, the MIT bag model, a simple phenomenological model that implements two key properties of QCD, *asymptotic freedom* and *confinement*, is introduced. Due to its simple analytic form, the MIT bag model is widely used in astrophysics to determine the properties of quark matter at high temperatures and large densities. We first summarize some important thermodynamic relations which will be used frequently in the remainder of this work. Subsequently we discuss the MIT bag model and employ it to calculate the QCD phase diagram and the EoS . The primary purpose of this chapter is to explain some of the key properties of the QCD phase diagram, as known from lattice QCD, qualitatively in terms of a very simple physical model and to set the stage for more refined models which are discussed in subsequent chapters.

2.1 Some important thermodynamic relations

All standard thermodynamical quantities can be derived from the partition function (1.22). For example, the pressure p, the particle density n, the entropy density s and the energy density ϵ for a spatial homogeneous system are

$$p = T\frac{\partial \ln \mathcal{Z}}{\partial V}, \quad n = \frac{T}{V}\frac{\partial \ln \mathcal{Z}}{\partial \mu}, \quad s = \frac{1}{V}\frac{\partial (T \ln \mathcal{Z})}{\partial T}, \quad \epsilon = -p + Ts + \mu n. \tag{2.1}$$

For an ideal gas, the trace in the partition function (1.22) can be explicitly calculated. The resulting expression for bosons is

$$\ln \mathcal{Z}_b(T,\mu) = \frac{\nu_b V}{2\pi^2}\int_0^\infty \mathrm{d}k\, k^2 \ln\left[1 - \exp\left(-\beta\sqrt{k^2+m_b^2}\right)\right], \tag{2.2}$$

while that for fermions is

$$\ln \mathcal{Z}_f(T,\mu) = \frac{\nu_f V}{2\pi^2}\int_0^\infty \mathrm{d}k\, k^2 \left\{\ln\left[1 + \exp\left(-\beta(\sqrt{k^2+m_f^2} - \mu)\right)\right] + \ln\left[1 + \exp\left(-\beta(\sqrt{k^2+m_f^2} + \mu)\right)\right]\right\}. \tag{2.3}$$

ν_b and ν_f are the degeneracy factors for bosons and fermions, respectively, and m_b and m_f denote the masses of the particles. In the limit $m_{b,f} \to 0$ the integrals in (2.2) and

(2.3) can be calculated analytically. For bosons we obtain

$$T \ln \mathcal{Z}_b = \nu_b V \frac{\pi^2}{90} T^4, \tag{2.4}$$

while for fermions the result is

$$T \ln \mathcal{Z}_f = \frac{\nu_f V}{12} \left(\frac{7}{30} \pi^2 T^4 + T^2 \mu^2 + \frac{1}{2\pi^2} \mu^4 \right). \tag{2.5}$$

If we neglect the small quark masses, the pressure and the energy density of a gas of non-interacting quarks and gluons are thus given by

$$\begin{aligned} p &= \frac{37}{90} \pi^2 T^4 + T^2 \mu_q^2 + \frac{1}{2\pi^2} \mu_q^4, \\ \epsilon &= \frac{37}{30} \pi^2 T^4 + 3T^2 \mu_q^2 + \frac{3}{2\pi^2} \mu_q^4. \end{aligned} \tag{2.6}$$

Gluons come in eight colors and two polarizations, thus $\nu_b = 8 \cdot 2 \equiv \nu_g$. Quarks have three color degrees of freedom, two flavors (if we only consider the two lightest quark flavors u and d) and two spin states, and consequently $\nu_f = 3 \cdot 2 \cdot 2 \equiv \nu_q$. The chemical potentials of u and d quarks have been taken to be equal, $\mu_u = \mu_d \equiv \mu_q$. The entropy density is given by

$$s = \frac{1}{V} \frac{\partial (T \ln \mathcal{Z})}{\partial T} = \frac{\partial p}{\partial T} = \frac{74}{45} \pi^2 T^3 + 2\mu_q^2 T, \tag{2.7}$$

and the quark number density is

$$n_q = \frac{T}{V} \frac{\partial \ln \mathcal{Z}}{\partial \mu_q} = \frac{\partial p}{\partial \mu_q} = 2 \left(\mu_q T^2 + \frac{\mu_q^3}{\pi^2} \right). \tag{2.8}$$

Since the baryon number of a quark is 1/3, the baryon number density reads

$$n_B = \frac{2}{3} \left(\mu_q T^2 + \frac{\mu_q^3}{\pi^2} \right). \tag{2.9}$$

2.2 The MIT bag model

The MIT bag model has been put forward in the mid-seventies as a microscopic model for hadrons [CJJ+74, CJJT74, DJJK75]. At that time QCD, the fundamental gauge theory of strong interactions, has already been formulated. The MIT bag model was one of the first phenomenological quark models that implemented two of the key properties of QCD, confinement and asymptotic freedom, in a constitutive way. In the MIT bag model, hadrons are made up of a gas of free (or only weakly interacting) quarks and gluons which are confined to a finite region of space: the "bag". The confinement mechanism is not a dynamical result of the underlying theory, but is put in by hand by choosing appropriate boundary conditions. The bag is stabilized by a term of the form $g^{\mu\nu} B$ which is added to

the energy-momentum tensor *inside* the bag. The energy-momentum tensor of a perfect fluid in the rest frame is given by

$$T^{\mu\nu}_{\text{fluid}} = \text{diag}(\epsilon, p, p, p), \tag{2.10}$$

where ϵ is the energy density and p the pressure of the system. Consequently, the bag constant B can be interpreted as a positive contribution to the energy density and a negative contribution to the pressure inside the bag. Equivalently, one may attribute a term $-g^{\mu\nu}B$ to the region *outside* the bag. This leads to the picture of a non-trivial vacuum with a negative energy density $\epsilon_{\text{vac}} = -B$ and a positive pressure $p_{\text{vac}} = +B$. The stability of hadrons then results from balancing this positive vacuum pressure with the pressure caused by the gas of quarks and gluons inside the bag. The MIT bag model cannot say anything about the origin of the non-trivial vacuum, but treats B as a free parameter.

If we interpret the bag constant as a positive contribution to the energy density inside the bag, the energy E_H of an hadron is made up of two parts:

$$E_H = BV + \frac{C}{R}. \tag{2.11}$$

Here, BV is the energy associated with the volume V of the bag and C/R is the kinetic energy of the quarks and gluons inside the bag. It is proportional to the inverse of the radius R of the bag as a consequence of the quantum mechanical uncertainty principle. For our purpose, it is not necessary to specify the constant of proportionality. The effective radius of the hadron is obtained by minimizing (2.11). In the case of a spherical bag, we find

$$\frac{\partial E_H}{\partial R} = \frac{\partial}{\partial R}\left(B\frac{4\pi R^3}{3} + \frac{C}{R}\right) = 0 \quad \Longrightarrow \quad R_0^4 = \left(\frac{C}{4\pi B}\right)^{\frac{1}{4}}. \tag{2.12}$$

Substituting (2.12) back into (2.11), the equilibrium energy is given by

$$E_0(R_0) = 4BV_0, \tag{2.13}$$

where $V_0 = 4\pi R_0^3$ is the equilibrium volume. For a proton with $E_0 \approx 1$ GeV and $R_0 \approx 0.7$ fm, we find $B \approx 175$ MeV/fm^3, or $B^{\frac{1}{4}} \approx 192$ MeV.

The bag model is used to describe quark-gluon matter in any enclosed finite volume. The partition function of an ideal gas of massless quarks and gluons inside the bag is then given by

$$T \ln \mathcal{Z}_{QGP} = \left(\frac{37\pi^2}{90}T^4 + T^2\mu_q^2 + \frac{1}{2\pi^2}\mu_q^4\right) V - BV, \tag{2.14}$$

and the expressions for the pressure and the energy density become

$$p_{QGP} = \left(\frac{37\pi^2}{90}T^4 + T^2\mu_q^2 + \frac{1}{2\pi^2}\mu_q^4\right) - B, \tag{2.15}$$

$$\epsilon_{QGP} = \left(\frac{37\pi^2}{30}T^4 + 3T^2\mu_q^2 + \frac{3}{2\pi^2}\mu_q^4\right) + B. \tag{2.16}$$

The quark number density and the entropy density remain unchanged.

If we only consider the two lightest quarks (u and d) and if there is no net concentration of baryons (i. e. $\mu_B = 0$), then the dominant hadronic degrees of freedom at low temperature are the pions, $\pi^{\pm}$ and π^0, which carry zero net baryon number and can be relatively easily pair-produced. Neglecting the rest mass, which is justified for $T \gtrsim 100$ MeV, the pressure and the energy density of an ideal gas of pions are given by

$$p_\pi = \frac{\pi^2}{30} T^4 \quad \text{and} \quad \epsilon_\pi = \frac{\pi^2}{10} T^4. \tag{2.17}$$

2.3 Comparison with lattice results

2.3.1 The phase boundary

According to Gibbs criteria, the equilibrium condition for two phases is that the temperature T, the chemical potential μ and the pressure p are equal in both phases. Consider a system of pions, and quarks and gluons in equilibrium. For simplicity we start with the case of a vanishing chemical potential. Then $T_{\mathrm{QGP}} = T_\pi = T_c$, $\mu_{\mathrm{QCD}} = \mu_\pi = 0$ and

$$\frac{37\pi^2}{90} T_c^4 - B = \frac{\pi^2}{30} T_c^4 \quad \Longrightarrow \quad B = \frac{34\pi^2}{90} T_c^4. \tag{2.18}$$

For two light flavors a critical temperature $T_c \approx 170$ MeV is found in lattice QCD simulations (see Table 1.1). For this value of T_c the bag constant is $B^{1/4} \approx 236$ MeV. There is a latent heat which corresponds to a jump in the energy density $\Delta\epsilon$, or in the entropy density Δs, $\Delta\epsilon = T_c \Delta s = 4B$.

In order to extend these considerations to the case where $\mu_B \neq 0$, we notice that the transition is taking place when the pressure approximately vanishes, that is when the kinetic pressure of the quarks and gluons approximately equilibrates the bag pressure. Taking this as a criterion for the phase transition, we obtain the condition

$$p_{\mathrm{QGP}} = \frac{37\pi^2}{90} T^4 + \frac{1}{9} T^2 \mu_B^2 + \frac{1}{162} \mu_B^4 - B = 0. \tag{2.19}$$

At zero temperature we find a critical chemical potential of $\mu_B = (162\pi^2 B)^{\frac{1}{4}} = 1594$ MeV. A plot of the phase diagram obtained from (2.19) is shown in Fig. 2.1. The bag model result is in good qualitative agreement with the lattice data, but does not lie within the error band given by the lattice calculation.

2.3.2 Thermodynamical quantities

The pressure and the energy density can be calculated using Eqns. (2.15), (2.16) and (2.17). Results are shown in Fig. 2.2. The solid line denotes the pressure and the energy density of an ideal gas of massless pions for $T \leq T_c$ and the pressure and the energy

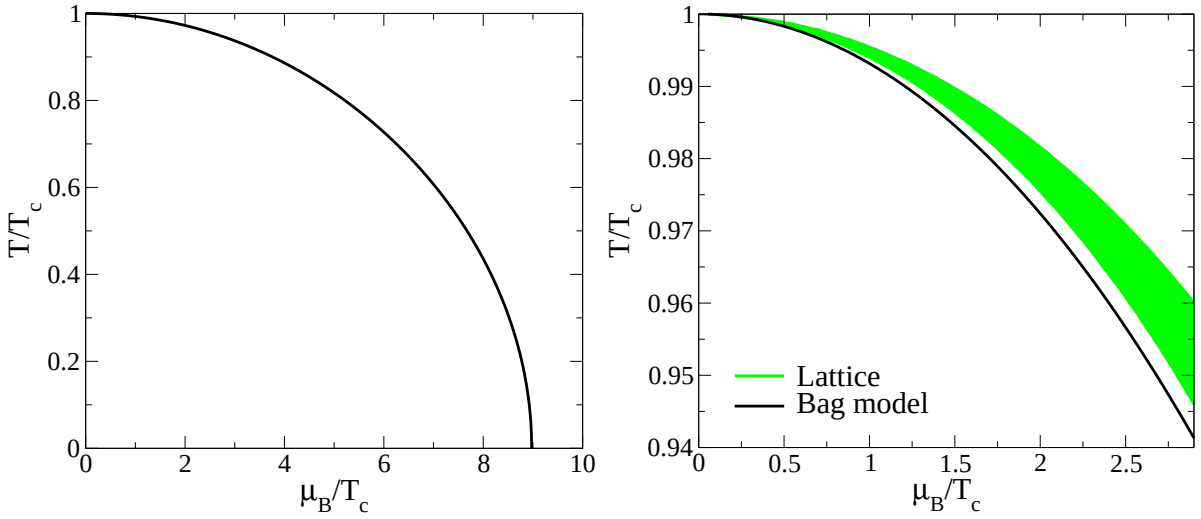

Figure 2.1: The phase boundary line $T_c(\mu)$ calculated with the bag model for $N_f = 2$. The shaded band in the right panel shows the one-sigma error band obtained in lattice calculations in [dFP02].

density obtained from the bag EoS for $T \geq T_c$. While the pressure is in good qualitative agreement with lattice results, the bag model energy density fails to reproduce the lattice data and even overshoots the ideal gas value. This is easy to understand from Eqn. (2.16): The first term is just the expression of an ideal gas, to which a constant energy density B is added. Since in Fig. 2.2 the energy density is plotted over T^4, the effect of the bag constant is biggest at T_c and becomes smaller for larger temperatures.

There are also lattice simulations of thermodynamical quantities at finite temperature and finite quark chemical potential for $N_f = 2 + 1$ [FKS03] and $N_f = 2$ [A$^+$03] flavors of quarks. In particular, these groups have calculated the scaled pressure difference $\Delta p(T, \mu_q) = (p(T, \mu_q) - p(T, 0))/T^4$ and the scaled quark number density $n_q(T, \mu_q)/T^3 = (\partial p/\partial \mu_q)/T^3$. In the bag model the scaled pressure difference is given by

$$\Delta p(T, \mu_q) = T^2 \mu_q^2 + \frac{1}{2\pi^2} \mu_q^4. \tag{2.20}$$

Since the bag constant B does not depend on the chemical potential, it drops out. The scaled quark number density reads

$$n_q = \frac{T}{V} \frac{\partial \ln \mathcal{Z}}{\partial \mu_q} = \frac{\partial p}{\partial \mu_q} = 2 \left(\mu_q T^2 + \frac{\mu_q^3}{\pi^2} \right). \tag{2.21}$$

These are merely the expressions for an ideal gas. It is obvious that these expressions cannot reproduce the non-trivial behavior of the (scaled) pressure difference and the (scaled) quark number density found in lattice simulations close to T_c.

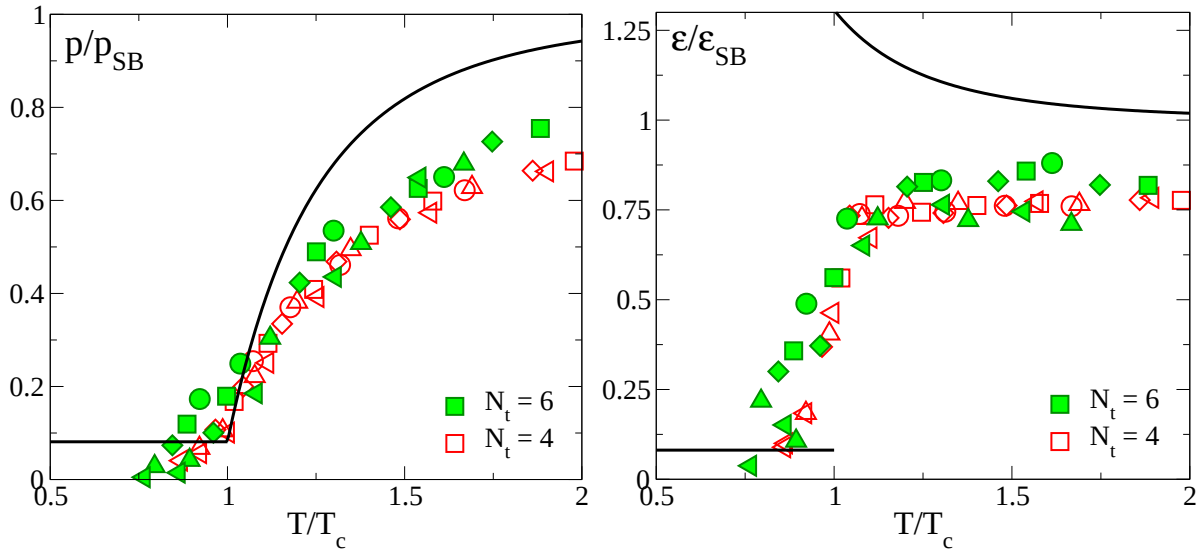

Figure 2.2: The pressure p/p_{SB} (left panel) and the energy density $\epsilon/\epsilon_{\mathrm{SB}}$ (right panel), divided by their respective Stefan-Boltzmann values from our model (solid lines) compared to lattice data from $16^3 \times 4$ and $16^3 \times 6$ lattices (symbols) [AK$^+$01a]. Different values of $m_{\mathrm{PS}}/m_{\mathrm{V}}$ used in the lattice calculations are denoted by different shapes of the symbols (see Fig. 1.2 or [AK$^+$01a]).

2.4 Summary

In this chapter we demonstrated that the basic features of the QCD phase diagram and the EoS can be understood using a simple phenomenological model, the MIT bag model, which is the most widely used EoS in astrophysics to study the properties of deconfined quark matter due to its simple analytic form. This model implements two of the key properties of QCD, asymptotic freedom and confinement. With only a single free parameter, the bag constant B, it can reproduce the phase boundary line that separates the hadronic phase and the QGP and the pressure obtained in lattice QCD simulations at least qualitatively. On the other hand, the model fails to describe the lattice energy density and the non-trivial behavior of lattice thermodynamic quantities at finite quark chemical potential. Thus, while the bag model is quite attractive due to its simplicity, it is clearly not adequate to perform precise numerical calculations of quark matter properties at finite temperature and finite quark chemical potential.

Chapter 3

Quasiparticle Model of the Quark-Gluon Plasma

In the previous chapter we employed the MIT bag model to explain some of the basic features of lattice QCD thermodynamics. In this model, quarks and gluons are confined in hadronic bags at low temperatures, while at high temperatures the individual bags merge to a single large bag in which quarks and gluons can move freely. This simple bag picture reproduces the lattice QCD phase diagram and the EoS qualitatively, but it fails to catch the essential behavior of the energy density, the quark number density and finite density corrections to the pressure. Lattice QCD thermodynamical quantities have been successfully described by a gas of non-interacting quark-gluon quasiparticles [GY95, PKPS96, LH98, PKS00]. Their thermally generated masses are based on perturbative calculations carried out in the Hard Thermal Loop (HTL) scheme [Kap89, Bel96]. However, the non-perturbative confinement physics which becomes important close to T_c was not properly taken into account by these quasiparticle models. Since confinement simply reduces the number of thermally active degrees of freedom in a statistical sense, it can be schematically incorporated in a model of non-interacting, massive quasiparticles by a modification of the particle distribution functions [SW01]. This model successfully describes and predicts a variety of lattice data including the Debye screening mass, which is not correctly estimated by other quasiparticle models. In this chapter we generalize this model to non-zero quark chemical potential in a thermodynamically self-consistent way and test it against a number of available lattice data. The main body of this work has been published in [TSW04].

3.1 Perturbative results

The average absolute three-momentum of quarks and gluons in a weakly interacting heatbath is given by $\langle p \rangle \approx 3\,T$. Assuming that the average momentum transfer between particles is of order p^2, we may substitute $\mu^2 \sim 10\,T^2$ in the running coupling $\alpha_s(\mu)$ of Eqn. (1.8) to get the leading order

$$\alpha_s(T) = \frac{12\pi}{\beta_0 \log(T^2/\Lambda_T^2)} \quad \text{with} \quad \Lambda_T \simeq \Lambda_{\rm QCD}/3 \simeq 100 \text{ MeV}. \tag{3.1}$$

Hence, at high temperatures α_s should become small and one may suspect that a perturbative description of the QCD plasma in terms of elementary partons might become reasonable. However, for temperatures of interest in the experimentally accessible region, the QCD coupling constant is presumably large: at $T = 3\,T_c$, $g_s(T) \simeq 2$ from Eqn. (3.1). The perturbative expansion in powers of g_s shows bad convergence already for much smaller values of the coupling, as apparent from the expression for the free energy $F(T)$ in pure SU(3) gauge theory [ZK95]:

$$\frac{F(T)}{F_{SB}} = 1 - 0.095 g_s^2 + 0.121 g_s^3 + [0.212 - 0.086 \log(1/g_s)] g_s^4 - 0.082 g_s^5. \tag{3.2}$$

Here, $F_{SB} = -16(\pi^2/90)T^4$ is the ideal gas value. With quarks, the resulting series behaves similarly. The series does not converge unless the coupling is tiny. The g_s^3 term is smaller than the g_s^2 term only if $g_s \sim 0.8 \Rightarrow \alpha_s \sim 1/20$. This corresponds to a temperature of 10^5 GeV, which is many orders of magnitude larger then the temperatures expected in heavy-ion collisions (approximately 0.5 GeV at RHIC). Thus bare perturbation theory is clearly inadequate to calculate QCD thermodynamical quantities in the temperature region accessible by today's heavy-ion collision experiments. However, the series in (3.2) is not the power series in α_s known from zero temperature perturbation theory; collective medium effects lead to the appearance of non-analytic terms of the form $\alpha_s^{n/2}$ and $\alpha_s^2 \log \alpha_s$. Consequently, the expansion point of perturbation theory should not be a bare particle, but a dressed quasiparticle taking into account the medium from the onset; of course, the resulting series in g_s has then to be treated self-consistently.

Such a quasiparticle description of QCD thermodynamics has been derived using resummed, approximately self-consistent HTL perturbation theory [BIR99a,BIR99b,BIR01, BI02]. The result can be seen in Fig. 3.1, where the pressure of an interacting gas of gluons is shown. The resulting EoS is in good qualitative agreement with lattice results, but fails to reproduce them quantitatively close to T_c. However, one should keep in mind that in the temperature region covered in Fig. 3.1 the coupling constant g_s is not small and the perturbative approach is questionable from the beginning. Apart from a trivial T^4 dependence, the temperature dependence of the pressure in this approach is entirely governed by the running coupling constant $\alpha_s(T)$ because there is no other scale in the problem than Λ_{QCD}. The resummation procedure only affects the normalization.

Various interpretations of the lattice data have been attempted in terms of physical quantities, most prominently as the EoS of a gas of massive quark and gluon quasiparticles. Their thermally generated masses are based on perturbative calculations carried out in the HTL scheme [GY95, PKPS96, LH98, PKS00]. This approach has been extended to non-vanishing quark chemical potential and good agreement with finite μ lattice calculations for $N_f = 2 + 1$ flavors has been found [ST03]. More recently, the QGP has also been described in terms of a condensate of Z_3 Wilson lines [Pis00] and by more refined quasiparticle models based on the HTL-resummed entropy and (next-to-leading order) extensions thereof [RR03]. These models have found support from resummed perturbation theory [BI02] for temperatures $T \gtrsim 3\,T_c$. However, they have difficulties explaining

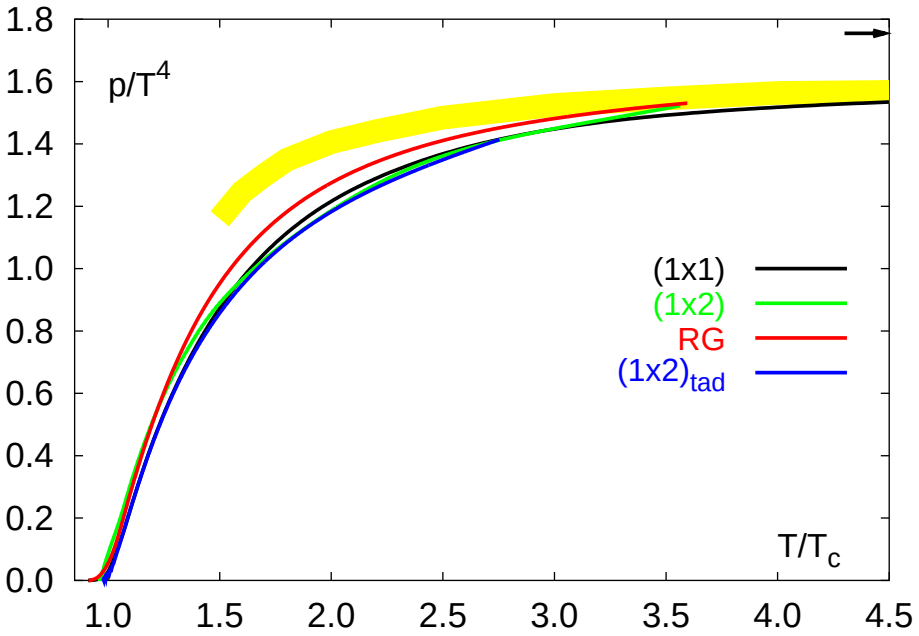

Figure 3.1: Approximately self-consistent HTL perturbation theory result for the pressure of an interacting gas of gluons [BIR99a, BIR99b, BIR01, BI02] (shaded band) vs. lattice results, calculated with different actions [B^+95a,B^+96,O^+99, BKLP99].

the dropping of the thermal gluon screening mass in the vicinity of the phase transition. An improved quasiparticle model [SW01] shows the correct temperature dependence of the Debye mass and reproduces lattice thermodynamical quantities such as the pressure, the energy density and the entropy density very well. The main new ingredient of this model is a phenomenological parametrization of (de)confinement. We will introduce this model in the following and show how it can be extended to finite quark chemical potential.

3.2 Thermodynamic self-consistency in a medium

In this section we show how the pressure p, the energy density ϵ, the particle number density n and the entropy density s for a general effective Hamiltonian $\mathcal{H}_{\text{eff}}(\alpha_1, \alpha_2, \ldots, \alpha_n)$ can be constructed. Here $\alpha_1, \alpha_2, \ldots, \alpha_n$ are phenomenological parameters, which are assumed to be functions of the temperature T and the chemical potential μ. For example, α_i may stand for a thermal quasiparticle mass. We follow the approach of [GY95] here. These results will then be used in subsequent parts of this chapter to construct a quasiparticle description of the QCD EoS .

To retain thermodynamical consistency, the pressure, the energy density, the particle

number density and the entropy density must satisfy the Gibbs-Duhem relation

$$\epsilon + p = Ts + \mu n = T\frac{\partial p}{\partial T} + \mu\frac{\partial p}{\partial \mu}. \tag{3.3}$$

The pressure and the energy density of a general thermodynamical system described by an effective Hamiltonian $\mathcal{H}_{\text{eff}}$ are given by

$$p(T,\mu) = \frac{T}{V}\ln \text{Tr} e^{-\beta(\mathcal{H}_{\text{eff}}-\mu Q)}, \tag{3.4}$$

$$\epsilon(T,\mu) = \frac{1}{V}\frac{\text{Tr}\,\mathcal{H}_{\text{eff}} e^{-\beta(\mathcal{H}_{\text{eff}}-\mu Q)}}{\text{Tr} e^{-\beta(\mathcal{H}_{\text{eff}}-\mu Q)}}, \tag{3.5}$$

where Q is a conserved charge or particle number and μ the associated chemical potential. To satisfy (3.3), all derivatives of the pressure with respect to the phenomenological parameters must vanish:

$$\left.\frac{\partial p}{\partial \alpha_i}\right|_{T,\mu,\{\alpha_{j\neq i}\}} = 0. \tag{3.6}$$

We will now apply this to an ideal gas of bosonic quasiparticle excitations with a medium dependent dispersion relation. The effective Hamiltonian for this system reads

$$\mathcal{H}_{id} = \sum_{\mathbf{k},s} \omega^*(k) a^\dagger_{\boldsymbol{k},i} a_{\boldsymbol{k},i} + E_0^*, \tag{3.7}$$

where the index $\boldsymbol{k}$ labels the momentum eigenstates and s the internal degrees of freedom, $\omega^*(k) \equiv \omega(k,\alpha_1,\ldots,\alpha_n)$ is the medium dependent dispersion relation, $a^\dagger_{\boldsymbol{k},i}$ and $a_{\boldsymbol{k},i}$ are Bose creation and annihilation operators, respectively, and $E_0^* = E_0(\alpha_1,\ldots,\alpha_n)$ is the system energy in the absence of quasiparticle excitations. If the dispersion relation is independent of the parameters $\alpha_1,\ldots,\alpha_n$, the zero-point energy E_0^* is constant and can be subtracted from the Hamiltonian, since only energy differences can be measured. For a medium dependent dispersion relation, however, the zero point energy depends on T and μ and cannot be neglected. Next we will calculate the pressure and the energy density for this system. For large V we may replace the sum over $\boldsymbol{k}$ in the effective Hamiltonian (3.7) by an integration over momentum phase space:

$$\sum_{\mathbf{k},s} \cdots \longrightarrow \nu\frac{V}{(2\pi)^3}\int \mathrm{d}^3k \cdots . \tag{3.8}$$

The degeneracy factor ν counts degrees of freedom like spin, isospin or color. Then the following expressions for the pressure and the energy density are obtained:

$$p(T,\mu,\alpha_1,\ldots,\alpha_n) = -T\frac{\nu}{2\pi^2}\int_0^\infty \mathrm{d}k\, k^2 \left[\ln\left(1-e^{\beta(\omega^*-\mu)}\right) + \ln\left(1-e^{\beta(\omega^*+\mu)}\right)\right] - B, \tag{3.9}$$

$$\epsilon(T,\mu,\alpha_1,\ldots,\alpha_n) = \frac{\nu}{2\pi^2}\int_0^\infty \mathrm{d}k\, k^2 \left[\frac{\omega^*}{e^{\beta(\omega^*-\mu)}-1} + \frac{\omega^*}{e^{\beta(\omega^*+\mu)}-1}\right] + B. \tag{3.10}$$

The first terms in (3.9) and (3.10) are the standard ideal gas expressions, while the second ones are additional medium contributions with

$$B = B(\alpha_1, \ldots, \alpha_n) \equiv \lim_{V\to\infty} \frac{E_0^*}{V}. \tag{3.11}$$

B is uniquely defined by (3.6). The statistical expressions for the particle number density $n(T,\mu)$ and the entropy density $s(T,\mu)$ keep their ideal gas form:

$$n(T,\mu,\alpha_1,\ldots,\alpha_n) = \frac{\nu}{2\pi^2}\int_0^\infty \mathrm{d}k\, k^2 \left[\frac{1}{e^{\beta(\omega^*-\mu)}-1} - \frac{1}{e^{\beta(\omega^*+\mu)}-1}\right], \tag{3.12}$$

$$s(T,\mu,\alpha_1,\ldots,\alpha_n) = \frac{\epsilon+p-\mu n}{T} + \frac{\epsilon+p+\mu n}{T}. \tag{3.13}$$

3.3 Quasiparticle model with confinement

In this section the quasiparticle model with confinement is introduced. For further details the reader is referred to Ref. [SW01].

At very high temperatures, spectral functions for gluons or quarks of the form $\delta(E^2 - k^2 - m^2(T))$ with $m(T) \sim g_s T$ are found in HTL perturbative calculations. Here, E is the particle energy, k the absolute value of its momentum, $m(T)$ its thermally generated mass and g_s the QCD coupling constant. As long as the spectral function at lower temperatures resembles qualitatively this asymptotic form, a quasiparticle description is expected to be applicable. QCD dynamics is then incorporated in the thermal masses of the quark and gluon quasiparticles. These thermal masses are obtained from the self-energies of the corresponding particles, evaluated at thermal momenta $k \sim T$:

$$m_q^2 = m_{0q}^2 + \frac{N_c^2-1}{8N_c}\left(T^2 + \frac{\mu^2}{\pi^2}\right) G^2(T,\mu), \tag{3.14}$$

$$m_g^2 = m_{0g}^2 + \frac{1}{6}\left[\left(N_c + \frac{N_f}{2}\right)T^2 + \frac{3}{2\pi^2}\sum_q \mu_q^2\right] G^2(T,\mu). \tag{3.15}$$

N_f is the number of flavors, N_c the number of colors. The effective coupling strength G is specified as

$$G(T,\mu=0) = \frac{g_0}{\sqrt{11N_c - 2N_f}}\left([1+\delta] - \frac{T_c}{T}\right)^\beta. \tag{3.16}$$

Setting $g_0 = 9.4$, $\beta = 0.1$, the effective masses as given in equations (3.14) and (3.15), approach the HTL result at high temperatures. (A small shift $\delta = 10^{-6}$ helps fine-tuning at $T \simeq T_c$). Because of the existence of a heat bath background, new partonic excitations, plasmons (longitudinal gluons) and plasminos (quark-hole excitations) are also present in the plasma. However, their spectral strengths are exponentially suppressed for hard momenta and large temperatures and consequently these states are essentially unpopulated [Bel96]. The functional dependence of $m_g(T)$ on T is based on the conjecture

that the phase transition is second order or weakly first order which suggests an almost power-like behavior $m \sim (T - T_c)^\beta$ with some critical exponent $\beta > 0$. It is assumed that the pseudocritical form of the effective coupling constant given in equation (3.16) also provides the correct approximate expression for the effective quark mass. This is supported by a non-perturbative dispersion relation analysis for a thermal quark interacting with the gluon condensate [ST99].

Close to T_c the picture of a non-interacting gas is not appropriate because the driving force of the transition, the confinement process, is not taken into account. Below T_c, the relevant degrees of freedom are pions and other hadrons. Approaching T_c from below, deconfinement sets in and the quarks and gluons are liberated, followed by a sudden increase in entropy and energy density. Conversely, when approaching the phase transition from above, the decrease in the thermodynamic quantities is not primarily caused by increasing masses of the quasiparticles, but by the reduction of the number of thermally active degrees of freedom due to the onset of confinement. For example, gluons begin to form heavy clusters (glueballs), so that the gluon density gets reduced as T_c is approached from above. This feature can be incorporated in the quasiparticle picture by modifying the number of effective degrees of freedom by a temperature dependent confinement factor $C(T)$:

$$C(T, \mu = 0) = C_0 \left([1 + \delta_c] - \frac{T_c}{T} \right)^{\beta_c}. \tag{3.17}$$

The confinement factor is taken to be universal. The parameters C_0, δ_c and β_c are fixed by reproducing the entropy density that results from lattice QCD thermodynamics. Since the results of lattice calculations with dynamical quarks are still dependent on the details of the simulations, C_0, δ_c and β_c should be finetuned for different lattice calculations.

For homogeneous systems of large volume V, the Helmholtz free energy F is related to the pressure p by $F(T, V) = -p(T)/V$. In the present framework of a gas of quasiparticles, its explicit expression reads

$$p(T) = \frac{\nu_g}{6\pi^2} \int_0^\infty \mathrm{d}k\, C(T) f_B(E_k^g) \frac{k^4}{E_k^g} + \frac{2N_c}{3\pi^2} \sum_{i=1}^{N_f} \int_0^\infty \mathrm{d}k\, C(T) f_D(E_k^i) \frac{k^4}{E_k^i} - B(T). \tag{3.18}$$

ν_g is the gluon degeneracy factor, $E_k^g = \sqrt{k^2 + m_g^2(T)}$ is the gluon energy, $E_k^q = \sqrt{k^2 + m_q^2(T)}$ the quark energy, $f_B(E_k^g) = (\exp((E_k^g)/T) - 1)^{-1}$ the Bose-Einstein distribution function of gluons and $f_D(E_k^q) = (\exp((E_k^q)/T) + 1)^{-1}$ the Fermi-Dirac distribution function of quarks. The energy density ϵ and the entropy density s take the form

$$\epsilon(T) = \frac{\nu_g}{2\pi^2} \int_0^\infty \mathrm{d}k\, k^2 C(T) f_B(E_k^g) E_k^g + \frac{2N_c}{\pi^2} \sum_{i=1}^{N_f} \int_0^\infty \mathrm{d}k\, k^2 C(T) f_D(E_k^i) E_k^i + B(T). \tag{3.19}$$

and

$$s(T) = \frac{\nu_g}{2\pi^2 T}\int_0^\infty \mathrm{d}k\, k^2 C(T) f_B(E_k^g)\frac{\frac{4}{3}k^2 + m_g^2(T)}{E_k^g} + \frac{2N_c}{\pi^2 T}\sum_{i=1}^{N_f}\int_0^\infty \mathrm{d}k\, k^2 C(T) f_D(E_k^i)\frac{\frac{4}{3}k^2 + m_q^2(T)}{E_k^i}. \tag{3.20}$$

The function $B(T)$ is introduced to act as a background field. It is necessary in order to maintain thermodynamic consistency: p, ϵ and $s = \partial p/\partial T$ have to satisfy the Gibbs-Duhem relation $\epsilon + p = Ts = T\partial p/\partial T$. $B(T)$ basically compensates the additional T-derivatives from the temperature-dependent masses in p and thus is not an independent quantity. Since $B(T)$ adds to the energy density of the quasiparticles, it can be interpreted as the thermal vacuum energy density. The entropy density, as a measure of phase space, is unaffected by $B(T)$.

3.4 Finite chemical potential

The quasiparticle model reviewed in the previous section accurately reproduces lattice thermodynamical quantities such as the pressure, the energy density and the entropy density in the temperature range $T_c < T \lesssim 4\,T_c$ at vanishing chemical potential [SW01]. However, many physical questions, e.g. the structure of quark cores in massive neutron stars, the baryon contrast prior to cosmic confinement or the evolution of the baryon number in the mid-rapidity region of central heavy-ion collisions, require a detailed understanding of the EoS at non-vanishing quark chemical potential. In this section, a thermodynamically self-consistent extension of the quasiparticle model to finite quark chemical potentials is presented. Results for various observables are then computed and compared to finite μ lattice results in the next section.

At vanishing quark chemical potential, it is conjectured from asymptotic freedom that QCD undergoes a phase transition from the hadronic phase to the QGP phase. At extremely high density, cold quark matter is necessarily in the Color-Flavor-Locked (CFL) phase in which quarks of all three colors and all three flavors form cooper pairs. It is expected that this phase is separated from the hadronic phase by the color superconducting 2SC phase. For a review of the QCD phase diagram, the reader is referred to [Raj99, Han01]. Our extension of the quasiparticle model provides a straightforward way to map the EoS at finite temperature and vanishing quark chemical potential into the $T-\mu$ plane without further assumptions. However, since this continuous mapping relies on quark and gluon quasiparticles, it cannot provide information about other possible phases with a different (quasiparticle) structure. It is therefore applicable in a limited range of not too large chemical potentials.

The pressure of an ideal gas of quark and gluon quasiparticles with effective masses

depending on temperature and quark chemical potential, is given by

$$\begin{aligned} p(T,\mu) =& \frac{\nu_g}{6\pi^2}\int_0^\infty \mathrm{d}k\, C(T,\mu) f_B(E_k^g)\frac{k^4}{E_k^g} \\ &+\frac{N_c}{3\pi^2}\sum_{q=1}^{N_f}\int_0^\infty \mathrm{d}k\, C(T,\mu)[f_D^+(E_k^q)+f_D^-(E_k^q)]\frac{k^4}{E_k^q} - B(T,\mu), \end{aligned} \tag{3.21}$$

with $f_D^\pm(E_k^q) = (\exp((E_k^q \mp \mu)/T)+1)^{-1}$. The effective coupling strength $G(T,\mu)$, the confinement factor $C(T,\mu)$ and the mean field contribution $B(T,\mu)$ now also depend on the quark chemical potential μ. $B(T,\mu)$ is calculated in Appendix A. The quark number density (which is related to the baryon number density n_B by $n_q = n_B/3$) retains the ideal gas form

$$n_q(T,\mu) = \frac{N_c}{\pi^2}\sum_{q=1}^{N_f}\int_0^\infty \mathrm{d}k\, C(T,\mu)[f_D^+(E_k^q) - f_D^-(E_k^q)]k^2, \tag{3.22}$$

but with the confinement factor $C(T,\mu)$ included.

In the previous section expressions for the coupling $G(T,\mu=0)$ and the confinement factor $C(T,\mu=0)$ are given. These expressions can be generalized to finite chemical potential in a thermodynamically self-consistent way using Maxwell relations. Imposing the Maxwell relation between the derivatives of the quark number density and the entropy,

$$\begin{aligned} \left.\frac{\partial s}{\partial \mu}\right|_T = \left.\frac{\partial n}{\partial T}\right|_\mu \quad &\Longrightarrow \quad \sum_i \left(\frac{\partial n}{\partial m_i^2}\frac{\partial m_i^2}{\partial T} - \frac{\partial s}{\partial m_i^2}\frac{\partial m_i^2}{\partial \mu}\right) = 0 \\ &\text{and} \quad \left(\frac{\partial n}{\partial C}\frac{\partial C}{\partial T} - \frac{\partial s}{\partial C}\frac{\partial C}{\partial \mu}\right) = 0, \end{aligned} \tag{3.23}$$

yields a set of first order quasilinear partial differential equations for the effective coupling constant $G^2(T,\mu)$ and the confinement factor $C(T,\mu)$:

$$a_T(T,\mu;G^2)\frac{\partial G^2}{\partial T} + a_\mu(T,\mu;G^2)\frac{\partial G^2}{\partial \mu} = b(T,\mu;G^2), \tag{3.24}$$

$$c_T(T,\mu;G^2)\frac{\partial C}{\partial T} + c_\mu(T,\mu;G^2)\frac{\partial C}{\partial \mu} = 0. \tag{3.25}$$

The coefficients a_T, a_μ, b, c_T, c_μ depend on T, μ, G^2 but not on C. It can be solved by the method of characteristics (see Appendix B). The flow of the effective coupling and the confinement factor is elliptic. In particular, one finds

$$a_T(T,\mu=0)=0, \quad a_\mu(T=0,\mu)=0, \quad c_T(T,\mu=0)=0, \quad c_\mu(T=0,\mu)=0. \tag{3.26}$$

Therefore, the characteristics are perpendicular to both the T and the μ axis. This guarantees that specifying the coupling constant and the confinement factor on the T

axis sets up a valid initial condition problem. Plots of the characteristic curves and the confinement factor are shown in Fig. 3.2 and 3.3.

3.5 Comparison with lattice results

Simulations of QCD at finite chemical potential are extremely difficult because the fermion determinant becomes complex. This prohibits Monte Carlo importance sampling, which interprets the measure as a probability factor and thus requires it to be positive. While this problem remains unsolved, there are some approaches which circumvent the sign problem and allow lattice simulations for small chemical potentials $\mu \lesssim T_c$. A brief review of some methods of these methods can be found in Chapter 1. For more details, the reader is referred to [LP03, MNNT03].

3.5.1 The phase boundary line

In the case of vanishing quark chemical potential, universal arguments and lattice simulations suggest a phase transition from the hadronic phase to the QGP phase at a critical temperature T_c. For QCD with three light flavors $m_u \sim m_d \sim m_s \sim 5$ MeV this transition is expected to be first order. For two light flavors $m_u \sim m_d \sim 5$ MeV and an infinitely large m_s there is no phase transition, only a smooth crossover [FK02a]. This suggests there is a critical strange mass m_s^c at which one finds a second order phase transition. Lattice calculations indicate that m_s^c is about half of the physical mass m_s. At finite quark chemical potential μ and vanishing T a first order phase transition is predicted. For the physical m_s this implies that there is a first order phase transition for small T and large μ which ends at a critical point (T^*, μ^*). At this point the phase transition is of second order. For large T and small μ the two phases are separated by a crossover. We refer to the line $T_c(\mu)$ that separates the hadronic phase from the QGP phase as the "phase boundary line". In the literature [DL03, dFP02, dFP03] this line is also frequently called the "pseudocritical line". $T_c(\mu)$ has been calculated on the lattice for $N_f = 4$ [FK02b, DL03], $N_f = 2$ [dFP02] and $N_f = 3$ [dFP03] flavors of quarks up to quark chemical potentials μ of order T_c. In the following we focus on the three-flavor results where the critical line has been calculated with an accuracy up to terms of order $(\mu/T)^6$. There, a Wilson gauge action and three degenerate flavors of staggered quarks have been employed, with bare masses in the range $0.025 < am < 0.04$, where a denotes the lattice spacing. The finite volume scaling behavior was monitored by using three lattice sizes, $8^3 \times 4$, $10^3 \times 4$ and $12^3 \times 4$.

In our quasiparticle model, the sudden decrease of the pressure, the energy density, the quark number density and the entropy density caused by gluons and quarks getting trapped in glueballs and hadrons when T_c is approached from above, is parametrized by the confinement factor $C(T, \mu)$. Consequently, it is natural to relate the critical line to

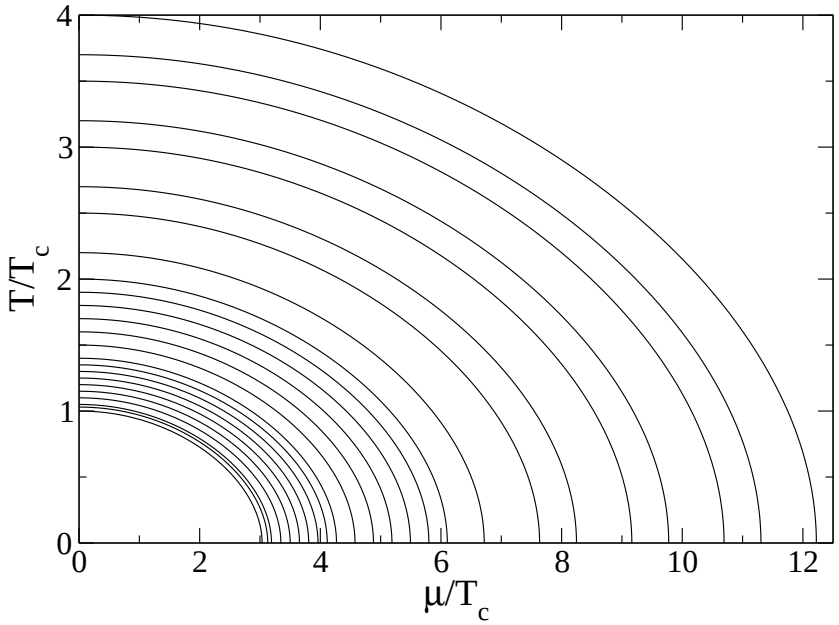

Figure 3.2: Characteristic curves of constant confinement factor $C(T, \mu) = const$, obtained when solving Eqn.(3.25).

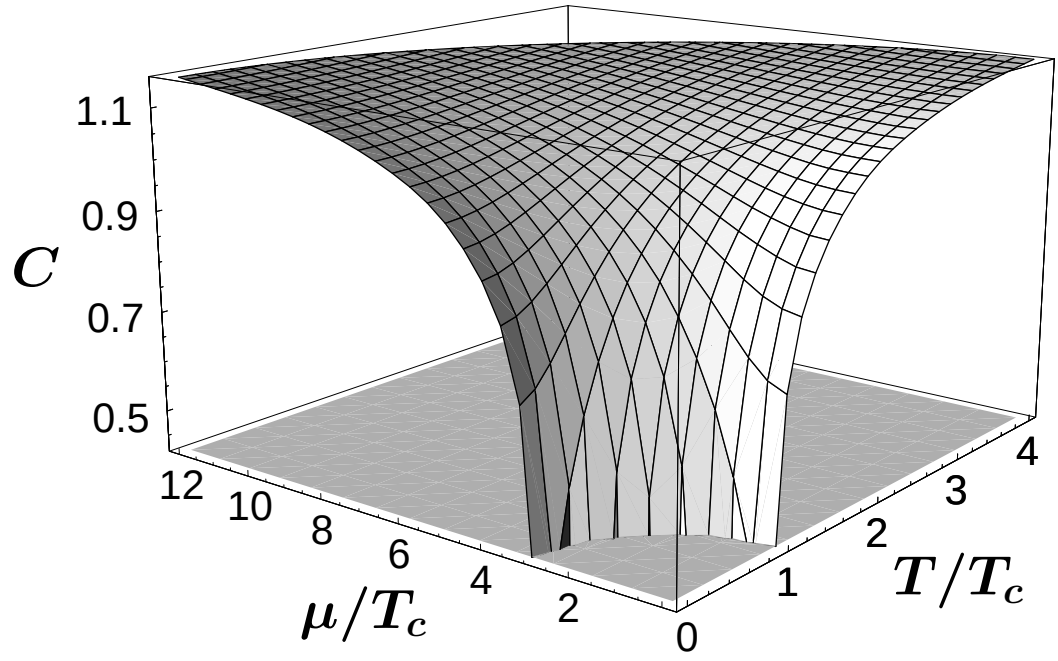

Figure 3.3: The confinement factor $C(T, \mu)$ as a function of the temperature T and the quark chemical potential μ.

the characteristic curve of the confinement factor through $T_c(\mu)$, as long as μ is small and the nature of the quasiparticles does not change qualitatively.

In order to calculate the confinement factor at finite chemical potential, we need to specify a valid initial condition, e.g. $C(T, \mu = 0)$. The functional form of $C(T, \mu = 0)$ is set by Eqn.(3.17). We have employed the following set of parameters, as found in ref. [SW01]:

	C_0	δ_c	β_c
3 flavors	1.03	0.02	0.2

We have checked that the form of the phase boundary line in the quasiparticle model depends only weakly on the exact choice of parameters and a small difference only shows up for values much larger than the range of μ covered by the lattice simulations. The lattice phase boundary line and our result are shown in Fig. 3.4. The quasiparticle result

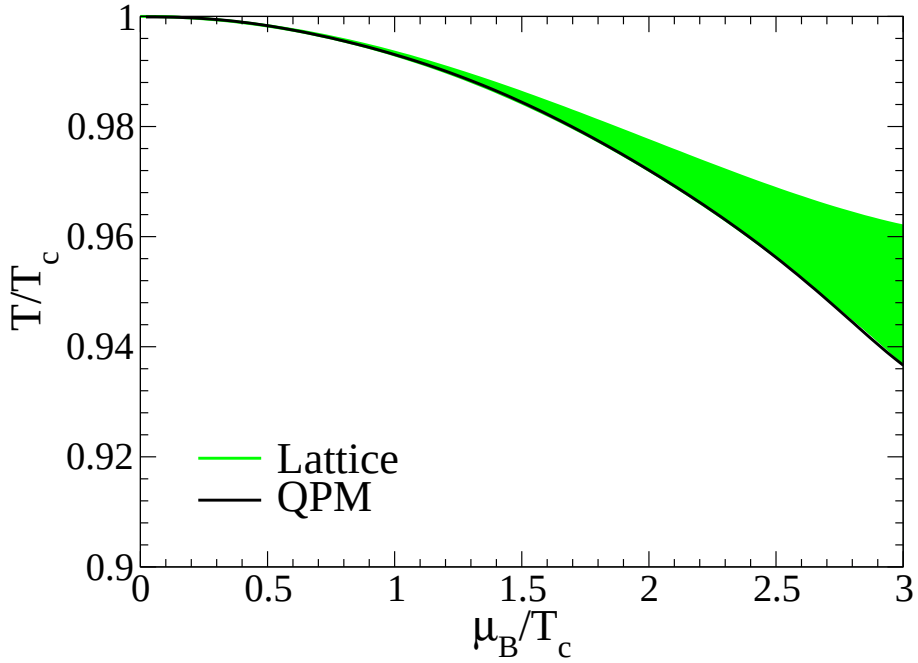

Figure 3.4: The phase boundary line $T_c(\mu)$ calculated with the quasiparticle model for $N_f = 3$. The shaded band shows the one-sigma error band obtained in lattice calculations in [dFP03].

is within the lattice estimate for $\mu_B \lesssim 2.5T_c$ and deviates only slightly from the lattice result for larger chemical potentials.

3.5.2 Thermodynamical quantities

There have been lattice calculations of thermodynamical quantities at finite chemical potential for $N_f = 2 + 1$ [FKS03] and $N_f = 2$ [A$^+$03] flavors of quarks. In the following

we focus on results from [A$^+$03] where a p4-improved staggered action on a $16^3 \times 4$ lattice was used. There, the N_t dependence is known to be small, in contrast to standard staggered fermion actions which show substantially larger cut-off effects. Estimates of the pressure, the quark number density and associated susceptibilities as functions of the quark chemical potential were made via a Taylor series expansion of the thermodynamic grand canonical potential Ω up to fourth order.

To calculate thermodynamical quantities within the quasiparticle model, we need to fix the parameters of the effective coupling constant and the confinement factor. Our calculations have shown that the results are not sensitive to the detailed choice of parameters for the effective coupling G. We have therefore used the parameters from Ref. [SW01] in our calculations. In principle, the parameters of the confinement factor can be fixed by comparing our calculations to lattice results at vanishing chemical potential. However, in ref. [A$^+$03] no $\mu = 0$ lattice data is given. Since lattice calculations including quarks give slightly different results depending on which action has been used, fitting the parameters in $C(T, \mu = 0)$ by comparing quasiparticle results to lattice data from a different simulation is not feasible and would lead to large differences. Consequently, we directly used the finite μ lattice results for fitting. Good agreement with the lattice thermodynamical observables was found for the following sets of parameters:

	C_0	δ_c	β_c
Set A	1.05	-0.016	0.15
Set B	1.12	0.02	0.2

While set A reproduces the lattice thermodynamical results slightly better, set B is in better agreement with the parameters found in [SW01] for $\mu = 0$ lattice simulations.

The temperature dependence of the scaled pressure difference $\Delta p(T, \mu) = (p(T, \mu) - p(T, \mu = 0))/T^4$ is shown in Fig. 3.5 and that of the scaled quark number density $n_q(T, \mu)/T^3$ in Fig. 3.6. Whereas the computation of the quark number density from equation (3.22) is straightforward, a numerical evaluation of (3.21) is difficult because of the derivatives of the effective masses and the confinement factor in $B(T, \mu)$ (see expressions in Appendix A). It turns out that it is simpler to calculate the pressure difference using the following relation:

$$\Delta p(T, \mu) = \frac{1}{T^4} \int_0^\mu \mathrm{d}\mu' n_q(T, \mu'). \tag{3.27}$$

The lattice pressure difference is well reproduced even for the largest values of the chemical potential. The quark number density is in very good agreement with the lattice data for $\mu/T_c = 0.2$ and 0.4. For larger values of μ our calculations underestimate the magnitude of the lattice results close to T_c, but show the same qualitative features.

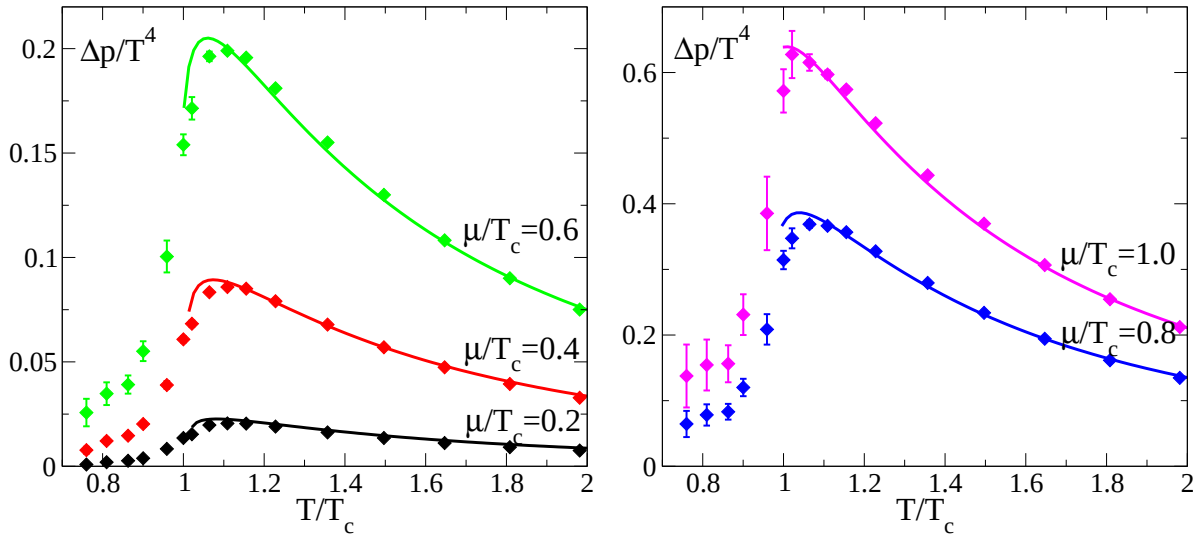

Figure 3.5: The scaled pressure difference $\Delta p(T,\mu)/T^4$ as a function of temperature compared to lattice results from [A+03] (symbols).

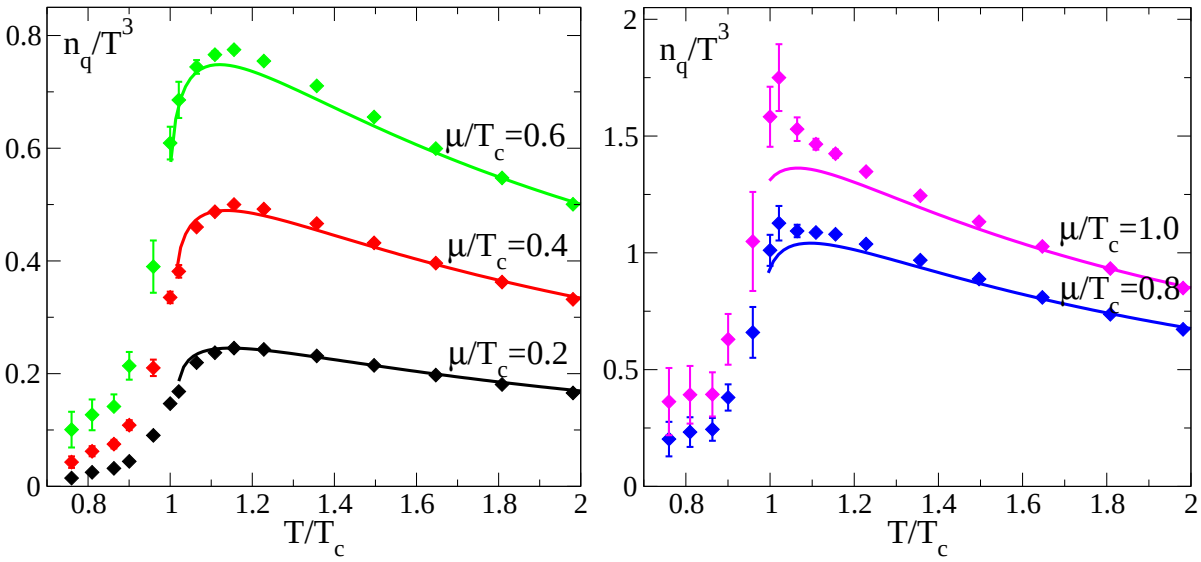

Figure 3.6: The scaled quark number density $n_q(T,\mu)/T^3$ as a function of temperature compared to lattice results from [A+03] (symbols).

3.6 Momentum dependent confinement

The quasiparticle description of the QCD EoS which we have developed in the previous part of this chapter reproduces lattice QCD results at finite temperature and finite quark chemical potential remarkably well. The main new ingredient of this model is a phenomenological parametrization of (de)confinement by a confinement factor $C(T)$:

$$C(T, \mu = 0) = C_0 \left([1 + \delta_c] - \frac{T_c}{T} \right)^{\beta_c}. \tag{3.28}$$

The confinement factor reduces the number of thermally active degrees of freedom close to T_c. Below T_c the relevant degrees of freedom are pions and other hadrons. When T_c is approached from below, deconfinement sets in and the quarks and gluons get liberated, followed by a sudden increase in pressure, entropy density and energy density, which is accounted for by the confinement factor. We have assumed that the confinement factor is universal and that it only depends on temperature and not on the momentum spectrum of the constituents. In the remainder of this chapter we will briefly discuss a model with momentum dependent confinement [EFR+89]. The model has been tested with pure $SU(2)$ gauge theory and good agreement with thermodynamical quantities like the pressure and the interaction measure has been found. Here we extend this model to pure $SU(3)$ gauge theory and full QCD and compare our results with lattice QCD simulations.

Lattice QCD simulations of pure $SU(3)$ gauge theory show that the scaled energy density ϵ/T^4 changes rapidly in a small interval around the critical temperature $T = T_c$. It grows from the value expected for an ideal gas of glueballs to the much larger value expected for an ideal gas of gluons:

$$\frac{\epsilon_{\mathrm{SB}}}{T^4} = \frac{8\pi^2}{45}. \tag{3.29}$$

However, the weak temperature dependence of ϵ for $T \gtrsim 1.5 T_c$ and its rapid convergence to values near ϵ_{SB} do not imply the absence of interactions in the deconfined phase. The scaled interaction measure

$$\frac{\Delta}{T^4} \equiv \frac{\epsilon - 3p}{T^4}, \tag{3.30}$$

vanishes for an ideal gas. For lattice $SU(3)$ gauge theory it differs from zero over a considerable range of temperatures above T_c. Δ/T^4 grows rapidly for $T > T_c$ and has a maximum at $T \approx 1.2\, T_c$ and decreases afterwards. This behavior can be explained if the momentum spectrum of the constituents contains massive glueball states at low momenta and massless gluons at high momenta. The absence of low momentum gluons, together with the temperature-dependence of the spectrum, results in a large and rapidly varying Δ/T^4 which can reproduce lattice QCD thermodynamical quantities.

To illustrate this, we will first consider an ideal Boltzmann gas of massless constituents, with a constant low momentum cutoff K. Its partition function is given by

$$\ln \mathcal{Z} = \frac{\nu V}{2\pi^2} \int_K^\infty \mathrm{d}k\, k^2 e^{-k/T}, \tag{3.31}$$

where ν is the degeneracy factor of the constituents and V is the volume of the system. The integral in Eqn. (3.31) can be calculated analytically. The pressure and the energy density are then given by

$$p = \frac{\nu}{2\pi^2}\left(T^2K^2 + 2T^3K + 2T^4\right)e^{-\frac{K}{T}}, \tag{3.32}$$

$$\epsilon = \frac{\nu}{2\pi^2}\left(TK^3 + 3T^2K^2 + 6T^3K + 6T^4\right)e^{-\frac{K}{T}}, \tag{3.33}$$

and the scaled interaction measure reads

$$\frac{\Delta}{T^4} = \frac{\nu K^3}{2\pi^2 T^3}e^{-\frac{K}{T}}. \tag{3.34}$$

Its maximum is at $T = K/3$ and it vanishes as T^{-3} for large T and goes to zero exponentially for $T \to 0$. While (3.34) reproduces the interaction measure found in $SU(3)$ lattice QCD simulations qualitatively, it yields a value of Δ/T^4 which is too small at the peak. Furthermore, it contains no information about the critical temperature T_c and hence cannot reproduce the rapid variation in the critical region. To incorporate the T_c dependence, we make the momentum cutoff K temperature dependent. Since we expect no gluons below T_c, a natural form of the cutoff is

$$\frac{K}{T_c} = r\left(\frac{T - T_c}{T_c}\right)^{-s}, \tag{3.35}$$

where r and s are free parameters. With this cutoff, the partition function (3.31) vanishes at T_c, while at high T the full gluon spectrum is recovered.

We will now make use of the ideas we have discussed in this section to account for the observed behavior of p/T^4, ϵ/T^4 and Δ/T^4 in $SU(3)$ lattice QCD simulations. To obtain a full model, we make the ansatz

$$\ln \mathcal{Z} = -\frac{\nu_{\mathrm{GB}} V}{2\pi^2}\int_0^K \mathrm{d}k\, k^2 \ln\left(1 - e^{-\beta\sqrt{k^2+M^2}}\right) - \frac{\nu_g V}{2\pi^2}\int_K^\infty \mathrm{d}k\, k^2 \ln\left(1 - e^{-\beta k}\right). \tag{3.36}$$

The first term is the contribution from heavy glueball states for momenta $k < K$ and the second term is the contribution from massless gluons for momenta $k > K$, where K is given by Eqn. (3.35). ν_{GB} is the degeneracy factor for the glueball states and M its mass. The lightest glueball state found in lattice QCD simulations [MP99] has a mass of about $M \approx 1$ GeV and its degeneracy factor $\nu_{\mathrm{GB}} = 1$ because it is a scalar particle and obviously a color singlet. Other glueball states are even heavier and are neglected here. The degeneracy factor for an ideal gas of gluons is $\nu_g = 16$. Thermodynamical quantities like the pressure, the entropy density, the energy density, and the interaction measure can now be easily calculated from Eqn. (3.36). The results for $r = 3$ and $s = 0.25$ are presented in Fig. 3.7. This simple model reproduces the interaction measure quite well in the whole temperature range where lattice data is available. It is in good agreement with the pressure, the entropy density and the energy density from lattice simulations for

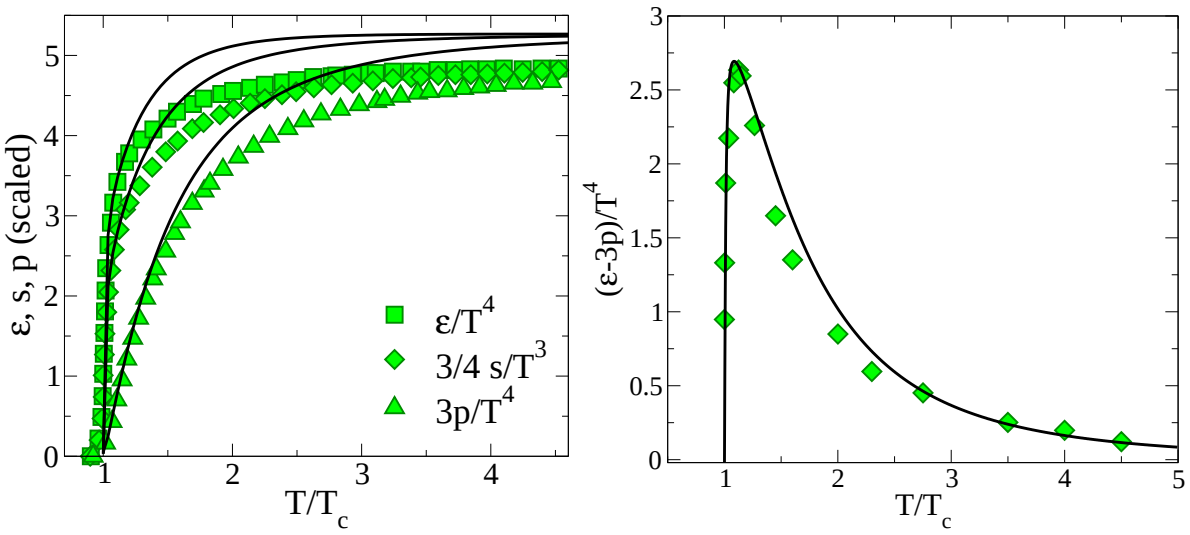

Figure 3.7: Left panel: Scaled pressure, entropy density and energy density as functions of temperature obtained from Eqn. (3.36) (solid lines), compared to continuum extrapolated $SU(3)$ lattice data (symbols) [B$^+$96]. Right panel: The interaction measure $\Delta = (\epsilon - 3p)/T^4$ obtained from Eqn. (3.36) (solid line) versus results (symbols) from a $32^3 \times 8$ lattice. The data symbols already represent the continuum interpolated values [B$^+$96].

temperatures $T_c < T \lesssim 1.5\,T_c$, but it exceeds the lattice results for $T \gtrsim 1.5\,T_c$. This can be corrected by introducing thermal quasiparticle masses which will bring the pressure, the entropy density and the energy density down at larger temperatures.

The model can also be extended to full QCD. The partition function is then given by

$$\begin{aligned}\ln \mathcal{Z} = &- \frac{\nu_{\rm GB} V}{2\pi^2} \int_0^K \mathrm{d}k\, k^2 \ln\left(1 - e^{-\beta\sqrt{k^2+M^2}}\right) - \frac{\nu_g V}{2\pi^2} \int_K^\infty \mathrm{d}k\, k^2 \ln\left(1 - e^{-\beta k}\right) \\ &- \frac{\nu_\pi V}{2\pi^2} \int_0^K \mathrm{d}k\, k^2 \ln\left(1 - e^{-\beta\sqrt{k^2+m_\pi^2}}\right) - \frac{\nu_q V}{2\pi^2} \int_K^\infty \mathrm{d}k\, k^2 \ln\left(1 + e^{-\beta k}\right). \end{aligned} \tag{3.37}$$

The first two terms are the contributions from heavy glueball states and massless gluons, respectively and are identical to the terms in Eqn. (3.36). The third term is the contribution from pions for momenta $k < K$ and the fourth term is the contribution from quarks for momenta $k > K$. $\nu_\pi = 3$ is the degeneracy factor of a pion gas and $\nu_q = 24$ the degeneracy factor of a quark gas. For simplicity we neglected the quark masses here. Results for the pressure, the energy density, and the interaction measure are shown in Fig. 3.8 and Fig. 3.9, respectively. The parameters r and s are the same as in the case of pure $SU(3)$ gauge theory.

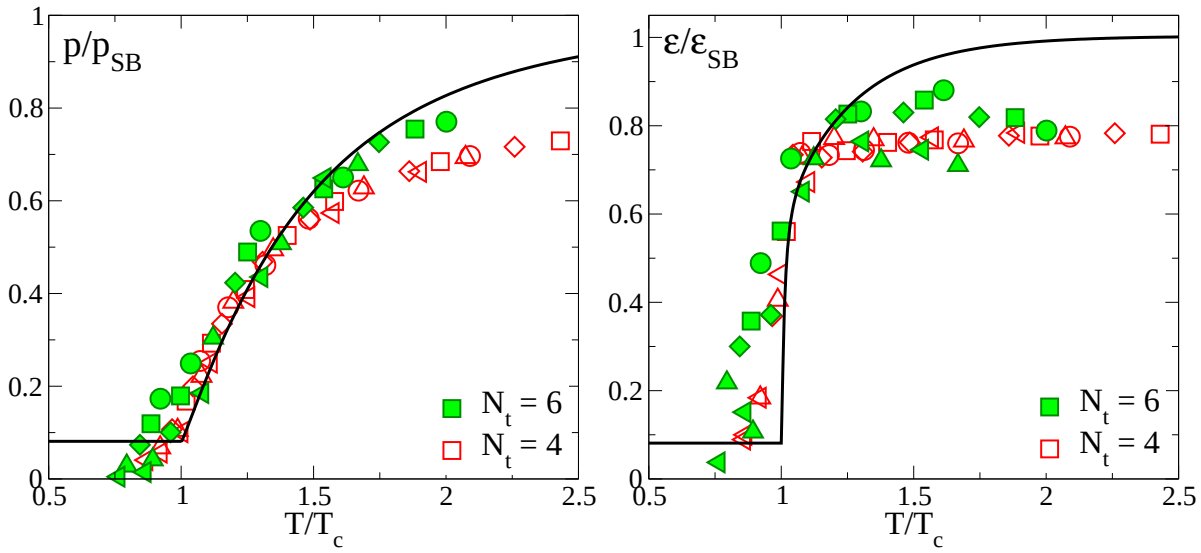

Figure 3.8: The pressure p/p_{SB} (left panel) and the energy density $\epsilon/\epsilon_{\mathrm{SB}}$ (right panel), divided by their respective Stefan-Boltzmann values from our model (solid lines) compared to lattice data from $16^3 \times 4$ and $16^3 \times 6$ lattices (symbols) [AK+01a]. Different values of $m_{\mathrm{PS}}/m_{\mathrm{V}}$ used in the lattice calculations are denoted by different shapes of the symbols (see Fig. 1.2 or [AK+01a]).

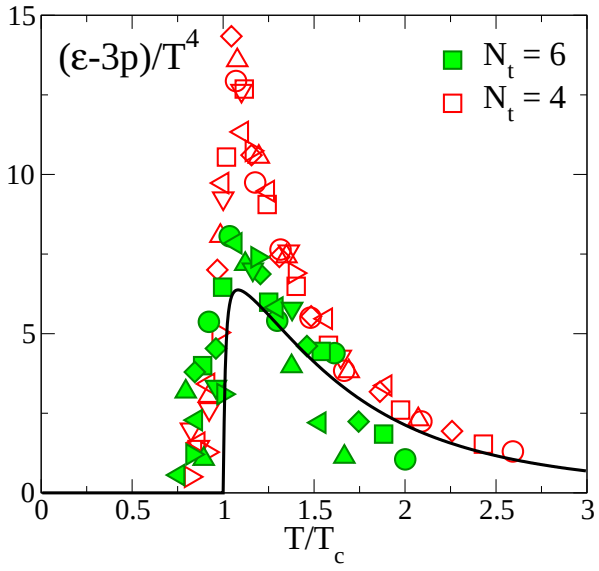

Figure 3.9: The scaled interaction measure $(\epsilon - 3p)/T^4$ from our model (solid lines) compared to lattice data from from $16^3 \times 4$ and $16^3 \times 6$ lattices (symbols) [AK+01a]. Different values of $m_{\mathrm{PS}}/m_{\mathrm{V}}$ used in the lattice calculations are denoted by different shapes of the symbols (see Fig. 1.2 or [AK+01a]).

3.7 Summary

In this chapter we have extended a novel quasiparticle description of the QCD EoS in the temperature range $T_c < T \lesssim 3\,T_c$, where current heavy-ion collision experiments operate, to finite quark chemical potential. Such an extension is important for a number of reasons: First, for current heavy ion collision experiments at SPS and RHIC the chemical freeze-out occurs at $\mu_{f.o.} \simeq 100$ MeV, (baryon chemical potential $\mu_B \simeq 300$ MeV) [BMHS99] and $\mu_{f.o.} \simeq 15$ MeV, ($\mu_B \simeq 45$ MeV) [BMMRS01], respectively. Thus, a finite quark chemical potential should be introduced to describe the deconfined quark matter created in these experiments. Second, first lattice QCD simulations at finite quark chemical potential are now available and it is of great theoretical interest to interpret these lattice results. Third, the introduction of an additional external control parameter helps to test the reliability of the quasiparticle approach.

The use of a quasiparticle model in QCD is based on the observation that in a strongly interacting system, the complex dynamics often rearranges itself in such a way that gross features of the physics can be described in terms of appropriate effective degrees of freedom. In the confinement quasiparticle model, the strong interactions between the quarks and gluons are incorporated in thermally generated masses. Since confinement simply reduces the number of thermally active degrees of freedom in a statistical sense, confinement can be included in the quasiparticle model by modifying the particle distribution functions with a confinement factor $C(T)$. To extend this model to finite quark chemical potentials we have used Maxwell relations to construct the effective coupling $G(T,\mu)$ and the confinement factor $C(T,\mu)$. We then used this model to calculate the phase boundary line $T_c(\mu)$ and the scaled pressure difference $\Delta p(T,\mu) = (p(T,\mu) - p(T,\mu=0))/T^4$ and the scaled quark number density $n_q(T,\mu)/T^3$. We compared our results to recent lattice calculations and found remarkably good agreement even for large quark chemical potentials $\mu \sim T_c$.

Finally we have dropped the assumption that the confinement process only depends on temperature and not on the momentum spectrum of the particles. We constructed a model with momentum dependent confinement and applied this model to pure $SU(3)$ gauge theory and full QCD with dynamical quarks. Lattice QCD results for the pressure, the energy density and the interaction measure are reproduced remarkably well in the temperature range $T_c \leq T \lesssim 2\,T_c$. For larger temperatures, the model does not reproduce the substantial deviations of the pressure and the energy from the Stefan-Boltzmann limit found in lattice QCD simulations. However, this can be accounted for by the introduction of thermal quasiparticle masses.

Chapter 4

Thermodynamics of the Nambu–Jona-Lasinio Model

The extension of the confinement quasiparticle model which we have developed in chapter 3 reproduces lattice QCD results at finite temperature and finite quark chemical potential remarkably well. However, the model also has shortcomings which limit its applicability: There is no obvious relation to a microscopic theory, i. e. there is no Lagrangian that can be used to calculate other physical quantities, e. g. meson masses. It also does not incorporate the symmetries and symmetry breaking patterns of QCD which are essential to understand the lightest hadrons. A model that is particularly well suited to study the symmetries and symmetry breaking patterns of QCD is the Nambu–Jona-Lasinio (NJL) model. It is an effective Lagrangian of relativistic fermions interacting through local fermion-fermion couplings. Historically, it goes back to two papers by Nambu and Jona-Lasinio in 1961 [NJL61a, NJL61b], i. e. to a time when QCD and even quarks were still unknown. In its original version the NJL model was therefore a model of interacting nucleons. After QCD was established, the NJL model was reinterpreted as a theory of quark degrees of freedom [Kle, Zic, Vol84, HK84]. In principle, the NJL Lagrangian can be obtained from QCD by "integrating out" the gluonic degrees of freedom, replacing them by a local four-point color-current interaction. This amounts to effectively replacing the local color gauge symmetry by a global one, with the assumption that colored (gluonic) excitations are far removed from the low-energy spectrum and hence "frozen". This picture is supported by the short gluon field strength correlation length $\lambda \lesssim 0.2$ fm observed in lattice QCD calculations, which suggests a short correlation distance for the "color transport" between quarks [DGP92, DGDSS02]. In this chapter we introduce the two-flavor NJL model and demonstrate how it can be used to analyze the properties of quark matter at finite temperature and finite quark chemical potential. Subsequent chapters are based on this formalism. For more details the reader is referred to [VW91, Kle92, HK94].

4.1 Vacuum properties

In QCD, the conserved current associated with a quark is a color-current

$$\boldsymbol{J}^a_\mu = \bar{\psi}\gamma_\mu t^a \psi. \tag{4.1}$$

This current couples to the gluon field. Two quarks interact with each other by absorbing and emitting gluons, thus by exchanging color charges. If color fields propagate only over very short distances, then the interaction between the quarks can be approximated by a local coupling between their color currents,

$$\mathcal{L}_{\rm int} = -G_c \sum_{a=1}^{8} \boldsymbol{J}_\mu^a \boldsymbol{J}_a^\mu, \tag{4.2}$$

where $G_c \sim \bar{g}_s^2 \lambda^2$ is an effective coupling strength of dimension (length)^2. It is given by the QCD coupling strength, averaged over the relevant distance scales times the squared correlation length, λ^2. Matrix elements of the interaction (4.2) involve both direct and exchange terms. To calculate exchange terms we construct a Fierz invariant interaction by adding the Fierz transform of the color-current interaction (4.2) to the original interaction. In mean-field approximation, calculating direct terms with the Fierz invariant interaction is equivalent to calculating both direct and exchange terms with the original color-current interaction (4.2). The Fierz transform gives both color-singlet and color-octet terms (see Appendix C). The color-singlet part reads

$$\mathcal{L}_{\rm int}^{\rm cs} = \frac{G}{2} \sum_{b=0}^{3} \Big[(\bar{\psi}\tau_b\psi)^2 + (\bar{\psi} i\gamma_5 \tau_b \psi)^2 - \frac{1}{2}(\bar{\psi}\gamma^\mu \tau_b \psi)^2 - \frac{1}{2}(\bar{\psi}\gamma^\mu\gamma_5 \tau_b \psi)^2 \Big], \tag{4.3}$$

where $G = \frac{16}{9} G_c$ is the effective coupling strength between quarks and anti-quarks and τ_j are the Pauli matrices in flavor (isospin) space. The local interaction between color-currents transformed into scalar-pseudoscalar and vector-axialvector interactions which operate in color-singlet channels with quantum numbers (flavor and spin) of the various mesons. The remaining color-octet part which includes the original interaction (4.2) and the color-octet terms of the Fierz transform, is

$$\begin{aligned} \mathcal{L}_{\rm int}^{\rm co} = &- \frac{9}{8}\frac{G}{2} \sum_{a=1}^{8} (\bar{\psi}\gamma^\mu t_a \tau_b \psi)^2 \\ &- \frac{3}{16}\frac{G}{2} \sum_{a=1}^{8}\sum_{b=0}^{3} \Big[(\bar{\psi} t_a \tau_b \psi)^2 + (\bar{\psi} i\gamma_5 t_a \tau_b \psi)^2 - \frac{1}{2}(\bar{\psi}\gamma^\mu t_a \tau_b \psi)^2 - \frac{1}{2}(\bar{\psi}\gamma^\mu\gamma_5 t_a \tau_b \psi)^2 \Big]. \end{aligned} \tag{4.4}$$

In this chapter we will restrict ourselves to the discussion of the color-singlet part (4.3) of the interaction because the color-octet part does not play any role for matrix elements taken between color-singlet states. These are the only states we look at in this chapter. For simplicity we will only consider the scalar and pseudoscalar channels:

$$\mathcal{L}_{\rm sym} = \bar{\psi}(i\partial\!\!\!/ - \hat{m}_0)\psi + \frac{G}{2} \sum_{b=0}^{3} \Big[(\bar{\psi}\tau_b\psi)^2 + (\bar{\psi} i\gamma_5 \tau_b \psi)^2 \Big], \tag{4.5}$$

where $\hat{m}_0 = \mathrm{diag}(m_u, m_d)$ is the current quark matrix and we shall work in the isospin-symmetric limit with $m_u = m_d \equiv m_0$. In the limit of vanishing quark masses this

Lagrangian is invariant under $SU(2)_L \otimes SU(2)_R$ transformations, just like the QCD Lagrangian (1.1). However, it also has an additional $U(1)_A$ symmetry which is not realized in nature and which can be removed by adding an anomaly term:

$$\mathcal{L}_{\text{det}} = K\left\{\det{}_f[\bar{\psi}(1+\gamma_5)\psi] + \det{}_f[\bar{\psi}(1-\gamma_5)\psi]\right\} \tag{4.6}$$

$$= \frac{K}{2}\left[(\bar{\psi}\psi)^2 + (\bar{\psi}i\gamma_5\vec{\tau}\psi)^2 - (\bar{\psi}i\gamma_5\psi)^2 - (\bar{\psi}\vec{\tau}\psi)^2\right]. \tag{4.7}$$

The complete NJL Lagrangian then reads

$$\mathcal{L}_{\text{NJL}} = \mathcal{L}_{\text{sym}} + \mathcal{L}_{\text{det}} = \bar{\psi}(i\partial\!\!\!/ - \hat{m}_0)\psi + \frac{G}{2}\left[\left(\bar{\psi}\psi\right)^2 + \left(\bar{\psi}i\gamma_5\vec{\tau}\psi\right)^2\right], \tag{4.8}$$

where we have assumed $G = K$. In principle, $\mathcal{L}_{\text{sym}}$ and $\mathcal{L}_{\text{det}}$ are regarded to have different origins, as discussed in Ref. [RA88]. Thus the choice of the coupling constants, $G = K$, should be considered as an approximation. The color-octet part is discussed in detail in the next chapter.

4.1.1 Constituent quarks and mesons

In this section we briefly review the vacuum properties of quarks and mesons described within the NJL model. Quarks in the NJL model are dressed by their strong interactions and acquire a dynamical mass $M = m_0 + \Sigma$, where Σ is the quark self-energy. Diagrammatically, in Hatree-Fock approximation the quark self-energy that arises from interaction terms in (4.8) is illustrated in Fig. 4.1.

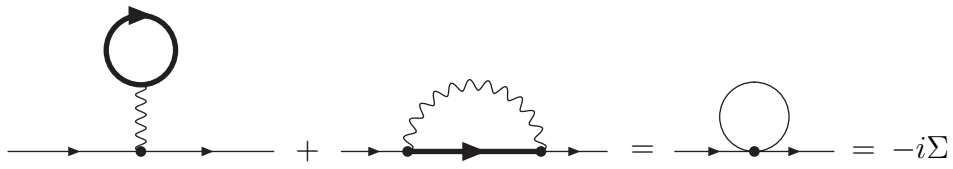

Figure 4.1: Hatree and Fock contributions to the self-energy for a particular interaction vertex.

To distinguish the Hatree and the Fock terms, the pointlike interactions are drawn as (non-local) interaction lines. Since in this approximation the self-energy is local, it only gives rise to a constant shift in the quark mass:

$$M = m_0 + 4iG\left(N_c N_f + \frac{1}{2}\right)\int\frac{\mathrm{d}^4p}{(2\pi)^4}\frac{M}{p^2 - M^2}. \tag{4.9}$$

In an $1/N_c$ expansion, the first term in the brackets is of zeroth order, while the second term is of first order. Since there are more diagrams contributing to $\mathcal{O}(1/N_c)$ which we are not taking into account, we also neglect this term in the following. The integral in Eqn. (4.9) is quadratically divergent and has to be regularized. This prescription is then

part of the model. When the model is applied to thermodynamics, it is convenient to regularizing the divergent integrals by a three-momentum cutoff. This has the advantage that it preserves the analytic structure, necessary, e. g., for the analytic continuation of functions given on imaginary Matsubara frequencies. Therefore we will employ the three-momentum cutoff-scheme in the following. Eqn. (4.9) then reads

$$M = m_0 + 4GN_cN_fM\int^\Lambda \frac{\mathrm{d}^3p}{(2\pi)^3}\frac{1}{2E_p} = m_0 + \frac{GN_cN_fM}{\pi^2}\int_0^\Lambda \mathrm{d}p\,\frac{p^2}{E_p}, \tag{4.10}$$

where

$$\int^\Lambda \frac{\mathrm{d}^3p}{(2\pi)^3} \equiv \int \frac{\mathrm{d}^3p}{(2\pi)^3}\theta(\Lambda - |\boldsymbol{p}|), \tag{4.11}$$

and $E_p = \sqrt{\boldsymbol{p}^2 + M^2}$. For sufficiently strong interactions G, this allows for non-trivial solutions $M \neq m_0$, even in the chiral limit $m_0 = 0$, producing a gap $\Delta E = 2M$ in the quark spectrum. In analogy to the BCS theory of superconductivity, this equation is often referred to as "gap equation". M is often called "constituent quark mass" because its numerical value is approximately the same as the values commonly used in naive non-relativistic quark models.

We now employ the effective Lagrangian (4.8) to study mesonic modes using a consistent combination of one- and two-body equations (the gap equation and the Bethe-Salpeter equation). This scheme is analogous to the Hatree-Fock plus RPA approach familiar from nuclear physics. The basic element in this calculation is the two-body interaction kernel generated by the interaction terms in (4.8). Given the symmetries of the Lagrangian, we can decompose the color-singlet two-body interaction kernel into flavor and Lorentz tensor covariants in the quark-antiquark channel:

$$\begin{aligned}\mathcal{K} = {} & K^S_{ij}(I_D\tau_i \otimes I_D\tau_j) + K^P_{ij}(i\gamma_5\tau_i \otimes i\gamma_5\tau_j) + K^V_{ij}(\gamma_\mu\tau_i \otimes \gamma^\mu\tau_j) \\ & + K^A_{ij}(\gamma_\mu\gamma_5\tau_i \otimes \gamma^\mu\gamma_5\tau_j).\end{aligned} \tag{4.12}$$

The K^α_{ij} are then given in terms of the coupling strength parameters of the Lagrangian (4.8):

$$K^S_{ij} = G, \quad K^P_{ij} = G, \quad K^V_{ij} = 0, \quad K^A_{ij} = 0. \tag{4.13}$$

The interaction kernel (4.12) is defined such that it represents the Born term of the quark-antiquark $\mathcal{T}$-matrix (see Fig. 4.2). An explicit expression for the $\mathcal{T}$-matrix is given by

$$\mathcal{T}(q) = \mathcal{K} + i\mathrm{Tr}\int\frac{\mathrm{d}^4p}{(2\pi)^4}[\mathcal{K}S(p)\mathcal{T}(q)S(p-q)], \tag{4.14}$$

where $S(p) = (\not{p} - M + i\epsilon)^{-1}$ is the quark propagator with the dynamical quark mass M. The integral in (4.14) is divergent and has to be regularized. To preserve the Ward-Takahashi identity, the same regularization scheme as for the gap equation has to be applied. Using the ansatz

$$\mathcal{T} = T(\Gamma, \Gamma')_{ij}(\Gamma\tau_i \otimes \Gamma'\tau_j). \tag{4.15}$$

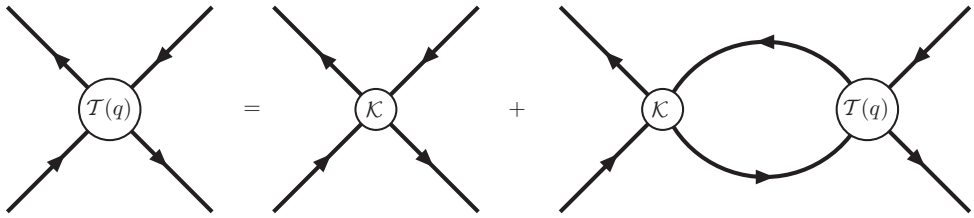

Figure 4.2: Illustration of the Bethe-Salpeter equation which determines the quark-antiquark $\mathcal{T}$-matrix.

we can write the $\mathcal{T}$-matrix as a matrix equation in Dirac-, color- and flavor-space:

$$T = K + KJT = K(1 + JT). \tag{4.16}$$

The formal solution of this equation is

$$T = \frac{K}{1 - JK}, \tag{4.17}$$

where

$$J(\Gamma, \Gamma')_{ij} = i\mathrm{Tr} \int \frac{\mathrm{d}^4 p}{(2\pi)^4} [\Gamma \tau_i S(p) \Gamma' \tau_j S(p - q)] \tag{4.18}$$

are the generators of the correlation functions characterized by the Dirac matrices Γ, Γ' and the flavor matrices τ_i, τ_j. The trace is taken in Dirac-, color- and flavor-space. In order to determine meson properties one interprets the T-matrix (4.16) as an effective meson exchange and parametrizes the pole structure as

$$T_{\mathcal{M}}(q^2) = \frac{-g^2_{\mathcal{M}qq}}{q^2 - m^2_{\mathcal{M}}}, \tag{4.19}$$

where $\mathcal{M}$ denotes the quantum numbers of the respective meson channel. The meson mass $m_{\mathcal{M}}$ and the effective coupling $g_{\mathcal{M}qq}$ are given by

$$1 - KJ(q^2 = m^2_{\mathcal{M}}) = 0 \quad \text{and} \quad g^{-2}_{\mathcal{M}qq} = \left. \frac{dJ_{\mathcal{M}}}{dq^2} \right|_{q^2 = m^2_{\mathcal{M}}}. \tag{4.20}$$

where $J = J(\Gamma, \Gamma')_{ij}$ is the generator of the correlation function with the quantum numbers $\mathcal{M}$.

4.1.2 Model parameters

The two-flavor NJL model has three parameters: the coupling constant G, the cutoff parameter Λ and the current quark mass m_0. There are three physical quantities which can be used to fix these parameters: the pion decay constant f_π, the quark condensate $\langle \bar{\psi}\psi \rangle = \langle \bar{u}u \rangle + \langle \bar{d}d \rangle$ and the pion mass m_π. Whereas the pion mass, $m_\pi = 139$ MeV and

the pion decay constant, $f_\pi = 92.4 \pm 0.2$ MeV [Hol90], are known quite accurately, the uncertainties for the quark condensate are rather large. Limits extracted from sum rules are 190 MeV $\lesssim -\langle\bar{u}u\rangle^{1/3} \lesssim$ 260 MeV at a renormalization scale of 1 GeV [DN98], while lattice calculations yield $\langle\bar{u}u\rangle^{1/3} = (231 \pm 4 \pm 8 \pm 6)$ MeV [GRTV99]. This allows for small variations of the parameters of the NJL model.

Employing a three momentum cutoff, the quark condensate is given by

$$\langle\bar{u}u\rangle = \langle\bar{d}d\rangle = -2N_c M \int^{\Lambda} \frac{\mathrm{d}^3p}{(2\pi)^3}\frac{1}{E_p} = -\frac{N_c M}{\pi^2}\int_0^{\Lambda}\mathrm{d}p\,\frac{p^2}{E_p}, \tag{4.21}$$

whereas the pion decay constant is given by

$$f_\pi^2 = N_c M^2 \int^{\Lambda} \frac{\mathrm{d}^3p}{(2\pi)^3}\frac{1}{E_p^3} = \frac{N_c M^2}{2\pi^2}\int_0^{\Lambda}\mathrm{d}p\,\frac{p^2}{E_p^3}. \tag{4.22}$$

The pion mass can be calculated using the first equation from (4.20) with

$$\begin{aligned} J_{PP} =& i2N_c\mathrm{tr}\int\frac{\mathrm{d}^4p}{(2\pi)^4}[i\gamma_5 S(p) i\gamma_5 S(p-q)] \\ =& i8N_c\int\frac{\mathrm{d}^4p}{(2\pi)^2}\frac{1}{p^2-M^2} - i4N_c q^2\int\frac{\mathrm{d}^4p}{(2\pi)^2}\frac{1}{(p^2-M^2)((p-q)^2-M^2)}, \end{aligned} \tag{4.23}$$

where the trace in the first line is taken in Dirac-space only. Applying a three-momentum cutoff one finds the condition

$$1 - \frac{2GN_c}{\pi^2}\int_0^{\Lambda}\mathrm{d}p\,\frac{p^2}{E_p}\left(1 - \frac{q_0^2}{q_0^2 - 4E_p^2}\right)\Bigg|_{q_0^2=m_\pi^2} = 0 \tag{4.24}$$

for the pion mass. Several sets of parameters are used in the literature. We will employ the parameters from [Kle92], which are listed in Table 4.1 with the resulting physical quantities.

Λ [GeV]	G[GeV^{-2}]	m_0[MeV]
0.651	10.08	5.5
$\lvert\langle\bar{\psi}_u\psi_u\rangle\rvert^{1/3}$[MeV]	f_π[MeV]	m_π[MeV]
251	92.3	139.3

Table 4.1: Parameter set used in this work for the two-flavor NJL model, and the resulting physical quantities.

4.2 Non-zero temperatures and densities

The NJL model has been employed to study quark and meson properties in hot or dense matter (see e. g. [VW91, Kle92, LKW92] and references therein). Calculations indicate a significant temperature and density dependence of the chiral condensate. Its melting is connected with the prediction of a partial restoration of chiral symmetry at high temperatures and/or large densities. The properties of mesons at finite temperature and finite density have also been studied in the framework of the NJL model. Due to its Goldstone boson nature, the pion plays a special role. Its mass stays nearly constant until the critical conditions for chiral symmetry restoration are reached. Then it turns into a non-Goldstone particle and its mass quickly increases. In this section we will discuss how the NJL model is employed to study quark matter at finite temperature and finite quark chemical potential.

Applying standard techniques of thermal field theory it is straight forward to evaluate the quark loop which enters the gap equation or the Bethe-Salpeter equation for the $\mathcal{T}$-matrix at non-vanishing temperature or chemical potential. Details are presented in Appendix D. The results have basically the same structure as the vacuum expressions, but are modified by thermal occupation numbers. For instance, the gap equation (4.10) becomes

$$M = m_0 + 4N_c N_f G M \int^{\Lambda} \frac{\mathrm{d}^3 p}{(2\pi)^3} \frac{1 - f_D^+(E_p) - f_D^-(E_p)}{2E_p}, \tag{4.25}$$

where $f_D^{\pm}(E_p) = (\exp((E_p \mp \mu)/T) + 1)^{-1}$ are the Fermi-Dirac distribution functions for particles and antiparticles and $E_p = \sqrt{\boldsymbol{p}^2 + M^2}$ is their on-shell energy. The constituent quark mass as a function of temperature and chemical potential obtained from Eqn. (4.25) is shown in Fig. 4.3.

The total quark number density is given by the standard expression for the particle density of a gas of non-interacting massive particles:

$$n_q = \frac{N_c N_f}{\pi^2} \int_0^{\Lambda} \mathrm{d}p\, p^2 [f_D^+(E_p) - f_D^-(E_p)]. \tag{4.26}$$

Both the constituent quark mass $M(T, \mu)$ and the density $n_q(T, \mu)$ are discontinuous functions of μ at small temperatures, but the constituent quark mass as a function of the density is continuous. A plot of the constituent quark mass as a function of temperature and baryon density $n_B = n_q/3$ is shown in Fig. 4.4.

To determine the pion mass, we have to evaluate the quark loops in (4.23) at finite temperature and finite quark chemical potential. The pole of the T-matrix in this channel

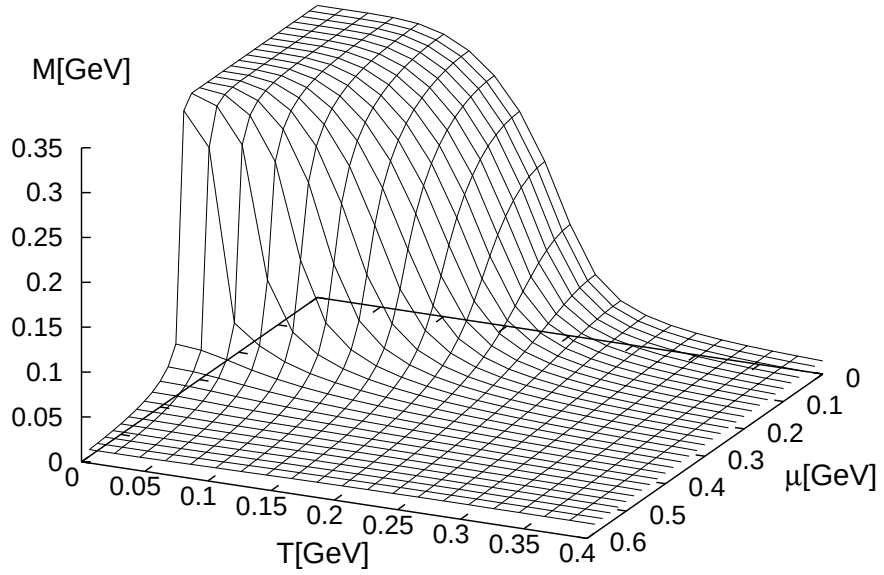

Figure 4.3: Constituent quark mass M as a function of temperature and quark chemical potential obtained from the gap equation (4.25).

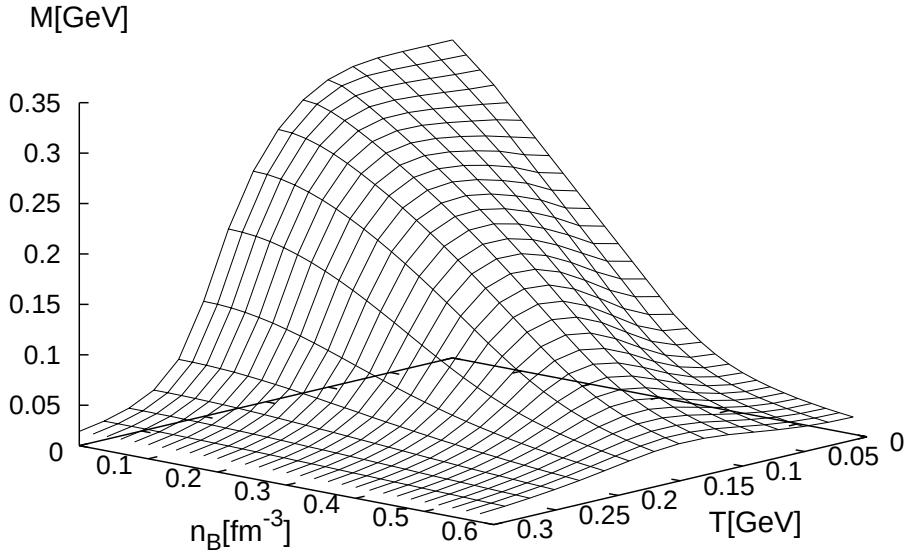

Figure 4.4: Constituent quark mass M as a function of temperature and the baryon number density obtained from the gap equation (4.25) and Eqn. (4.26).

is given by

$$1 - \frac{2GN_c}{\pi^2}\int_0^\Lambda \mathrm{d}p\,\frac{p^2}{E_p}\left(1-\frac{q_0^2}{q_0^2-4E_p^2}\right)\left[1-f_D^+(E_p)-f_D^-(E_p)\right]\Big|_{q_0^2=m_\pi^2}$$
$$= 1 + \frac{8GN_c}{\pi^2}\int_M^{\Lambda_E}\mathrm{d}E\,\frac{E^2\sqrt{E^2-M^2}(1-f_D^+(E)-f_D^-(E))}{q_0^2-4E^2}\Big|_{q_0^2=m_\pi^2} = 0. \tag{4.27}$$

In the last line we have changed the variable of integration from p to E and defined $\Lambda_E \equiv \sqrt{\Lambda^2+M^2}$. The sigma mass can be calculated using the first equation from (4.20) with

$$\begin{aligned} J_{SS} =& i2N_c\mathrm{tr}\int\frac{\mathrm{d}^4p}{(2\pi)^4}[\mathbf{1}S(p)\mathbf{1}S(p-q)] \\ =& i8N_c\int\frac{\mathrm{d}^4p}{(2\pi)^2}\frac{1}{p^2-M^2} + i4N_c(4M^2-q^2)\int\frac{\mathrm{d}^4p}{(2\pi)^2}\frac{1}{(p^2-M^2)((p-q)^2-M^2)}, \end{aligned} \tag{4.28}$$

where again the trace in the first line is taken in Dirac-space only. The pole of the T-matrix in this channel is then given by

$$1 + \frac{8GN_c}{\pi^2}\int_M^{\Lambda_E}\mathrm{d}E\,\frac{(E^2-M^2)\sqrt{E^2-M^2}(1-f_D^+(E)-f_D^-(E))}{q_0^2-4E^2}\Big|_{q_0^2=m_\sigma^2} = 0. \tag{4.29}$$

The pion mass as a function of temperature and chemical potential is shown in Fig. 4.5 and as a function of temperature and baryon number density in Fig. 4.6. The sigma mass as a function of temperature and quark chemical potential is shown in Fig. 4.7 and as a function of temperature and baryon number density in Fig. 4.8.

Our results are in good agreement with a very detailed study making use of a field-theoretical approach for the calculation of the pseudoscalar and scalar correlation functions at finite temperature [MRST01]. In that work, phenomenological forms for the non-perturbative features of the gluon propagator were introduced and the Schwinger-Dyson and Bethe-Salpeter equations were solved.

4.3 Thermodynamic potential

It is straightforward to evaluate the loop integrals that enter the gap equation and the Bethe-Salpeter equation at finite temperature and finite quark chemical potential. Equivalently, we can also calculate the thermodynamic potential Ω of the system and deduce thermodynamic properties from it. This formalism is important because it is directly applicable to the NJL model with confinement which we discuss in subsequent parts of this work.

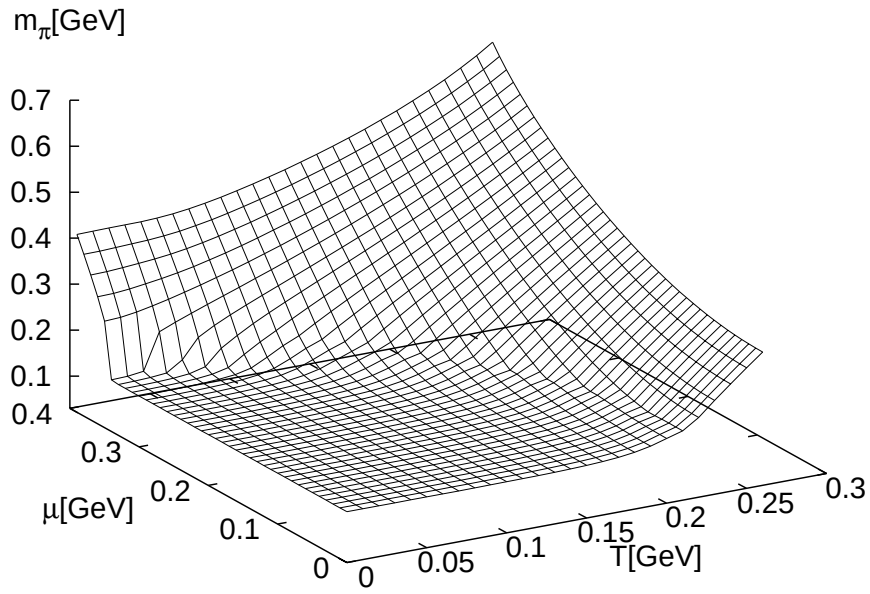

Figure 4.5: Pion mass as a function of temperature and quark chemical potential obtained from Eqn. (4.27).

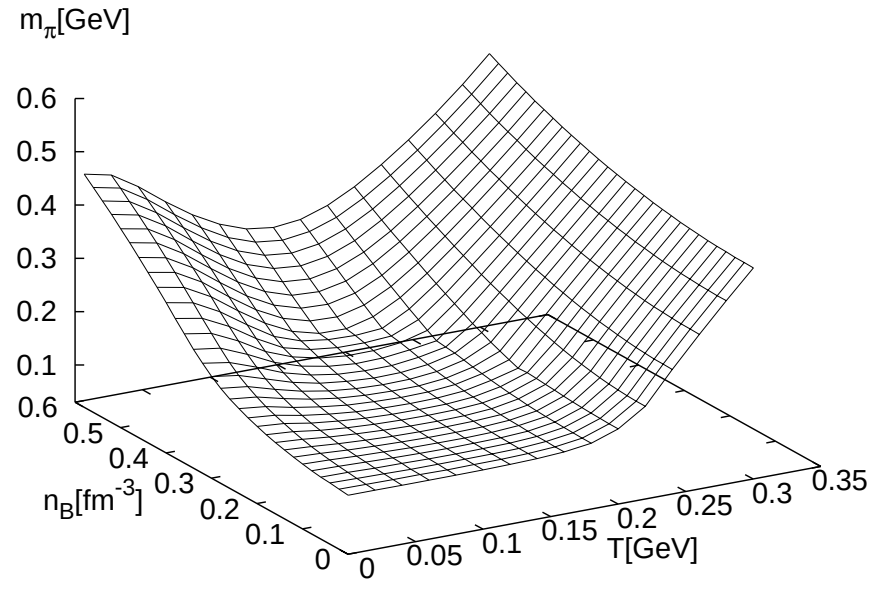

Figure 4.6: Pion mass as a function of temperature and baryon number density obtained from Eqn. (4.27) and Eqn. (4.26).

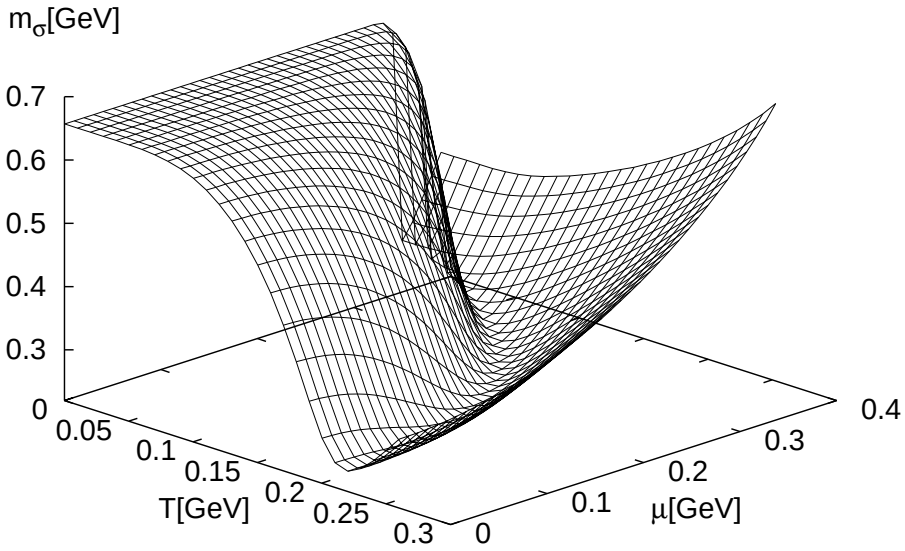

Figure 4.7: Sigma mass as a function of temperature and quark chemical potential obtained from Eqn. (4.29).

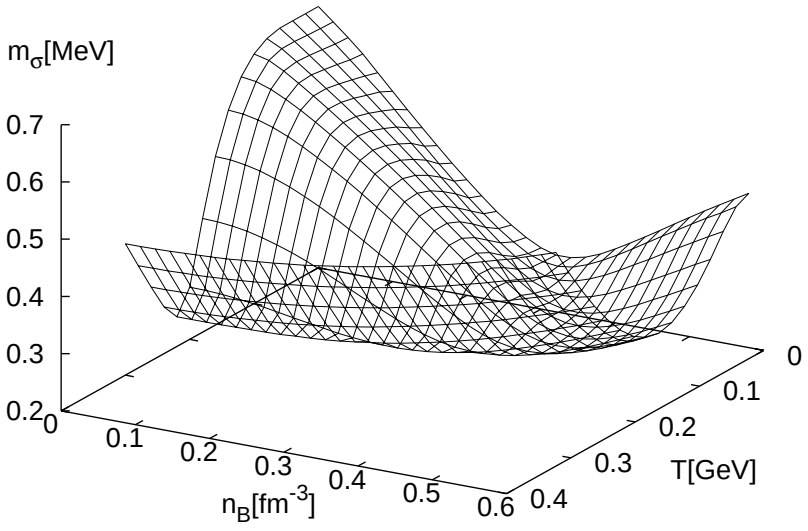

Figure 4.8: Sigma mass as a function of temperature and baryon number density obtained from Eqn. (4.29) and Eqn. (4.26).

To derive the thermodynamic potential, it is useful to work with the bosonized form of the Lagrangian (4.8). We start from the NJL path integral

$$\mathcal{Z} = \mathcal{N} \int \mathcal{D}\psi \mathcal{D}\bar{\psi} \exp\left[i \int \mathrm{d}^4x \, \mathcal{L}_{\mathrm{NJL}} \right]. \tag{4.30}$$

$\mathcal{N}$ is an (infinite) constant which is not relevant here. Our final goal is to integrate over the fermionic degrees of freedom, but this is not possible at this stage since the interaction term is quadratic in the quark fields. We therefore multiply (4.30) by the constant

$$\int \mathcal{D}\sigma \mathcal{D}\pi \exp\left[i \int \mathrm{d}^4x \left(-\frac{\sigma^2 + \vec{\pi}^2}{2G} \right) \right], \tag{4.31}$$

and obtain the equivalent path integral

$$\mathcal{Z} = \mathcal{N} \int \mathcal{D}\sigma \mathcal{D}\vec{\pi} \mathcal{D}\psi \mathcal{D}\bar{\psi} \exp\left[i \int \mathrm{d}^4x \, \bar{\psi}(i\partial\!\!\!/ - \hat{m}_0)\psi + \frac{G}{2}\left[(\bar{\psi}\psi)^2 + (\bar{\psi} i\gamma_5 \vec{\tau}\psi)^2 \right] - \frac{\sigma^2 + \vec{\pi}^2}{2G} \right]. \tag{4.32}$$

The bosonic fields can now be shifted according to

$$\sigma \to \sigma + G\bar{\psi}\psi \qquad \text{and} \qquad \vec{\pi} \to \vec{\pi} + G\bar{\psi} i\gamma_5 \vec{\tau}\psi, \tag{4.33}$$

so that the functional integral (4.30) becomes

$$\mathcal{Z} = \mathcal{N} \int \mathcal{D}\sigma \mathcal{D}\vec{\pi} \mathcal{D}\psi \mathcal{D}\bar{\psi} \exp\left[i \int \mathrm{d}^4x \left(\bar{q}\left(S^{-1}\right) q - \frac{\sigma^2 + \vec{\pi}^2}{2G} \right) \right]. \tag{4.34}$$

The inverse quark propagator (in Nambu-Gorkov representation) reads

$$S^{-1} = \begin{pmatrix} i\partial\!\!\!/ - \hat{m}_0 + \sigma + i\gamma_5 \vec{\tau}\vec{\pi} & 0 \\ 0 & i\partial\!\!\!/ - \hat{m}_0 + \sigma + i\gamma_5 \vec{\tau}\vec{\pi} \end{pmatrix}, \tag{4.35}$$

and

$$q(x) = \frac{1}{\sqrt{2}} \begin{pmatrix} \psi(x) \\ \psi(x) \end{pmatrix}. \tag{4.36}$$

We have formally doubled the fermion fields. The advantage of this notation will be apparent when a quark chemical potential is introduced. We can now integrate over $q(x)$ and $\bar{q}(x)$ since (4.34) is bilinear in the quark fields and obtain the bosonized Lagrangian

$$\tilde{\mathcal{L}}_{\mathrm{NJL}} = -\frac{\sigma^2 + \vec{\pi}^2}{2G} - \frac{i}{2}\mathrm{Tr}\ln S^{-1}. \tag{4.37}$$

The trace in (4.37) is taken over color, flavor and Dirac indices and the factor $1/2$ accounts for the double counting of the fermion fields.

The quantity to be minimized at finite temperature is the thermodynamic potential per unit volume, which can be written as:

$$\Omega\left(T, \mu\right) = -\frac{T}{2} \sum_n \int^{\Lambda} \frac{\mathrm{d}^3p}{(2\pi)^3} \mathrm{Tr}\ln\left(\frac{1}{T} \tilde{S}^{-1}\left(i\omega_n, \boldsymbol{p}\right) \right) + \frac{\sigma^2}{2G}. \tag{4.38}$$

Here $\omega_n = (2n+1)\pi T$ are the Matsubara frequencies for fermions. The inverse quark propagator becomes

$$\tilde{S}^{-1}\left(p^0, \boldsymbol{p}\right) = \begin{pmatrix} \not{p} - \hat{m}_0 + \sigma - \mu\gamma_0 & 0 \\ 0 & \not{p} - \hat{m}_0 + \sigma + \mu\gamma_0 \end{pmatrix}, \tag{4.39}$$

where a quark chemical potential μ has been introduced. The expectation value $\langle\vec{\pi}\rangle$ of the pseudoscalar isotriplet field is equal to zero for isospin-symmetric systems. In (4.39) we have suppressed color and flavor indices. In fact, each of the elements of the matrix is a matrix in color-, flavor- and Dirac-space and thus (4.39) is a tensor product of matrices. To carry out the trace we use the identity $\mathrm{Tr}\ln(X) = \ln\det(X)$. The determinant can be calculated using the identity $\det(A\otimes B) = (\det A)^m(\det B)^n$, where A and B are two square matrices of dimension n and m [Eve80]. The result reads

$$\mathrm{Tr}\ln\left(\frac{1}{T}\tilde{S}^{-1}\right) = 2N_cN_f\left[\ln\left(\frac{(\omega_n+i\mu)^2+E_p^2}{T^2}\right) + \ln\left(\frac{(\omega_n-i\mu)^2+E_p^2}{T^2}\right)\right], \tag{4.40}$$

where we have introduced the quark quasiparticle energy $E_p = \sqrt{\boldsymbol{p}^2+M^2}$ with $M = m_0 - \sigma$. We can reorder the terms to obtain

$$\begin{aligned}
&\ln\left(\frac{(\omega_n+i\mu)^2+E_p^2}{T^2}\right) + \ln\left(\frac{(\omega_n-i\mu)^2+E_p^2}{T^2}\right) \\
&= \ln\left(\frac{[(\omega_n+i\mu)^2+E_p^2][(\omega_n-i\mu)^2+E_p^2]}{T^4}\right) = \ln\left(\frac{[\omega_n^2+(E_p-\mu)^2][\omega_n^2+(E_p+\mu)^2]}{T^4}\right) \\
&= \ln\left(\frac{\omega_n^2+(E_p-\mu)^2}{T^2}\right) + \ln\left(\frac{\omega_n^2+(E_p+\mu)^2}{T^2}\right).
\end{aligned} \tag{4.41}$$

Using the relation

$$T\sum_{n=-\infty}^{\infty}\ln\left(\frac{\omega_n^2+\lambda^2}{T^2}\right) = \lambda + 2T\ln\left(1+e^{-\lambda/T}\right), \tag{4.42}$$

we finally obtain

$$\begin{aligned}
\Omega(T,\mu;M) = &-2N_cN_f\Bigg\{\int^{\Lambda}\frac{\mathrm{d}^3p}{(2\pi)^3}E_p + T\int^{\Lambda}\frac{\mathrm{d}^3p}{(2\pi)^3}\ln\left[1+\exp\left(-\frac{E_p-\mu}{T}\right)\right] \\
&+ T\int^{\Lambda}\frac{\mathrm{d}^3p}{(2\pi)^3}\ln\left[1+\exp\left(-\frac{E_p+\mu}{T}\right)\right]\Bigg\} + \frac{\sigma^2}{2G}.
\end{aligned} \tag{4.43}$$

The second and the third integral in (4.43) are not divergent, so in principle there is no need to regularize them. Removing the cutoff from these integrals has the advantage that thermodynamical quantities like the pressure and the energy density approach the Stefan-Boltzmann limit at high temperatures. On the other hand, this heuristic procedure breaks chiral symmetry explicitly. It is nevertheless justified as long as temperature and quark chemical potential are well below the cutoff Λ [Rip97]. Our studies show that the effect of the additional symmetry breaking on quantities like the quark condensate and the constituent quark mass is small in the temperature region $0 \le T \lesssim (2-3)\,T_c$ that we consider in this work. From now on we will therefore not regularize integrals that are not divergent, unless stated otherwise.

4.4 Comparison with the bag model

In chapter 2 we have discussed the MIT bag model, a simple model that implements two of the key properties of QCD, asymptotic freedom and confinement. The MIT bag model treats quarks and gluons as a gas of non-interacting particles confined to a finite region of space, the bag. In the following, we will briefly compare the MIT bag model and the NJL model.

In the NJL model, the pressure is given by

$$\begin{aligned} p =& -\Omega = -\frac{\sigma^2}{2G} + 2N_cN_f \int^{\Lambda} \frac{\mathrm{d}^3p}{(2\pi)^3} E_p \\ &+ 2N_cN_f \int \frac{\mathrm{d}^3p}{(2\pi)^3} \left\{ T \ln\left[1 + \exp\left(-\frac{E_p - \mu}{T}\right)\right] + T \ln\left[1 + \exp\left(-\frac{E_p + \mu}{T}\right)\right] \right\}, \end{aligned} \tag{4.44}$$

and the energy density reads

$$\begin{aligned} \epsilon =& -p + Ts + \mu n \\ =& \frac{\sigma^2}{2G} - 2N_cN_f \int^{\Lambda} \frac{\mathrm{d}^3p}{(2\pi)^3} E_p + 2N_cN_f \int \frac{\mathrm{d}^3p}{(2\pi)^3} E_p \left[f_D^+(E_p) + f_D^-(E_p)\right], \end{aligned} \tag{4.45}$$

where $s = \partial p/\partial T$ is the entropy and $n = \partial p/\partial \mu$ is the particle number density. The Gibbs-Duhem relation

$$\epsilon + p = Ts + \mu n \tag{4.46}$$

is automatically fulfilled in the NJL model. The last term in (4.44) and (4.45) can be interpreted as the pressure and the energy density of a gas of non-interacting quasiparticles with mass M. The part

$$\frac{\sigma^2}{2G} - 2N_cN_f \int^{\Lambda} \frac{d^3p}{(2\pi)^3} E_p + B_0 \equiv B(T,\mu), \tag{4.47}$$

can be seen as a temperature and chemical potential dependent bag constant $B(T,\mu)$. Here we have introduced a constant B_0 to adjust $B(T,\mu)$ at zero temperature and chemical potential. Since $B(T,\mu)$ adds to the energy density of the quasiparticles, it can be interpreted as a thermal vacuum energy density.

In the limit $M = m_0 = 0$ the pressure and the energy density are given by

$$\begin{aligned} p =& \frac{N_cN_f}{\pi^2} \int_0^{\infty} \mathrm{d}q\, q^2 \left\{ T \ln\left[1 + \exp\left(-\frac{q - \mu}{T}\right)\right] + T \ln\left[1 + \exp\left(-\frac{q + \mu}{T}\right)\right] \right\} - B \\ =& \frac{2N_cN_f}{12} \left(\frac{7}{30}\pi^2 T^4 + T^2\mu^2 + \frac{1}{2\pi^2}\mu^4 \right) - B, \end{aligned} \tag{4.48}$$

and

$$\begin{aligned}\epsilon &= \frac{N_c N_f}{\pi^2}\int_0^\infty \mathrm{d}p\, p^2 E_p \left[f_D^+(E_p) + f_D^-(E_p)\right] + B \\ &= \frac{2N_c N_f}{4}\left(\frac{7}{30}\pi^2 T^4 + T^2\mu^2 + \frac{1}{2\pi^2}\mu^4\right) + B. \end{aligned} \tag{4.49}$$

From Eqn. (4.48) or Eqn. (4.49) we could now calculate the deconfinement phase boundary line in the same manner as in the MIT bag model. This is surprising because the NJL model does not confine quarks, whereas the bag model is confining by construction. The solution is, that Eqns. (4.48) and (4.49) are only valid in the limit $M = m_0 = 0$. Then massless quarks, just like the bag model quarks, are restricted to the chirally restored phase and are not permitted to enter the non-trivial vacuum and hence they are confined. In the NJL model, however, quarks develop a dynamical mass and chiral symmetry is spontaneously broken and thus the NJL-model quarks are permitted to enter the non-trivial vacuum. Thus, while chiral symmetry breaking gives a microscopic explanation of the bag pressure, it also prevents the quarks from being confined.

4.5 Summary

In this chapter we have discussed the 'classic' NJL model, which was introduced in 1961 by Nambu and Jona-Lasinio as a model of interacting nucleons. After the development of QCD, the NJL model was reinterpreted as a schematic quark model. While schematically simple and analytically tractable, the model has many of the properties of QCD, in particular the chiral symmetry and its spontaneous breaking. Chiral symmetry breaking implies a non-vanishing chiral condensate. Quarks develop quasiparticle masses by propagating in this chiral condensate. Above a critical temperature $T \geq T_c$ the chiral symmetry is restored and the constituent quark masses approach the current quark masses.

We have applied the NJL model to study the properties of strongly interacting quark matter at finite temperature and quark chemical potential. The chiral condensate shows a significant dependence on temperature and quark chemical potential. By solving Bethe-Salpeter equations in the color-singlet quark-antiquark channels, we employed the NJL model to generate the lightest mesons as quark-antiquark excitations of the correlated QCD ground state with its condensate structure. The pion plays a special role due to its Goldstone boson nature. Its mass stays nearly constant until the critical condition for chiral symmetry restoration is reached. Then its mass rapidly increases because the pion no longer is a Goldstone boson. Finally we briefly compared the NJL model and the bag model, which is the most commonly used model to describe the EoS of deconfined quark matter. While in the bag model the bag constant B is a free model parameter, in

the NJL model the bag constant arises dynamically as a consequence of the spontaneous chiral symmetry breaking.

Chapter 5

Color-Octet Modes

In the previous chapter we have studied the color-singlet sector of the NJL model. We have neglected the color-octet part which is introduced by the Fierz-transformation of the original color-current interaction. Color-octet quark-antiquark modes are the remnants of gluon degrees of freedom in this model. The color octet-sector of the NJL model will be studied in detail in this chapter. Colored quark-antiquark pairs have never been observed in nature. The requirement that quarks at low energies have to be part of a bound color-singlet state is called *color confinement* and is an important feature of QCD. However, the NJL model does not confine quarks and thus allows for colored quark-antiquark excitations. The aim of this chapter is to show that such excitations are only possible at energies far above the cutoff of the theory and that they are thus insignificant for the low-energy spectrum.

5.1 Vacuum properties

By solving the Bethe-Salpeter equation in the color-octet channel, the NJL model generates color-octet quark-antiquark states. Possible bound states below the quark-antiquark threshold are determined by the poles of the scattering matrix. Above the quark-antiquark threshold color-octet bound states show up as a resonance structure in the real and imaginary parts of the scattering matrix. The color-octet part of the two-body interaction kernel reads:

$$\begin{aligned}\mathcal{K} = {} & K^S_{abij}(I_D t_a \tau_i \otimes I_D t_b \tau_j) + K^P_{abij}(i\gamma_5 t_a \tau_i \otimes i\gamma_5 t_b \tau_j) + K^V_{abij}(\gamma_\mu t_a \tau_i \otimes \gamma^\mu t_b \tau_j) \\ & + K^A_{abij}(\gamma_\mu\gamma_5 t_a \tau_i \otimes \gamma^\mu\gamma_5 t_b \tau_j).\end{aligned} \tag{5.1}$$

The coefficients K_{abij} can be read from the color-octet interaction (4.4) and are given by:

$$\begin{gathered}K^S_{abij} = -\frac{3}{16}G, \quad K^P_{abij} = -\frac{3}{16}G, \\ K^V_{abij} = \frac{3}{32}G, \quad i,j \neq 0, \quad K^V_{ab00} = -\frac{229}{288}G, \quad K^A_{abij} = \frac{3}{32}G.\end{gathered} \tag{5.2}$$

An explicit expression for the $\mathcal{T}$-matrix is given by

$$\mathcal{T}(q) = \mathcal{K} + i\mathrm{Tr}\int\frac{\mathrm{d}^4p}{(2\pi)^4}[\mathcal{K}S(p)\mathcal{T}(q)S(p-q)]. \tag{5.3}$$

The integral in Eqn. (5.3) is divergent and has to be regularized. We can make the following ansatz for the $\mathcal{T}$-matrix:

$$\mathcal{T} = T(\Gamma, \Gamma')_{abij}(\Gamma t_a \tau_i \otimes \Gamma' t_b \tau_j). \tag{5.4}$$

The formal solution reads

$$T = \frac{K}{1 - JK}, \tag{5.5}$$

where

$$J(\Gamma, \Gamma')_{abij} = i\mathrm{Tr} \int \frac{\mathrm{d}^4 p}{(2\pi)^4} \left[\Gamma t_a \tau_i S(p + q/2) \Gamma' t_b \tau_j S(p - q/2)\right], \tag{5.6}$$

are the color-octet generators of the correlation functions characterized by the Dirac matrices Γ, Γ', the color matrices t_a, t_b and the flavor matrices τ_i, τ_j. The trace is taken in Dirac-, color- and flavor-space.

We can use the longitudinal projection operator $L_{\mu\nu} = q_\mu q_\nu / q^2$ and the transversal projection operator $T_{\mu\nu} = g_{\mu\nu} - q_\mu q_\nu / q^2$ to project out the spin 0 and spin 1 parts of the interaction kernel $\mathcal{K}$:

$$\mathcal{K}_s = K^S_{ij}(I_D \tau_i \otimes I_D \tau_j) + K^A_{ij}(-i\gamma_\mu \hat{q}^\mu \tau_i \otimes i\gamma_\nu \hat{q}^\nu \tau_b), \tag{5.7}$$

$$\mathcal{K}_p = K^P_{ij}(i\gamma_5 \tau_i \otimes i\gamma_5 \tau_j) + K^A_{ij}(-i\gamma_\mu \gamma_5 \hat{q}^\mu \tau_i \otimes i\gamma_\nu \gamma_5 \hat{q}^\nu \tau_j), \tag{5.8}$$

$$\mathcal{K}_v = T^\mu_\nu K^V_{ij}(\gamma_\mu \tau_i \otimes \gamma^\nu \tau_j), \tag{5.9}$$

$$\mathcal{K}_a = T^\mu_\nu K^A_{ij}(\gamma_\mu \gamma_5 \tau_i \otimes \gamma^\nu \gamma_5 \tau_j), \tag{5.10}$$

with $\hat{q}_\mu = q_\mu / \sqrt{q^2}$. Note, that we inserted $-i \cdot i = 1$ in the first two equations. $\mathcal{K}_s$, $\mathcal{K}_p$, $\mathcal{K}_v$ and $\mathcal{K}_a$ are the scalar, pseudoscalar, vector and axial vector parts of the kernel $\mathcal{K}$, respectively. The scattering matrix separates into four independent Dirac channels:

$$\mathcal{T}(q) = \mathcal{T}_s(q) + \mathcal{T}_p(q) + \mathcal{T}_v(q) + \mathcal{T}_a(q). \tag{5.11}$$

Consequently the Bethe-Salpeter equation can be separated into four independent equations in color- and flavor space. The correlation matrix is given for each of the four channels by (5.6). Γ, Γ' are the corresponding Dirac matrices.

The zeroes of $1 - JK$ represent the singularities of the quark-antiquark T-matrix in the various color-octet channels. These singularities define the masses of the color-octet modes. For each scalar, pseudoscalar, vector or axial vector channel, these masses are determined by the set of conditions

$$D(q) \equiv \det[1 - JK] = 0 \quad \text{at} \quad q^2 = m^2. \tag{5.12}$$

where each $D(q)$ is specified by a given color-octet channel. Non-diagonal elements of $1 - JK$ appear as a consequence of flavor singlet-triplet mixing and/or mixing of different channels in Dirac space.

5.1.1 Pseudoscalar-isovector channel

First we discuss the pseudoscalar-isovector channel, which is the color-octet 'pionic' channel. The correlation matrix elements are given by

$$\begin{aligned} J(\Gamma,\Gamma') &= i\mathrm{Tr}\int\frac{\mathrm{d}^4p}{(2\pi)^2}\Gamma t_a\tau_i S(p+q/2)\Gamma' t_b\tau_j S(p-q/2) \\ &= i4\mathrm{tr}\int\frac{\mathrm{d}^4p}{(2\pi)^2}\Gamma S(p+q/2)\Gamma' S(p-q/2), \end{aligned} \tag{5.13}$$

where Tr denotes the trace in flavor-, color- and Dirac-space, while tr denotes the trace in Dirac-Space only. The trace in color space is $\mathrm{tr}[t_at_b]=2\delta_{ab}$ and the trace in flavor space is $\mathrm{tr}[\tau_i\tau_j]=2\delta_{ij}$. We can express Eqn. (5.13) using the elementary integrals [KLVW90]

$$I_1(m) \equiv i16\int^\Lambda\frac{\mathrm{d}^4p}{(2\pi)^4}\frac{1}{p^2-m^2+i\epsilon}, \tag{5.14}$$

$$I_2(q^2,m_1,m_2) \equiv i8\int^\Lambda\frac{\mathrm{d}^4p}{(2\pi)^4}\frac{1}{(p+q/2)^2-m_1^2+i\epsilon}\frac{1}{(p-q/2)^2-m_2^2+i\epsilon}, \tag{5.15}$$

where we have introduced a covariant Euclidean cutoff

$$\int^\Lambda\frac{\mathrm{d}^4p}{(2\pi)^4} \equiv \int\frac{\mathrm{d}^4p}{(2\pi)^4}\theta(\Lambda^2-p_0^2-\boldsymbol{p}^2). \tag{5.16}$$

As an exception we work here with a covariant Euclidean cutoff since this cutoff scheme allows to give explicit analytic expressions for the elementary integrals. We will employ the following set of parameters for these calculations: $\Lambda = 1.015$ GeV, $G = 7.626$ GeV^{-2} and $m_0 = 5.5$ MeV [Kle92]. To preserve the Ward-Takahashi identity, the same regularization scheme has to be applied to the gap equation.

The integral I_1 can be calculated easily and gives the following analytic expression:

$$I_1(m) = \frac{1}{\pi^2}\left[\Lambda^2 - m^2\log\left(1+\frac{\Lambda^2}{m^2}\right)\right]. \tag{5.17}$$

By performing a Wick-rotation and using Feynman parameters, the integral I_2 can be written as

$$I_2(q^2,m_1,m_2) = \frac{1}{2\pi^2}\int_0^1\mathrm{d}z\left(\frac{\Lambda^2}{\Lambda^2+y}+\log\frac{y}{\Lambda^2+y}\right), \tag{5.18}$$

with $y = q^2(z^2-z)+m_1^2-z(m_1^2-m_2^2)$. We can perform an integration in the complex z-plane to obtain (for $m_1 < m_2$):

- $q^2 < (m_1+m_2)^2$:

$$\begin{aligned} I_2(q^2,m_1,m_2) =& \frac{1}{2\pi^2}\left[\omega\log\frac{m_1^2}{m_1^2+\Lambda^2} + 2\sqrt{\frac{4m_1^2-q^2\omega^2}{q^2}}\arctan\sqrt{\frac{q^2\omega^2}{4m_1^2-q^2\omega^2}}\right. \\ &\left. + \frac{q^2\omega^2-2\Lambda^2-4m_1^2}{\sqrt{q^2(m_1^2+\Lambda^2)-\frac{q^4\omega^2}{4}}}\arctan\sqrt{\frac{q^2\omega^2}{4(m_1^2+\Lambda^2)-q^2\omega^2}}\right]. \end{aligned} \tag{5.19}$$

- $(m_1+m_2)^2 < q^2 < 4(\Lambda^2+m_1^2)$:

$$\begin{aligned}\mathrm{Re}\, I_2(q^2,m_1,m_2) =& \frac{1}{2\pi^2}\Bigg[\omega \log\frac{m_1^2}{m_1^2+\Lambda^2} + 2\sqrt{\frac{q^2\omega^2-4m_1^2}{q^2}}\log\frac{q\omega+\sqrt{q^2\omega^2-4m_1^2}}{q\omega-\sqrt{q^2\omega^2-4m_1^2}} \\ &+ \frac{q^2\omega^2-2\Lambda^2-4m_1^2}{\sqrt{q^2(m_1^2+\Lambda^2)-\frac{q^4\omega^2}{4}}}\arctan\sqrt{\frac{q^2\omega^2}{4(m_1^2+\Lambda^2)-q^2\omega^2}}\Bigg],\end{aligned} \tag{5.20}$$

$$\mathrm{Im}\, I_2(q^2,m_1,m_2) = -\frac{1}{2\pi}\sqrt{\frac{q^2\omega^2-4m_1^2}{q^2}}, \tag{5.21}$$

with $\omega \equiv 1+\frac{m_1^2-m_2^2}{q^2}$.

The correlation integrals for the pseudoscalar-isovector channel are then given by

$$J(i\gamma_5, i\gamma_5) \equiv J_{PP} = I_1(m) - q^2 I_2(q^2,m,m), \tag{5.22}$$
$$J(i\gamma_5, -i\gamma_\mu\gamma_5\hat{q}^\mu) \equiv J_{PA} = 2qmI_2(q^2,m,m), \tag{5.23}$$
$$J(i\gamma_\mu\gamma_5\hat{q}^\mu, -i\gamma_5) \equiv J_{AP} = 2qmI_2(q^2,m,m), \tag{5.24}$$
$$J(i\gamma_\nu\gamma_5\hat{q}^\nu, -i\gamma_\mu\gamma_5\hat{q}^\mu) \equiv J_{AA} = -4m^2 I_2(q^2,m,m), \tag{5.25}$$

and the matrix equation in this channel reads

$$\begin{pmatrix} T_{PP} & T_{PA} \\ T_{AP} & T_{AA} \end{pmatrix} = \begin{pmatrix} K_P & 0 \\ 0 & K_A \end{pmatrix}\left[\begin{pmatrix} 1 & 0 \\ 0 & 1 \end{pmatrix} + \begin{pmatrix} J_{PP} & J_{PA} \\ J_{AP} & J_{AA} \end{pmatrix}\begin{pmatrix} T_{PP} & T_{PA} \\ T_{AP} & T_{AA} \end{pmatrix}\right]. \tag{5.26}$$

The solutions for the $\mathcal{T}$-matrix elements are given by

$$T_{PP} = \frac{K_P}{D_{PP}(q^2)}(1-K_A J_{AA}), \tag{5.27}$$
$$T_{PA} = T_{AP} = \frac{K_A K_P J_{PA}}{D_{PP}(q^2)}, \tag{5.28}$$
$$T_{AA} = \frac{K_A}{D_{PP}(q^2)}(1-K_P J_{PP}), \tag{5.29}$$

with

$$D_{PP}(q^2) = (1-K_P J_{PP})(1-K_A J_{AA}) - K_A K_P (J_{PA})^2. \tag{5.30}$$

The $\mathcal{T}$-matrix is real below $q^2 < 4\,m^2$ and becomes complex above this threshold. The masses of possible bound states below the quark-antiquark threshold $q^2 < 4\,m^2$ are determined by the zeros of the function D_{PP}. In the following we present results for D_{PP}, for the real part of the scattering matrix $\mathrm{Re}\, T_{PP}$ and the imaginary part $\mathrm{Im}\, T_{PP}$ as a function of the four-momentum squared q^2. $D_{PP}(q^2)$ is shown in Fig. 5.1. Obviously there are no bound states below the quark-antiquark threshold because the interaction in this channel is repulsive. The real and the imaginary part of the scattering matrix is shown in Fig. 5.2. Apparently there is a resonance structure, however the corresponding mass of the pseudoscalar-isovector color-octet mode is far above the cutoff of the theory. A lower bound for the mass is given by $m \sim 2$ GeV.

5.1.2 Scalar-isovector channel

In this section the scalar-isovector channel is studied, which is the color-octet 'sigma' channel. The correlation matrix is given by Eqn. (5.6). Its only non-vanishing element is

$$J(I_D, I_D) = I_1(m) + (m^2 - q^2) I_2(q^2, m, m). \tag{5.31}$$

The solution for the T-matrix in this channel reads

$$T_{SS} = \frac{K_S}{D_{SS}(q^2)}, \tag{5.32}$$

with

$$D_{SS}(q^2) = 1 - K_S J_{SS}. \tag{5.33}$$

Again, $D_{SS}(q^2)$ determines the masses of bound quark-antiquark pairs below the threshold $q^2 < 4\,m^2$. The results for $D_{SS}(q^2)$, $\mathrm{Re}\,T_{SS}(q^2)$ and $\mathrm{Im}\,T_{SS}(q^2)$ are shown in Figs. 5.3 and 5.4. The form of these functions is similar to pseudoscalar-isovector case. There are no bound states below the quark-antiquark threshold. A scalar resonance with a mass far above the cutoff of the theory is observed. A lower bound for the mass of the scalar resonance is again given by $m \sim 2$ GeV.

5.1.3 Vector-isovector channel

Next we study the correlation matrix for the vector-isovector channel. It also has only one non-vanishing element which is given by

$$\begin{aligned} J^{(T)}_{VV} T^{\mu}_{\ \nu} &\equiv J(T_{\nu\beta}\gamma^{\beta}, T^{\mu\alpha}\gamma_{\alpha}), \\ J_{VV} &= \frac{2}{3}[(2m^2 + q^2) I_2 - 2m^2 I_2^0], \end{aligned} \tag{5.34}$$

where $I_2^0 \equiv I_2(q^2 = 0)$. The solution of the T-matrix in this channel reads

$$T_{VV} = -\frac{K_V}{D_{VV}(q^2)}, \tag{5.35}$$

with

$$D_{VV}(q^2) = 1 - K_V J_{VV}. \tag{5.36}$$

The results for $D_{VV}(q^2)$, $\mathrm{Re}\,T_{VV}(q^2)$ and $\mathrm{Im}\,T_{VV}(q^2)$ are presented in Figs. 5.5 and 5.6. Again there are no bound states below the quark-antiquark threshold and the mass of the vector resonance is even higher then the corresponding masses of the pseudoscalar and scalar resonances. However, its width is notably smaller.

5.1.4 Axial vector-isovector channel

The axial vector-isovector channel behaves like the vector-isovector channel. The only non-vanishing element of the correlation matrix is

$$J_{AA}^{(T)} = \frac{2}{3}[(-4m^2 + q^2)I_2 - 2m^2 I_2^0]. \tag{5.37}$$

The solution for the T-matrix is given by

$$T_{SS} = -\frac{K_A}{D_{AA}(q^2)}, \tag{5.38}$$

with

$$D_{AA}(q^2) = 1 - K_A J_{AA}. \tag{5.39}$$

The results for $D_{AA}(q^2)$, $\mathrm{Re}\, T_{AA}(q^2)$ and $\mathrm{Im}\, T_{AA}(q^2)$ are presented in Figs. 5.7 and 5.8. Again there is no bound state below the quark-antiquark threshold. A axial vector resonance with a mass similar to the mass of the vector resonance is observed far above the cutoff of the theory.

5.2 Non-zero temperatures and densities

In this section we study the change of the masses of the color-octet modes at finite temperature and finite quark chemical potential. In this section we will regularize all divergent integrals with a three-momentum cutoff and we will use the Matsubara formalism to evaluate the correlation matrix elements

$$J(\Gamma, \Gamma') = i\mathrm{Tr} \int \frac{\mathrm{d}^4 p}{(2\pi)^2} \Gamma t_a \tau_i S(p) \Gamma' t_b \tau_j S(p-q) \tag{5.40}$$

at finite temperature. The correlation matrix elements for the various combinations of Dirac-, color- and flavor matrices can again be expressed in terms of the elementary integrals

$$I_1(m) \equiv i16 \int \frac{\mathrm{d}^4 p}{(2\pi)^4} \frac{1}{p^2 - m^2 + i\epsilon}, \tag{5.41}$$

$$I_2(q^2, m_1, m_2) \equiv i8 \int \frac{\mathrm{d}^4 p}{(2\pi)^4} \frac{1}{(p + q/2)^2 - m_1^2 + i\epsilon} \frac{1}{(p - q/2)^2 - m_2^2 + i\epsilon}. \tag{5.42}$$

At finite temperature and non-zero quark chemical potential, the following expressions are obtained for Eqn. (5.41) and (5.42):

$$\begin{aligned} I_1(m) &= \frac{4}{\pi^2} \int_m^{\Lambda_E} \mathrm{d}E \sqrt{p^2 - m^2} [1 - f_D^+(E) - f_D^-(E)], \\ I_2(q^2, m) &= \mathcal{P} \frac{4}{\pi^2} \int_m^{\Lambda_E} \mathrm{d}E \frac{\sqrt{E^2 - m^2}(1 - f_D^+(E) - f_D^+(E))}{q_0^2 - 4E^2} \\ &\quad - \frac{i}{2\pi q_0} \sqrt{q_0^2 - 4m^2} \left[1 - f_D^+\left(\frac{q_0}{2}\right) - f_D^-\left(\frac{q_0}{2}\right)\right] \theta[(2\Lambda_E - q_0)(q_0 - 2m)]. \end{aligned} \tag{5.43}$$

At zero temperature and vanishing quark chemical potential the results are similar to those we have discussed in the previous section, using a four-momentum cutoff. There are no bound states below the quark-antiquark threshold and a resonance structure can be clearly seen in the plots of the real and imaginary parts of the associated scattering matrices.

At finite temperature and quark chemical potential, the mass of the pseudoscalar resonance is to good approximation given by

$$m \approx 2\Lambda_E = 2\sqrt{\Lambda^2 + M^2}. \tag{5.44}$$

Consequently, a decrease of the mass of the pseudoscalar resonance related to the drop of the constituent quark mass when chiral symmetry is restored, is observed. For large temperatures or chemical potentials, the mass of the pseudoscalar resonances is given by $m \approx 2\Lambda$. The mass of the pseudoscalar resonance as a function of temperature and quark chemical potential is shown in Fig. 5.9. The masses of the scalar, vector and axial vector resonances behave similarly.

5.3 Summary

In this chapter we have studied the color-octet sector of the NJL model. One of the shortcomings of this model is that it does not confine quarks because the gluon dynamics is integrated out and replaced by pointlike couplings between the quarks. However, one of the key properties of QCD is color confinement, which means that quarks at low energies have to be part of bound color-singlet states. In this chapter we have shown that, although the NJL model does not explicitly confine quarks, the mass of color-octet modes are of order $\mathcal{O}(2\text{ GeV})$, much larger than the cutoff of the theory which is of order $\mathcal{O}(650\text{ MeV})$. Thus, all color-octet modes are far removed from the low-energy spectrum of the theory and the NJL model is consistent with the observed particle spectrum. This does not change qualitatively at finite temperature and non-zero quark chemical potential.

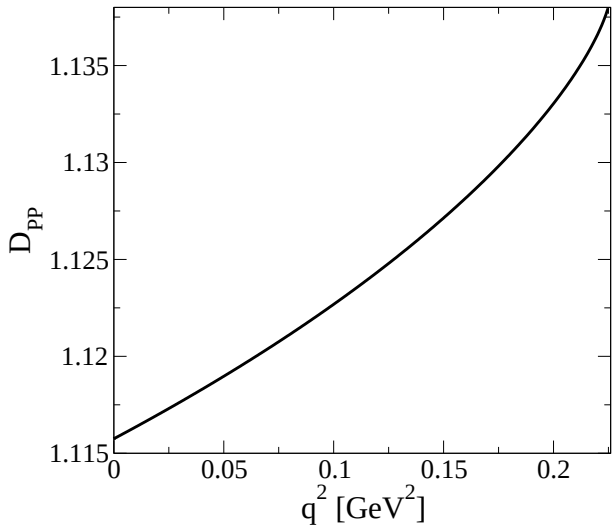

Figure 5.1: $D_{PP}(q^2)$ for the pseudoscalar-isovector channel below the quark-antiquark threshold.

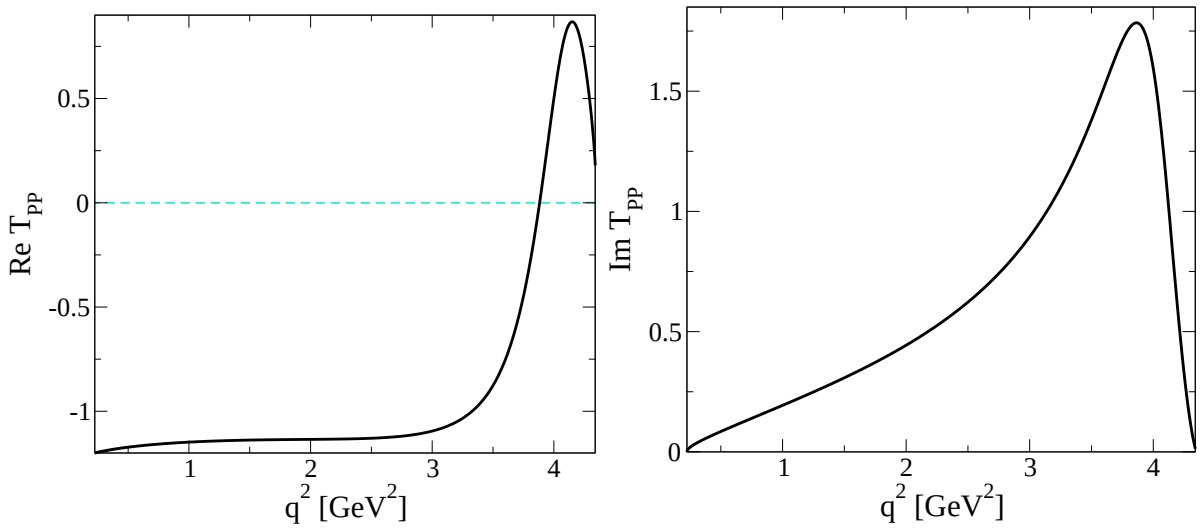

Figure 5.2: Re $T_{PP}(q^2)$ and Im $T_{PP}(q^2)$ for the pseudoscalar-isovector channel above the quark-antiquark threshold.

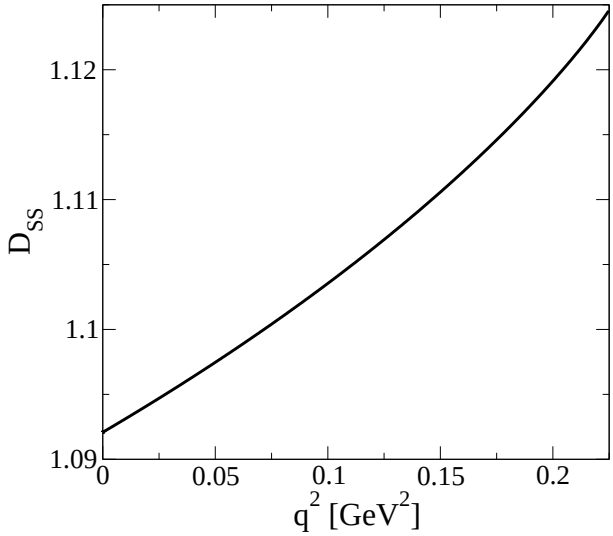

Figure 5.3: $D_{SS}(q^2)$ for the scalar-isovector channel below the quark-antiquark threshold.

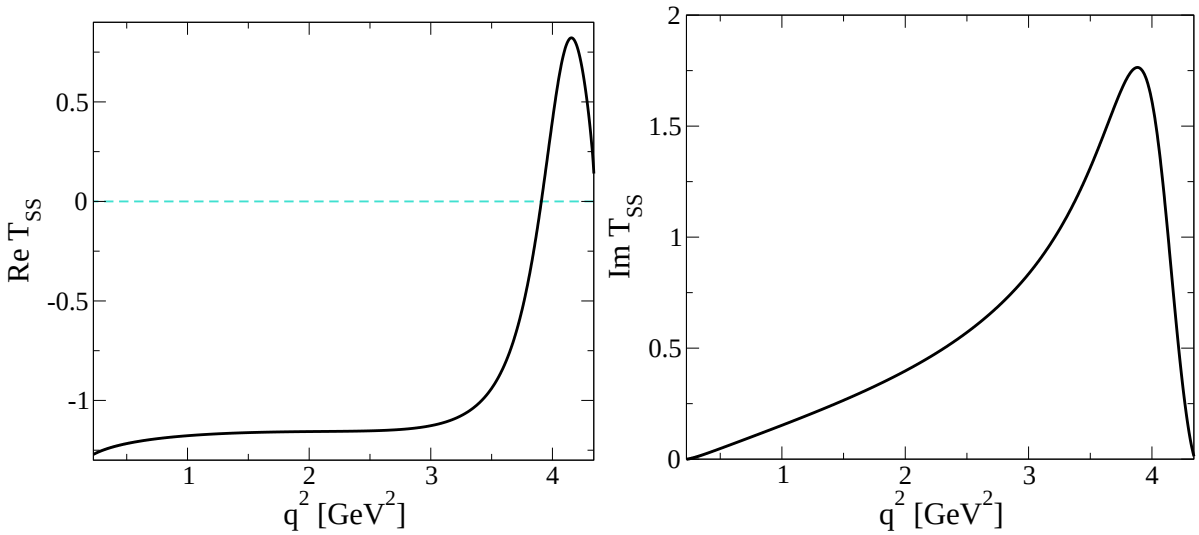

Figure 5.4: Re $T_{SS}(q^2)$ and Im $T_{SS}(q^2)$ for the scalar-isovector channel above the quark-antiquark threshold.

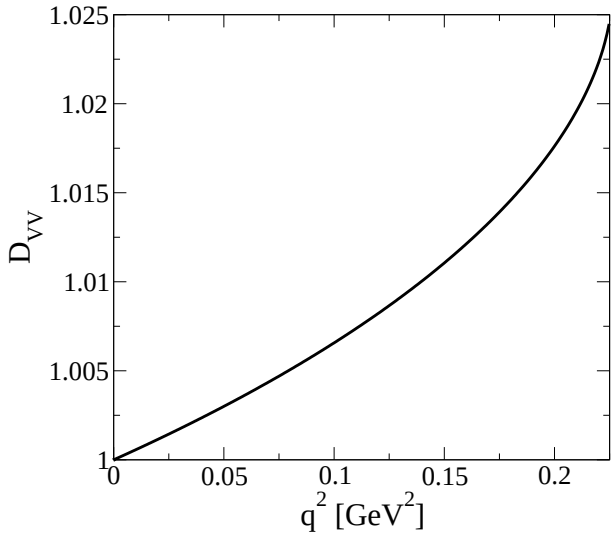

Figure 5.5: $D_{VV}(q^2)$ for the vector-isovector channel below the quark-antiquark threshold.

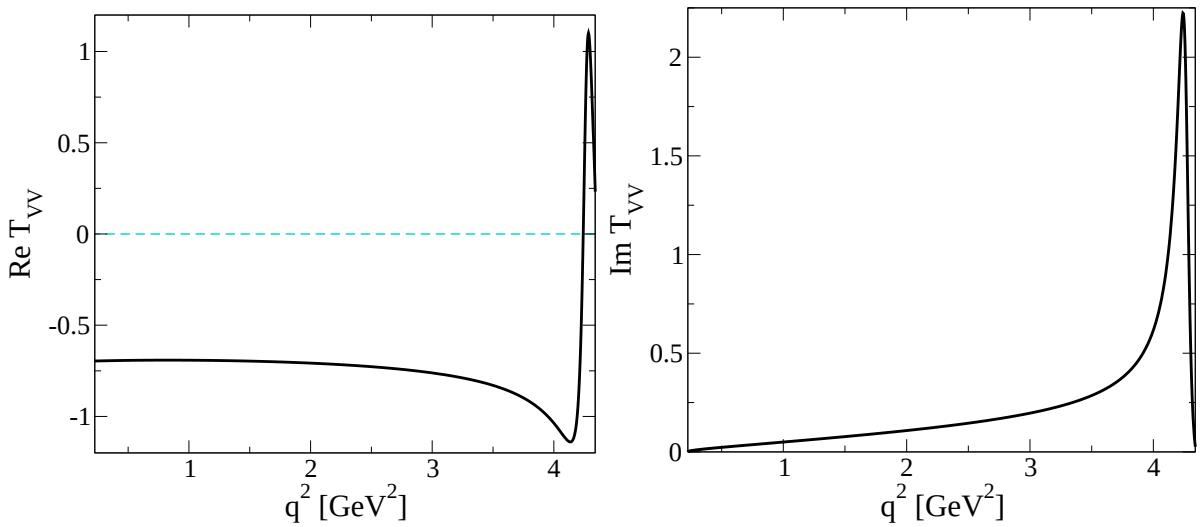

Figure 5.6: Re $T_{VV}(q^2)$ and Im $T_{VV}(q^2)$ for the vector-isovector channel above the quark-antiquark threshold.

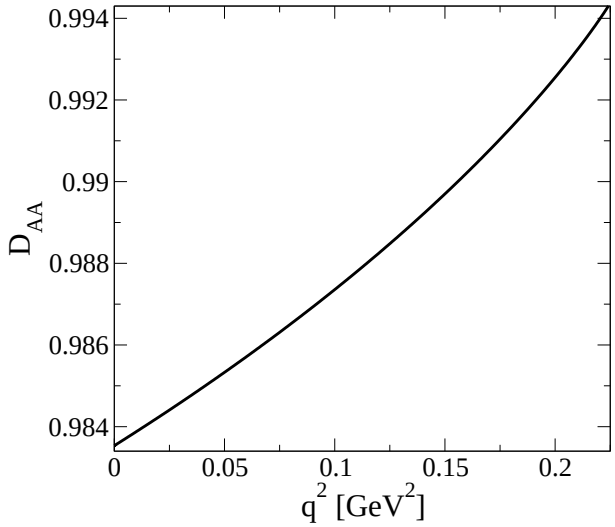

Figure 5.7: $D_{AA}(q^2)$ for the axial vector-isovector channel below the quark-antiquark threshold.

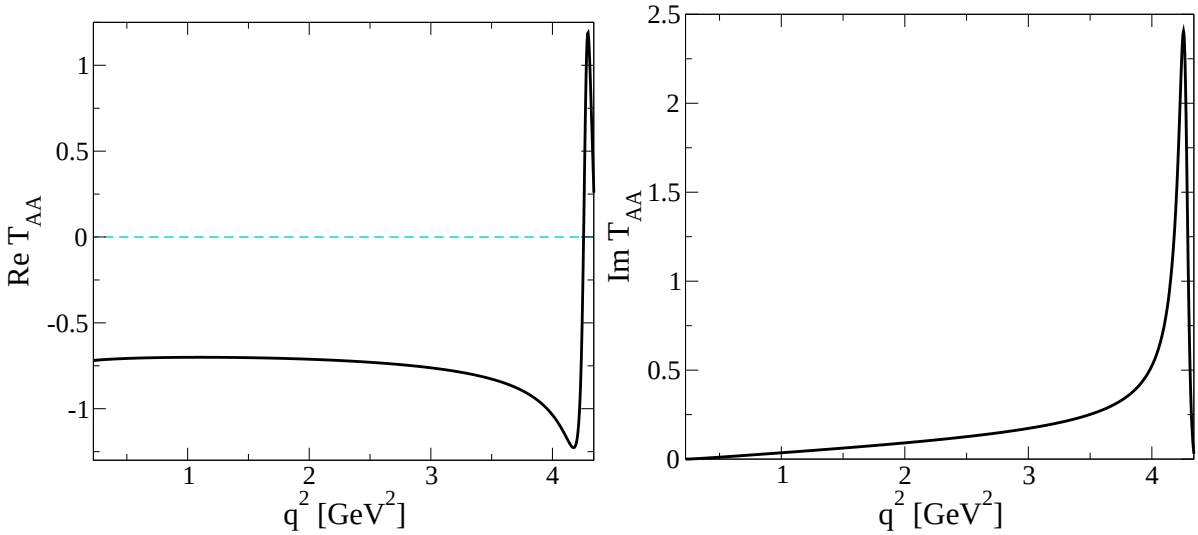

Figure 5.8: Re $T_{AA}(q^2)$ and Im $T_{AA}(q^2)$ for the axial vector-isovector channel above the quark-antiquark threshold.

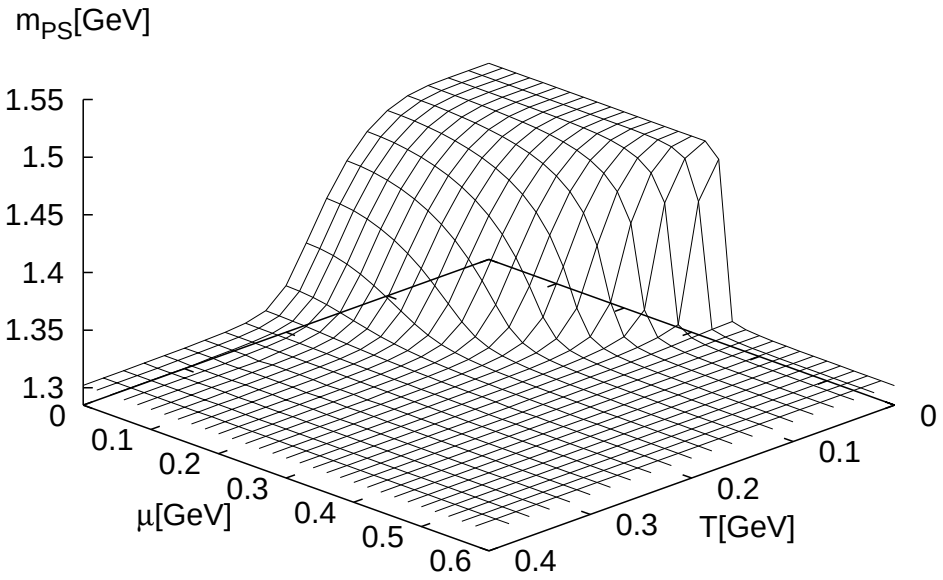

Figure 5.9: The mass m_{PS} of the pseudoscalar color-octet resonance as function of temperature and quark chemical potential.

Chapter 6

Nambu–Jona-Lasinio Model with Confinement

Bulk thermodynamical quantities at vanishing and finite quark chemical potential are remarkably well reproduced by the generalized confinement quasiparticle model which we have developed in chapter 3. In chapter 4 and 5 we then turned to a more microscopic description of the QGP. The basis for this was the NJL model, an effective Lagrangian of relativistic quarks interacting through local fermion-fermion couplings. This Lagrangian can in principle be obtained from QCD by "integrating out" the gluonic degrees of freedom, replacing them by local four-point color-current interactions. The NJL model incorporates many of the symmetries and symmetry breaking patterns of QCD, in particular the chiral symmetry and its spontaneous breaking at low temperatures. However, it does not confine quarks and thus allows for colored quark-antiquark excitations which have never been observed in nature. In chapter 5 we have shown that such colored modes are far removed from the low-energy spectrum of the theory and that the NJL model is consistent with the observed particle spectrum. On the other hand, for the physics close to the phase transition confinement is the driving force. Thus, the NJL model cannot reproduce lattice QCD thermodynamical quantities in this temperature regime.

Since confinement simply reduces the number of thermally active degrees of freedom in a statistical sense, it can be incorporated in a model of free massive quasiparticles by a modification of the particle distribution functions with a confinement factor $C(T, \mu)$. This function parametrizes our ignorance about details of the confinement mechanism. However, it would be desirable to construct a more microscopic description of the confinement process that then can be used to calculate thermodynamical quantities. This is the aim of the current chapter. Our starting point is the heavy-quark limit, in which the confinement-deconfinement phase transition is well defined and an order parameter, the so-called Polyakov loop, can be established. Subsequently we construct an effective theory for the Polyakov loop and study its thermodynamic properties. If quarks are added no order parameter can be established, but the Polyakov loop still changes rapidly close to T_c and serves as an indicator of a rapid crossover towards deconfinement. For a complete discussion of QCD at finite temperature, we must also incorporate the chiral symmetry breaking and its restoration at high temperatures. To this end, we introduce a generalized two-flavor NJL Lagrangian with quarks coupled to a (spatially

constant) temporal background $SU(3)$ gauge field representing Polyakov loop dynamics. This Polyakov loop extended (PNJL) model incorporates both chiral symmetry restoration and confinement. We test the effectiveness of the PNJL approach by confronting it with lattice QCD thermodynamics. The main body of this work has been published in [RTW05].

6.1 Center symmetry

The confinement-deconfinement phase transition of QCD is only well-defined in the heavy-quark limit $m_q \to \infty$. In this case, the confined and deconfined phases are characterized by distinct symmetry properties: the $Z(3)$ center symmetry of the $SU(3)$ gauge group is spontaneously broken in the deconfined phase, while it is restored in the confined phase [tH78]. The associated order parameter is the Polyakov loop, a Wilson line closed around the periodic Euclidean time direction [Pol78, Sus79]. In this section we discuss the symmetry properties of the QCD Lagrangian in the heavy-quark limit. We introduce topological non-trivial gauge transformations and show how they give rise to the $Z(3)$ center symmetry of QCD [HW00]. Finally we introduce the Polyakov loop as the order parameter associated with the center symmetry.

In the limit $m_q \to \infty$ the QCD Lagrangian (1.1) reduces to

$$\mathcal{L}_{\text{Gauge}} = -\frac{1}{2}\text{Tr}(G_{\mu\nu}G^{\mu\nu}). \tag{6.1}$$

The partition function can be expressed in terms of the Euclidean path integral

$$\mathcal{Z} = \int \mathcal{D}A \exp\left(-\int_0^\beta \mathrm{d}\tau \int_V \mathrm{d}^3x\, \mathcal{L}^E_{\text{Gauge}}\right), \tag{6.2}$$

where $\mathcal{L}^E_{\text{Gauge}}$ is the Euclidean version of (6.1). Since we will always work in Euclidean space in the following, we will omit the superscript from now on. The measure $\mathcal{D}A$ in the path integral (6.2) contains fields that obey periodic boundary conditions [Kap89, Bel96],

$$A_\mu(\boldsymbol{x}, \tau + \beta) = A_\mu(\boldsymbol{x}, \tau). \tag{6.3}$$

Under a local gauge transformation $g(x) = e^{i\omega_a(x)t_a}$ with arbitrary real functions $\omega_a(x)$, the gluon field transforms as

$${}^gA_\mu = g(A_\mu + \partial_\mu)g^\dagger. \tag{6.4}$$

Consequently, the field strength tensor transforms as

$${}^gG_{\mu\nu} = gG_{\mu\nu}g^\dagger, \tag{6.5}$$

and the Lagrangian (6.1) is invariant because

$$\text{Tr}\,{}^gG_{\mu\nu}{}^gG_{\mu\nu} = \text{Tr}\, gG_{\mu\nu}g^\dagger gG_{\mu\nu}g^\dagger = \text{Tr}\, G_{\mu\nu}G_{\mu\nu}. \tag{6.6}$$

Here we used $gg^\dagger = \mathbf{1}$ and the fact that the trace is cyclic. In order to maintain the boundary condition (6.3) for the vector potential, we first consider gauge transformations that are strictly periodic in Euclidean time:

$$g(\boldsymbol{x}, \tau + \beta) = g(\boldsymbol{x}, \tau). \tag{6.7}$$

Thus, a strictly periodic vector potential transforms as

$$\begin{aligned} {}^gA_\mu(\boldsymbol{x}, \tau + \beta) &= g(\boldsymbol{x}, \tau + \beta)(A_\mu(\boldsymbol{x}, \tau + \beta) + \partial_\mu)g^\dagger(\boldsymbol{x}, \tau + \beta) \\ &= g(\boldsymbol{x}, \tau)(A_\mu(\boldsymbol{x}, \tau) + \partial_\mu)g^\dagger(\boldsymbol{x}, \tau) \\ &= {}^gA_\mu(\boldsymbol{x}, \tau). \end{aligned} \tag{6.8}$$

However, in addition there are topologically non-trivial gauge transformations [tH78] that also preserve the boundary condition (6.3). These gauge transformations are periodic up to a constant twist matrix z in the center $Z(3)$ of $SU(3)$:

$$g(\boldsymbol{x}, \tau + \beta) = zg(\boldsymbol{x}, \tau). \tag{6.9}$$

The elements of the center of a group commute with all elements of the group. For $SU(3)$ they are given by

$$z = e^{\frac{2\pi i n}{3}}\mathbf{1}, \quad n \in \{1, 2, 3\}. \tag{6.10}$$

Under such a twisted transformation, a strictly periodic vector potential transforms as

$$\begin{aligned} {}^gA_\mu(\boldsymbol{x}, \tau + \beta) &= g(\boldsymbol{x}, \tau + \beta)(A_\mu(\boldsymbol{x}, \tau + \beta) + \partial_\mu)g^\dagger(\boldsymbol{x}, \tau + \beta) \\ &= zg(\boldsymbol{x}, \tau)(A_\mu(\boldsymbol{x}, \tau) + \partial_\mu)g^\dagger(\boldsymbol{x}, \tau)z^\dagger \\ &= z\,{}^gA_\mu(\boldsymbol{x}, \tau)z^\dagger \\ &= {}^gA_\mu(\boldsymbol{x}, \tau). \end{aligned} \tag{6.11}$$

In the last line we used the fact that z is an element of the center of $SU(3)$.

The $Z(3)$ symmetry gets explicitly broken in the presence of quark fields, which are anti-periodic in Euclidean time [Kap89, Bel96],

$$\psi(\boldsymbol{x}, \tau + \beta) = -\psi(\boldsymbol{x}, \tau), \tag{6.12}$$

and transform as

$${}^g\psi = g\psi. \tag{6.13}$$

Consequently, under a twisted transformation, the quark fields transform as

$$\begin{aligned} {}^g\psi(\boldsymbol{x}, \tau + \beta) &= g(\boldsymbol{x}, \tau + \beta)\psi(\boldsymbol{x}, \tau + \beta) \\ &= -zg(\boldsymbol{x}, \tau)\psi(\boldsymbol{x}, \tau) \\ &= -z\,{}^g\psi(\boldsymbol{x}, \tau). \end{aligned} \tag{6.14}$$

To maintain the boundary condition (6.12) only $z = 1$ is possible and the center symmetry disappears.

The twisted transformations (6.9) represent a global $Z(3)$ symmetry of the Euclidean gauge action. Unlike the $SU(3)$ gauge symmetry, it can break spontaneously and should not be considered as a subgroup of the local gauge group. The center symmetry is a symmetry of the Euclidean action, not the Hamiltonian. While the Hamiltonian acts at a given instant, the center symmetry transformations are characterized by non-trivial boundary conditions in Euclidean time and thus affect the entire time evolution. Hence it is meaningless to ask how states in the physical Hilbert space transform under such transformations. Instead, the center symmetry is a symmetry of the spatial transfer matrix, which acts on a different Hilbert space. At finite temperature the spatial transfer matrix is at least as useful as the Hamiltonian, because its spectrum is sensitive to temperature, while the spectrum of the Hamiltonian is not.

6.2 The Polyakov loop as an order parameter for deconfinement

A system of gluons may be probed using an infinitely heavy test quark which does not break the $Z(3)$ center symmetry. The operator that describes such a static quark is a Wilson loop winding around the periodic imaginary time direction, the so-called Polyakov loop [Pol78, Sus79]:

$$\Phi(\boldsymbol{x}) = \frac{1}{3}\mathrm{Tr}\left[\mathcal{P}\exp\left(i\int_0^\beta \mathrm{d}\tau A_4(\boldsymbol{x},\tau)\right)\right]. \tag{6.15}$$

Here $\mathcal{P}$ denotes path ordering of the exponential and $A_4 = iA^0$ is the temporal component of the Euclidean gauge field $(\boldsymbol{A}, A_4)$. The Polyakov loop is a complex scalar field that depends on the spatial position $\boldsymbol{x}$ of the static color source. It transforms non-trivially under twisted $Z(3)$ transformations:

$$\begin{aligned}
{}^g\Phi(\boldsymbol{x}) &= \frac{1}{3}\mathrm{Tr}\left[\mathcal{P}\exp\left(i\int_0^\beta \mathrm{d}\tau\, {}^gA_4(\boldsymbol{x},\tau)\right)\right] \\
&= \frac{1}{3}\mathrm{Tr}\left[g(\boldsymbol{x},\tau+\beta)\mathcal{P}\exp\left(i\int_0^\beta \mathrm{d}\tau A_4(\boldsymbol{x},\tau)\right)g^\dagger(\boldsymbol{x},\tau)\right] \\
&= \frac{1}{3}\mathrm{Tr}\left[zg(\boldsymbol{x},\tau)\mathcal{P}\exp\left(i\int_0^\beta \mathrm{d}\tau A_4(\boldsymbol{x},\tau)\right)g^\dagger(\boldsymbol{x},\tau)\right] = z\Phi(\boldsymbol{x}).
\end{aligned} \tag{6.16}$$

On the other hand, it is invariant under strictly periodic gauge transformations (with $z = 1$) as it should as a gauge invariant physical quantity.

The partition function of a system of gluons in the presence of a static infinitely heavy test quark is given by

$$\mathcal{Z}_Q = \int \mathcal{D}A\,\Phi(\boldsymbol{x})e^{-S_{\mathrm{Gauge}}[A]}, \tag{6.17}$$

where

$$S_{\text{Gauge}} = \int_0^\beta \mathrm{d}\tau \int_V \mathrm{d}^3x \, \mathcal{L}^E_{\text{Gauge}} \tag{6.18}$$

is the Euclidean gauge action. The thermal expectation value of the Polyakov loop,

$$\langle \Phi \rangle = \frac{1}{\mathcal{Z}} \int \mathcal{D}A \, \Phi(\boldsymbol{x}) e^{-S_{\text{Gauge}}[A]} = \frac{\mathcal{Z}_Q}{\mathcal{Z}} = e^{-\beta F}, \tag{6.19}$$

is the ratio of the partition functions of the gluonic systems with and without the external color source and hence measures the free energy F of an external static quark. Therefore, $\langle \Phi \rangle$ is zero in the confined phase in which the free energy of a single quark is infinite. This can be understood as follows: At low temperatures T the extent $\beta = 1/T$ of the Euclidean time direction is large and the Polyakov loop extends through many space-time regions that are essentially uncorrelated in color space. As a consequence, the Polyakov loop behaves essentially as a random variable and its thermal expectation value averages to zero. On the other hand, asymptotic freedom suggests that quarks and gluons become deconfined in the high-temperature phase. Then F is finite and $\langle \Phi \rangle \neq 0$. In that case the Euclidean time direction is short and the Polyakov loop extends only through a small space-time region which is highly correlated in color space. Thus the Polyakov loop picks up a non-zero expectation value.

6.3 The Polyakov loop model

In this section we will construct an effective theory for the Polyakov loop. We will mainly follow [Sve86] here. In principle, one can imagine to integrate out the gluon fields and derive an effective action for the Polyakov loop directly from the underlying $SU(3)$ gauge theory:

$$e^{-S_{\text{eff}}[\Phi]} = \int \mathcal{D}A \, \delta\left[\Phi(\boldsymbol{x}) - \frac{1}{3}\mathrm{Tr}\, \mathcal{P} e^{i\int_0^\beta \mathrm{d}\tau A_4(\boldsymbol{x},\tau)}\right] e^{-S_{\text{Gauge}}[A]}. \tag{6.20}$$

The δ-functional ensures that $\Phi(\boldsymbol{x})$ obeys Eqn. (6.15). Unfortunately, the resulting effective action is non-local and impossible to compute in practice. However, to calculate the change of bulk thermodynamical quantities close to the confinement-deconfinement transition, it is sufficient to construct a simple effective theory that incorporates the relevant symmetries and symmetry breaking patterns of the original theory and study its properties. The details of this effective theory can then be arranged by comparing its properties with lattice QCD results. S_{eff} in general has the form:

$$\begin{aligned} S_{\text{eff}}[\Phi] = &\int \mathrm{d}^3x \, \mathcal{V}(\Phi(\boldsymbol{x}), \Phi^*(\boldsymbol{x})) + \int \mathrm{d}^3x \int \mathrm{d}^3y \, \Phi^*(\boldsymbol{x}) S_2(\boldsymbol{x}-\boldsymbol{y}) \Phi(\boldsymbol{y}) \\ &+ \int \mathrm{d}^3x \int \mathrm{d}^3y \int \mathrm{d}^3z \int \mathrm{d}^3w \, \Phi^*(\boldsymbol{x}) \Phi^*(\boldsymbol{y}) S_4(\boldsymbol{x},\boldsymbol{y},\boldsymbol{z},\boldsymbol{w}) \Phi(\boldsymbol{z}) \Phi(\boldsymbol{w}) + \cdots . \end{aligned} \tag{6.21}$$

Here, Φ^* is the charge conjugated Polyakov loop. The kernels $S_2, S_4, \ldots$ depend on the temperature of the system and must have a range λ given roughly by the correlation

length ξ of the fields integrated out in (6.20), i. e. , the space-like components A_i. The essential argument for the construction of an effective theory from (6.20) is, that ξ stays finite at the phase transition because the transition is first order and thus all kernels should be short ranged. One can then envisage to integrate out all degrees of freedom at length scales less then λ, hence the effective action becomes

$$S_{\text{eff}}[\Phi] = \int \mathrm{d}^3x \left[(\partial_i\Phi)(\partial_i\Phi^*) + \mathcal{V}(\Phi,\Phi^*)\right]. \tag{6.22}$$

The effective potential $\mathcal{V}(\Phi,\Phi^*)$ can be calculated for asymptotically high temperatures [Wei81, Wei82] and in the strong coupling limit on a lattice [Sve86].

We will not use the asymptotic forms of the effective potential $\mathcal{V}(\Phi,\Phi^*)$ for large T or g_s, but rather construct a simple effective potential that incorporates the $Z(3)$ symmetry and its spontaneous breaking at high temperatures. For illustration, we will first deduce an effective potential for a $U(1)$ gauge theory which also confines on the lattice for strong bare coupling.

The center of $U(1)$ is of course also $U(1)$ and consequently $\mathcal{V}(\Phi,\Phi^*)$ must be symmetric under $\Phi \to e^{i\theta}\Phi$. Therefore, the simplest form for the effective potential is a type of mass term,

$$\mathcal{V}(\Phi,\Phi^*) = m^2\Phi^*\Phi. \tag{6.23}$$

In general, the effective $U(1)$ potential takes the form $\mathcal{V}(\Phi,\Phi^*) = f(\Phi^*\Phi) = f(|\Phi|^2)$. In mean-field approximation fluctuations are neglected and the equilibrium state of the system is represented by the absolute minimum of $\mathcal{V}$. In the low temperature, confined phase the center symmetry is unbroken and the absolute minimum of the effective potential should be $\Phi = 0$. At the critical temperature T_c the absolute minimum moves away from zero, either smoothly or discontinuously, giving rise to a second- or a first-order phase transition, respectively. We cannot distinguish between the two possibilities without further information about $f(|\Phi|^2)$. The simplest possible choice is

$$f(z^2) = az^2 + bz^4 + cz^6, \tag{6.24}$$

with $z^2 = |\Phi|^2$. Suppose a varies rapidly with T while b and c (with $c > 0$) stay roughly constant. If $b < 0$, then the absolute minimum jumps discontinuously as a is varied. This is illustrated in Fig. 6.1. On the other hand, if $b > 0$, then the minimum moves continuously away from $z = 0$ as a passes through zero. $a = 0$ is the critical point in the later case. This is illustrated in Fig. 6.2.

Next we will deduce a simple effective Polyakov loop potential $\mathcal{V}(\Phi,\Phi^*)$ for $SU(3)$ gauge theory. The center of $SU(3)$ is $Z(3)$, so this must be a symmetry of the effective potential. As we have seen, the potential $\mathcal{V}(\Phi,\Phi^*) = f(\Phi^*\Phi) = f(|\Phi|^2)$ is invariant under $U(1)$, of which $Z(3)$ is a subgroup. The simplest terms which are invariant under $Z(3)$, but not $U(1)$ are

$$\Phi^3 + (\Phi^*)^3 \qquad \text{and} \qquad i\left[\Phi^3 - (\Phi^*)^3\right]. \tag{6.25}$$

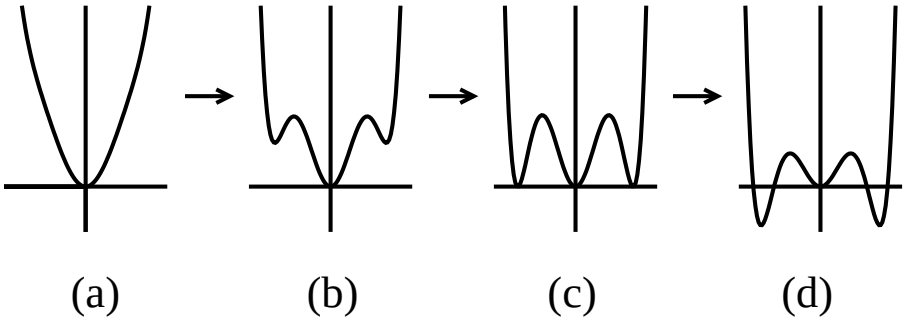

Figure 6.1: The effective $U(1)$ Polyakov loop potential $\mathcal{V}(\Phi, \Phi^*)$ for real Φ and $b < 0$. (a) $a \gg a_{\rm tr}$, where $a_{\rm tr}$ is the value of the coefficient a at the transition: there is a unique minimum at $\Phi = 0$. (b) $a > a_{\rm tr}$: a relative minimum at $\Phi \neq 0$ appears. (c) $a = a_{\rm tr}$: the minima are degenerate. (d) $a < a_{\rm tr}$: the absolute minima are at $\Phi \neq 0$.

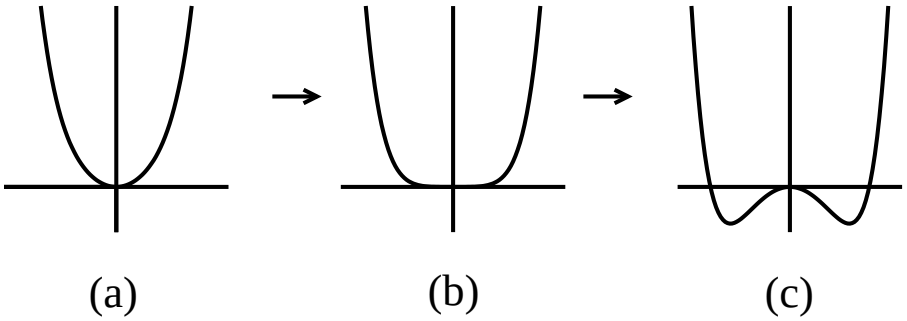

Figure 6.2: The effective $U(1)$ Polyakov loop potential $\mathcal{V}(\Phi, \Phi^*)$ for real Φ and $b > 0$. (a) $a > 0$: there is a unique minimum at $\Phi = 0$. (b) $a = 0$: the critical point, the minima are degenerate. (c) $a < 0$: the absolute minima are at $\Phi \neq 0$.

The factor of i in the second term is added to ensure that in all, the term is real. The charge conjugation symmetry of QCD further restricts the form of the effective potential: gluons are invariant under charge conjugation, under which $A_\mu \to -A_\mu$ and $\Phi \to \Phi^*$. The first term in (6.25) is invariant under charge conjugation, while the second term is not. Thus, in general the effective potential will take the form

$$\mathcal{V}(\Phi, \Phi^*) = f(|\Phi|^2) + g(|\Phi|^2, \mathrm{Re}\,\Phi^3). \tag{6.26}$$

Expanding (6.26) about the origin, with Φ chosen real, we obtain

$$\mathcal{V}(\Phi) = a\Phi^2 + b\,\Phi^3 + c\Phi^4 + \cdots . \tag{6.27}$$

If a is sufficiently large, we find a unique minimum at $\Phi = 0$. If a is decreased, a relative minimum appears at $\Phi \neq 0$, and it becomes the absolute minimum for $a = a_{\rm tr} > 0$. A

first order transition is thus forced by the cubic term, as expected for a $Z(3)$ mean-field theory.

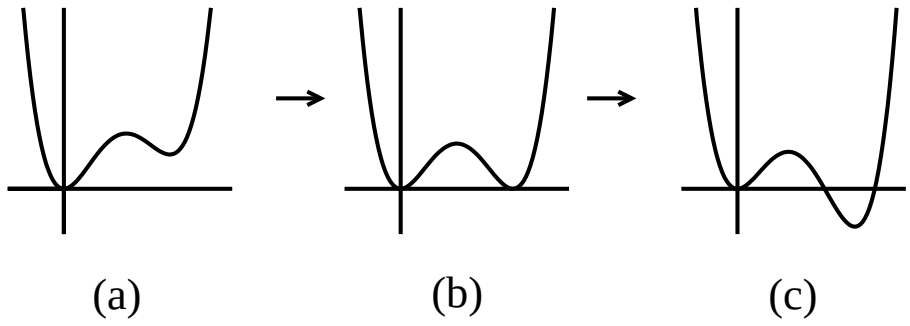

Figure 6.3: The effective $SU(3)$ Polyakov loop potential $\mathcal{V}(\Phi, \Phi^*)$ for real Φ when a cubic term is allowed. (a) $a > a_{\rm tr}$, where $a_{\rm tr}$ is the value of the coefficient a at the transition: there is a unique minimum at $\Phi = 0$ and a relative minimum at $\Phi \neq 0$. (b) $a = a_{\rm tr}$: the minima are degenerate. (c) $a < a_{\rm tr}$: the absolute minima is at $\Phi \neq 0$.

The spontaneous breaking of the center symmetry at high temperatures is also observed in lattice QCD simulations [Sch00]. This is illustrated in Fig. 6.4, where the distribution of the Polyakov loop Φ (in the figure the Polyakov loop is denoted by L) in the complex plane is given for a large sample of configurations. In the black center of the picture the system is in the symmetric phase (at a temperature $T < T_c$) and the Polyakov loop is clustered around the origin of the coordinate system. In the non-symmetric phase ($T > T_c$) the Polyakov loop favors the sector $\mathrm{Re}\,\Phi > 0$ and $\mathrm{Im}\,\Phi = 0$.

6.4 Thermodynamics of the Polyakov loop model

In this section we will construct an effective thermodynamic potential from (6.26), from which thermodynamical quantities like the pressure, the entropy density, the energy density or the Polyakov loop expectation value can be derived. For $N_c = 3$ the Polyakov loop is a complex valued field and we make the ansatz

$$\mathcal{U}(\Phi, \Phi^*; T) = \left[-\frac{b_2(T)}{2}\Phi^*\Phi - \frac{b_3}{6}\left((\Phi^*)^3 + \Phi^3\right) + \frac{b_4}{4}\left(\Phi^*\Phi\right)^2 \right] T^4, \tag{6.28}$$

where $b_2(T)$, b_3 and b_4 are dimensionless coefficients. $b_2(T)$ is a function of the temperature, while b_3 and b_4 are taken to be constants. The Polyakov loop is the trace of a phase factor and hence a dimensionless field. The only scale to make up the correct powers of dimension is the temperature. This accounts for the overall T^4. Lattice simulations for pure gauge QCD show that the Polyakov loop favors the sector $\mathrm{Re}\,\Phi > 0$ and $\mathrm{Im}\,\Phi = 0$ for $T > T_c$ as demonstrated in Fig. 6.4. Consequently, in the following we assume that

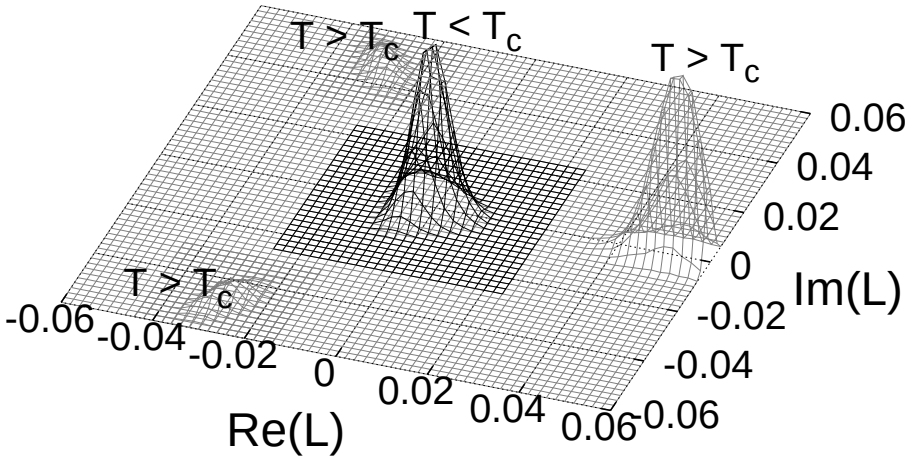

Figure 6.4: The distribution of the Polyakov loop Φ in the complex plane in the symmetric phase (black) and the non-symmetric phase (light gray). In the figure the Polyakov loop is denoted by L. Figure taken from [Sch00].

Φ is real. Eqn. (6.28) then simplifies to

$$\mathcal{U}(\Phi;T) = \left[-\frac{b_2(T)}{2}\Phi^2 - \frac{b_3}{3}\Phi^3 + \frac{b_4}{4}\Phi^4\right] T^4, \tag{6.29}$$

which we will employ in the following. For $b_2(T)$ we make the ansatz

$$b_2(T) = a_0 + a_1\left(\frac{T_0}{T}\right) + a_2\left(\frac{T_0}{T}\right)^2 + a_3\left(\frac{T_0}{T}\right)^3, \tag{6.30}$$

where a_0, a_1, a_2 and a_3 are dimensionless constants and T_0 is the critical temperature for deconfinement. We can fix three of the coefficients a_i and b_i by imposing that the Polyakov loop approaches unity for large temperatures, that the relative minimum $\Phi_{\min} > 0$ becomes the absolute minimum at $T = T_c$ and that the pressure reaches the ideal gas limit for large temperatures. Imposing $\lim_{T\to\infty}\Phi_{\min}(T) = 1$, where

$$\frac{\partial\mathcal{U}(\Phi,T)}{\partial\Phi} = 0 \quad \Longrightarrow \quad \Phi_{\min}(T) = \frac{b_3 + \sqrt{b_3^2 + 4b_2b_4}}{2b_4}, \tag{6.31}$$

is the value of $\Phi(T)$ at the minimum, we find $b_3 = b_4 - a_0$. The constraint that the relative minimum $\Phi_{\min} > 0$ becomes the absolute one at $T = T_c$ fixes a_3:

$$a_3 = -\frac{2a_0^2 + 5a_0b_4 + 9a_1b_4 + 9a_2b_4 + 2b_4^2}{9b_4}. \tag{6.32}$$

Finally, the pressure of a gas of gluons should approach the Stefan-Boltzmann limit for high temperatures $T \to \infty$. This fixes b_4:

$$b_4 = \frac{2}{15}(16\pi^2 - 15a_0). \tag{6.33}$$

The remaining coefficients a_0, a_1, a_2 are fitted to reproduce the lattice data [B$^+$96] for QCD thermodynamics in the pure gauge sector. The deconfining temperature T_0 appearing in Eqn. (6.30) is fixed at the lattice value $T_0 = 270$ MeV (see Table 1.1). The resulting effective potential below T_c at $T = 200$ MeV and above T_c at $T = 320$ MeV is shown in Fig. 6.5.

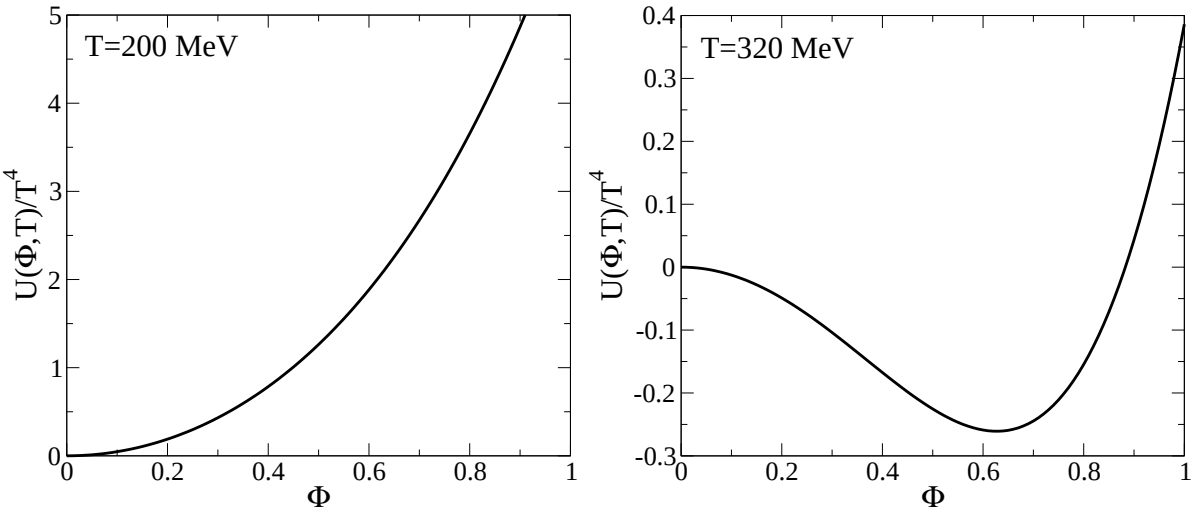

Figure 6.5: Scaled effective Polyakov loop potential $\mathcal{U}(\Phi;T)/T^4$ as a function of Φ below T_c at $T = 200$ MeV and above T_c at $T = 320$ MeV.

The pressure is obtained by minimizing the thermodynamic potential with respect to Φ:

$$p(T) = -\mathcal{U}(\Phi_{\min}(T);T), \tag{6.34}$$

where $\Phi_{\min}(T)$ is given by (6.31). The entropy density and the energy density are obtained by means of standard thermodynamic relations. In Fig. 6.6 we show the (scaled) pressure, energy density and entropy density in the pure gauge sector, as functions of temperature. The lattice data are reproduced extremely well using the ansatz (6.29, 6.30), with parameters summarized in Table 6.1.

With the same parametrization, we are also able to reproduce the lattice data [KKPZ02] for the temperature dependence of the Polyakov loop itself. A comparison between these data and our results is also shown in Fig. 6.6. The Polyakov loop vanishes below the critical temperature T_0, at which point it jumps discontinuously to a finite value, indicating a first order phase transition. It tends to one at large temperatures, as expected.

6.5 Polyakov loop model with quarks

The Polyakov loop model reproduces lattice QCD thermodynamical quantities remarkably well, however with the caveat that quarks are not yet included. In this section we

a_0	a_1	a_2	a_3	b_3	b_4
6.75	-1.95	2.625	-7.44	0.75	7.5

Table 6.1: Parameter set used in this work for the Polyakov loop potential (6.29) and (6.30).

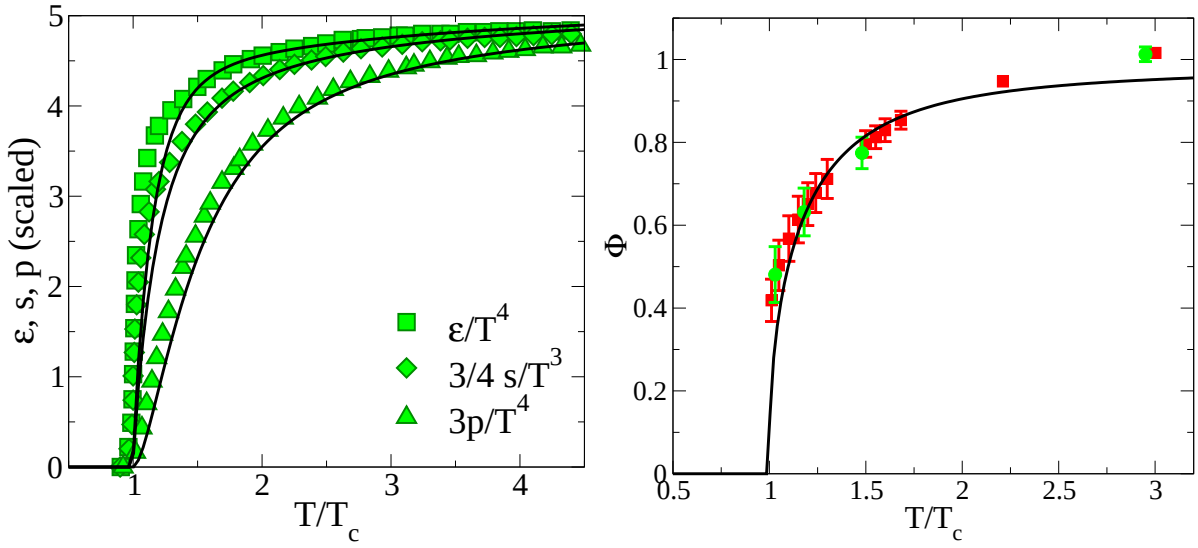

Figure 6.6: Left panel: Scaled pressure, entropy density and energy density as functions of temperature in the pure gauge sector, compared to corresponding lattice data taken from Ref. [B+96]. Right panel: Polyakov loop as a function of temperature in the pure gauge sector, compared to corresponding lattice data taken from Ref. [KKPZ02].

briefly discuss a simple extension of the Polyakov loop model to systems with dynamical quarks. We will mainly follow [DPZ05] here.

Quark fields break the $Z(3)$ center symmetry explicitly because they are anti-periodic in Euclidean time. The simplest symmetry-breaking term that can be added to the effective Polyakov loop potential (6.26) is

$$\mathcal{V}'(\Phi, \Phi^*) = -\frac{h}{2}\left(e^{\mu/T}\Phi + e^{-\mu/T}\Phi^*\right). \tag{6.35}$$

This term acts like a background magnetic field. Its strength is characterized by the parameter h. For massive quarks with $m \gg \mu$, $e^{\mu/T}\Phi$ represents the propagation of a particle forward in imaginary time, while $e^{-\mu/T}\Phi^*$ represents an anti-particle moving backward in imaginary time. Under charge conjugation, the chemical potential changes its sign, $\mu \to -\mu$, thus (6.35) is invariant under charge conjugation, as it should. However,

for a given value of $\mu \neq 0$, charge conjugation symmetry is of course violated: the number of quarks in the system is not equal to the number of anti-quarks. In the absence of quarks, the deconfinement transition is first order. The presence of quarks tends to weaken the transition. Eventually the transition becomes second order at $h = h^{\text{crit}}$ and turns into a smooth crossover for $h > h^{\text{crit}}$.

If we decompose Φ and Φ^* into real and imaginary parts, (6.35) can be written as

$$\begin{aligned}\mathcal{V}' =& -\frac{h}{2}\left(e^{\mu/T}\Phi + e^{-\mu/T}\Phi^*\right) = -\frac{h}{2}\left[e^{\mu/T}(\mathrm{Re}\,\Phi + i\,\mathrm{Im}\,\Phi) + e^{-\mu/T}(\mathrm{Re}\,\Phi - i\,\mathrm{Im}\,\Phi)\right] \\ =& -h\left[\frac{e^{\mu/T}+e^{-\mu/T}}{2}\mathrm{Re}\,\Phi + i\frac{e^{\mu/T}-e^{-\mu/T}}{2}\mathrm{Im}\,\Phi\right] \\ =& -h\left[\cosh\left(\frac{\mu}{T}\right)\mathrm{Re}\,\Phi + i\sinh\left(\frac{\mu}{T}\right)\mathrm{Im}\,\Phi\right]. \end{aligned} \tag{6.36}$$

At zero quark chemical potential, quarks generate a real background $Z(N_c)$ field for the real component of the Polyakov loop, $\mathrm{Re}\,\Phi$. At finite quark chemical potential, however, the $Z(N_c)$ background field contains a part proportional to the imaginary part of the Polyakov loop, $\mathrm{Im}\,\Phi$, with a coefficient that is itself imaginary. For two colors, the Polyakov loop is always real and thus $\mathrm{Im}\,\Phi = 0$. For three or more colors, the Polyakov loop is a complex field and consequently (6.36) is manifestly complex. However, if a given Polyakov loop $\Phi(\boldsymbol{x})$ contributes to the partition function, its charge conjugate $\Phi^*(\boldsymbol{x})$ also does. Adding the contributions of $\Phi(\boldsymbol{x})$ and $\Phi^*(\boldsymbol{x})$ together, we can rewrite the partition function in a form that is manifestly real,

$$\begin{aligned}\mathcal{Z} =& \frac{1}{2}\int \mathcal{D}\Phi\, e^{\mathcal{V}(\Phi,\Phi^*)}\left\{e^{-h[\cosh(\mu/T)\mathrm{Re}\Phi + i\sinh(\mu/T)\mathrm{Im}\Phi]} + e^{-h[\cosh(\mu/T)\mathrm{Re}\Phi - i\sinh(\mu/T)\mathrm{Im}\Phi]}\right\} \\ =& \int \mathcal{D}\Phi\, e^{\mathcal{V}(\Phi,\Phi^*) - h\cosh(\mu/T)\mathrm{Re}\Phi}\,\frac{e^{-ih\sinh(\mu/T)\mathrm{Im}\Phi} + e^{ih\sinh(\mu/T)\mathrm{Im}\Phi}}{2} \\ =& \int \mathcal{D}\Phi\, e^{\mathcal{V}(\Phi,\Phi^*) - h\cosh(\mu/T)\mathrm{Re}\Phi}\cos\left(h\sinh(\mu/T)\mathrm{Im}\Phi\right) = \int \mathcal{D}\Phi\, e^{-\tilde{\mathcal{V}}(\Phi,\Phi^*)}\cos(\tilde{h}\,\mathrm{Im}\Phi), \end{aligned} \tag{6.37}$$

where we have defined

$$\tilde{\mathcal{V}}(\Phi,\Phi^*) = \mathcal{V}(\Phi,\Phi^*) - h\cosh\left(\frac{\mu}{T}\right)\mathrm{Re}\,\Phi, \tag{6.38}$$

$$\tilde{h} = h\sinh\left(\frac{\mu}{T}\right). \tag{6.39}$$

The potential $\tilde{\mathcal{V}}(\Phi,\Phi^*)$ is even under charge conjugation of the gluons, while $\tilde{h}\,\mathrm{Im}\Phi$ is odd. We can use this to write the expectation values of the Polyakov loop as

$$\langle\Phi\rangle = \frac{1}{\mathcal{Z}}\int \mathcal{D}\Phi\, e^{-\tilde{\mathcal{V}}(\Phi,\Phi^*)}\left(\cos(\tilde{h}\,\mathrm{Im}\,\Phi)\mathrm{Re}\Phi - \sin(\tilde{h}\,\mathrm{Im}\Phi)\mathrm{Im}\Phi\right), \tag{6.40}$$

while that of the charge conjugated Polyakov loop is

$$\langle\Phi^*\rangle = \frac{1}{\mathcal{Z}}\int \mathcal{D}\,\Phi e^{-\tilde{\mathcal{V}}(\Phi,\Phi^*)}\left(\cos(\tilde{h}\,\mathrm{Im}\,\Phi)\mathrm{Re}\Phi + \sin(\tilde{h}\,\mathrm{Im}\Phi)\mathrm{Im}\Phi\right). \tag{6.41}$$

Because quarks at finite quark chemical potential induce an imaginary background field for the imaginary part of Φ, the expectation values of Φ and Φ^* are both real, but unequal. Physically, this is natural: the Polyakov loop is proportional to the trace of the wave function of a quark, the charge conjugated loop to that of an anti-quark. At finite quark chemical potential the number of quarks and antiquarks is not equal and thus they propagate differently.

For the thermodynamic potential, we make the ansatz

$$\mathcal{U}'(\Phi,\Phi^*;T,\mu) = \Bigg[-\frac{b_2(T)}{2}\Phi^*\Phi - \frac{b_3}{6}\left((\Phi^*)^3+\Phi^3\right) + \frac{b_4}{4}\left(\Phi^*\Phi\right)^2 - \frac{h}{2}\left(e^{\mu/T}\Phi + e^{-\mu/T}\Phi^*\right)\Bigg] T^4, \tag{6.42}$$

and we assume that the expectation values $\Phi_{\rm min}(T,\mu)$ and $\Phi^*_{\rm min}(T,\mu)$ are given by minimizing the thermodynamic potential with respect to Φ and Φ^* at fixed temperature T and quark chemical potential μ. The pressure is $p(T,\mu) = -\mathcal{U}'(\Phi_{\rm min}(T,\mu),\Phi^*_{\rm min}(T,\mu);T,\mu)$ and all other thermodynamical quantities can be obtained from the pressure by using standard thermodynamic relations. Fig. 6.7 shows the Polyakov loop at vanishing quark chemical potential for several values of h. The parameters have been taken to be the same as in the pure $SU(3)$ gauge case. Fig. 6.7 also shows the Polyakov loop and its charge conjugate as a function of temperature at finite quark chemical potential μ. Φ and Φ^* are both real, but unequal. For $T\to\infty$ we find that $\Phi=\Phi^*$ because the quark chemical potential is divided by temperature and thus $T\to\infty$ corresponds to $\mu\to 0$.

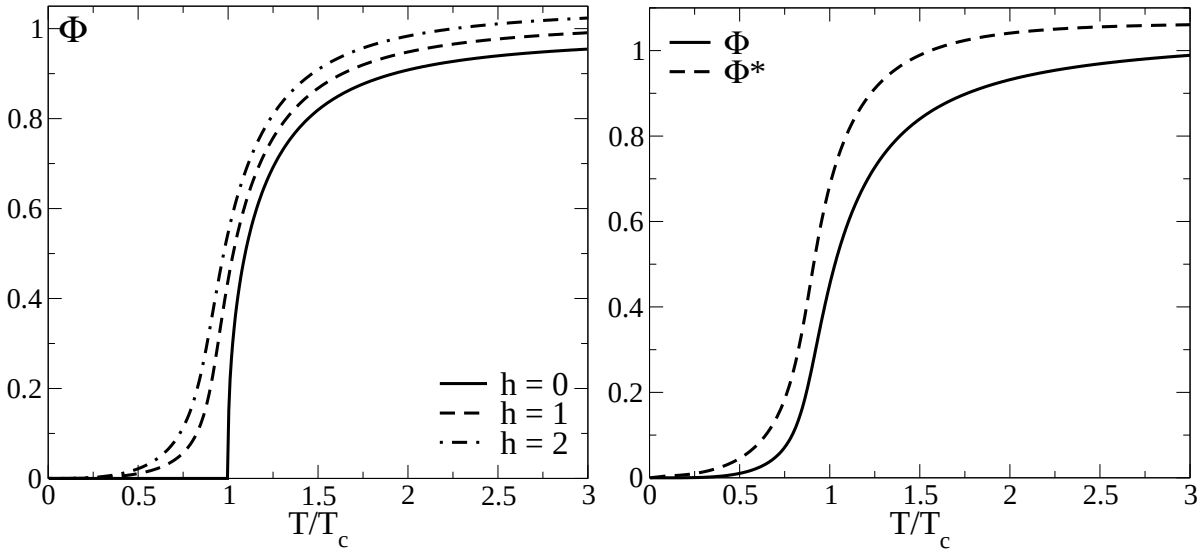

Figure 6.7: Left panel: Polyakov loop obtained from (6.42) for $h=0$, 1, 2 at zero quark chemical potential as a function of temperature. Right panel: Φ and Φ^* for $h=1$ and $\mu=100$ MeV as a function of temperature.

6.6 The PNJL model

In the previous section we have discussed how the Polyakov loop model can be extended to systems with dynamical quarks. We have found that quarks tend to weaken the confinement-deconfinement transition. For sufficiently large values of the parameter h they will turn the first-order transition that occurs in the absence of quarks into a smooth crossover. At finite quark chemical potential, the Polyakov loop and its charge conjugate are both real, but unequal.

However, a complete discussion of full QCD at finite temperature must also incorporate chiral symmetry breaking and its restoration at high temperatures. As we have seen, the 'classic' NJL model accounts for the chiral symmetry restoration at high temperatures. Following [MO96, Fuk04] we introduce a generalized $N_f = 2$ Nambu–Jona-Lasinio Lagrangian with quarks coupled to a (spatially constant) temporal background $SU(3)$ gauge field representing Polyakov loop dynamics (the PNJL model):

$$\mathcal{L}_{\mathrm{PNJL}} = \bar{\psi}\left(i\not{D} - \hat{m}_0\right)\psi + \frac{G}{2}\left[\left(\bar{\psi}\psi\right)^2 + \left(\bar{\psi}i\gamma_5\vec{\tau}\psi\right)^2\right] - \mathcal{U}\left(\Phi[A], \Phi^*[A]; T\right), \tag{6.43}$$

where

$$D_\mu = \partial_\mu + iA_\mu \qquad \text{and} \qquad A_\mu = \delta_{\mu 0} A_0. \tag{6.44}$$

The gauge coupling g_s is conveniently absorbed in the definition of $A_\mu \equiv g_s A_\mu^a \frac{\lambda_a}{2}$. A local, chirally symmetric scalar-pseudoscalar four-point interaction of the quark fields is introduced with an effective coupling strength G. $\mathcal{U}(\Phi, \Phi^*; T)$ is given by (6.28). The coupling between Polyakov loop and quarks is uniquely determined by the covariant derivative D_μ in the PNJL Lagrangian (6.43). Note that in the chiral limit ($\hat{m}_0 \to 0$), this Lagrangian is invariant under the chiral flavor group, $SU(2)_L \times SU(2)_R$ just like the original QCD Lagrangian.

In a convenient gauge (the so-called Polyakov gauge), the $SU(3)$ Polyakov loop can be parametrized as follows [Fuk04]:

$$\Phi = \frac{1}{3}\mathrm{Tr}_c\, L \quad \text{with} \quad L = \begin{pmatrix} \mathrm{e}^{i\phi} & 0 & 0 \\ 0 & \mathrm{e}^{i\phi'} & 0 \\ 0 & 0 & \mathrm{e}^{-i(\phi+\phi')} \end{pmatrix}. \tag{6.45}$$

The perturbative vacuum corresponds to $\phi = \phi' = 0$. Using this ansatz the traced Polyakov loop has the form:

$$\Phi = \frac{1}{3}\mathrm{Tr}_c L = \frac{1}{3}\left(e^{i\phi} + e^{i\phi'} + e^{-i\phi - i\phi'}\right). \tag{6.46}$$

Φ^* is the charge conjugate of this. Φ and Φ^* are constrained by the fact that L is a $SU(3)$ matrix with $\det L = 1$. Using the bosonization technique described in chapter 4, the Lagrangian (6.43) can be rewritten in terms of the auxiliary field variables σ and $\vec{\pi}$:

$$\mathcal{L}_{\mathrm{eff}} = -\frac{\sigma^2 + \vec{\pi}^2}{2G} - \mathcal{U}\left(\Phi, \Phi^*; T\right) - i\mathrm{Tr}\ln S^{-1}, \tag{6.47}$$

where an irrelevant constant has been dropped and

$$S^{-1} = i\gamma_\mu \partial^\mu - \gamma_0 A^0 - \hat{M} \tag{6.48}$$

is the inverse quark propagator with

$$\hat{M} = \hat{m}_0 - \sigma - i\gamma_5 \vec{\tau} \cdot \vec{\pi}\,. \tag{6.49}$$

The trace in (6.47) is taken over color, flavor and Dirac indices. The field equations for σ, $\vec{\pi}$, Φ and Φ^* are solved in mean field approximation[1]. The expectation value $\langle\vec{\pi}\rangle$ of the pseudoscalar isotriplet field is equal to zero for isospin-symmetric systems. The σ field has a non-vanishing vacuum expectation value as a consequence of spontaneous chiral symmetry breaking. Solving the field equations for σ, the effective quark mass M is determined by the self-consistent gap equation

$$M = m_0 - \langle\sigma\rangle = m_0 - G\langle\bar{\psi}\psi\rangle. \tag{6.50}$$

Note that $\langle\sigma\rangle = G\langle\bar{\psi}\psi\rangle$ is negative in our representation, and the chiral (quark) condensate is $\langle\bar{\psi}\psi\rangle = \langle\bar{\psi}_u\psi_u + \bar{\psi}_d\psi_d\rangle$. The Polyakov loop Φ and its charge conjugate Φ^* vanish in the confining vacuum and tend to one at high temperatures. The parameters a_i and b_i are taken to be the same as in the pure gauge case and are listed in Table 6.1. The parameters of the NJL part also remain unchanged and are given in Table 4.1.

Before passing to the actual calculations, we summarize basic assumptions behind Eqn. (6.43) and comment on limitations to be kept in mind. In fact the PNJL model (6.43) is quite schematic in several respects. It reduces gluon dynamics to a) chiral point couplings between quarks, and b) a simple static background field representing the Polyakov loop. This picture cannot be expected to work beyond a limited range of temperatures. At large T, transverse gluons are known to be thermodynamically active degrees of freedom, but they are ignored in the PNJL model. To what extent this model can reproduce lattice QCD thermodynamics is nonetheless a relevant question. We can assume that its range of applicability is, roughly, $T \leq (2-3)T_c$, based on the conclusion drawn in Ref. [MOM04] that transverse gluons start to contribute significantly for $T > 2.5\,T_c$.

6.6.1 Finite temperature and chemical potential

Using the formalism from section 4.3, we can extend the model to finite temperature and quark chemical potential. We consider the isospin symmetric case, with an equal number of u and d quarks (and therefore a single quark chemical potential μ) . The quantity to be minimized at finite temperature is the thermodynamic potential per unit volume:

$$\Omega\,(T,\mu) = \mathcal{U}\,(\Phi,\Phi^*;T) - \frac{T}{2}\sum_n \int \frac{\mathrm{d}^3p}{(2\pi)^3}\mathrm{Tr}\ln\left(\frac{1}{T}\tilde{S}^{-1}\,(i\omega_n,\vec{p})\right) + \frac{\sigma^2}{2G}. \tag{6.51}$$

[1] In the mean field approximation the fields are replaced by their expectation values for which, in later sections, we will continue using the notation σ, Φ and Φ^* for simplicity and convenience.

Here $\omega_n = (2n+1)\pi T$ are the Matsubara frequencies for fermions. The inverse quark propagator (in Nambu-Gorkov representation) becomes

$$\tilde{S}^{-1}\left(p^0,\vec{p}\right) = \begin{pmatrix} \gamma_0 p^0 - \vec{\gamma}\cdot\vec{p} - M - \gamma_0(\mu + iA_4) & 0 \\ 0 & \gamma_0 p^0 - \vec{\gamma}\cdot\vec{p} - M + \gamma_0(\mu + iA_4) \end{pmatrix}. \tag{6.52}$$

Here we have suppressed color and flavor indices. In fact, each of the elements of the matrix (6.52) is a matrix in color-, flavor- and Dirac-space and consequently (6.52) is a tensor product of matrices. To carry out the trace we use the identity $\mathrm{Tr}\ln(X) = \ln\det(X)$. The determinant can then be calculated using the identity $\det(A\otimes B) = (\det A)^m(\det B)^n$, for square matrices A and B of dimensions m and n, respectively. The result reads

$$\mathrm{Tr}\ln\left(\frac{1}{T}\tilde{S}^{-1}\right) = 2N_f\mathrm{Tr}_c\left[\ln\left(\frac{(\omega_n - i\mu + A_4)^2 + E_p^2}{T^2}\right) + \ln\left(\frac{(\omega_n + i\mu - A_4)^2 + E_p^2}{T^2}\right)\right], \tag{6.53}$$

where we have introduced the quark quasiparticle energy $E_p = \sqrt{\boldsymbol{p}^2 + M^2}$. The terms can be reordered to obtain

$$\mathrm{Tr}\ln\left(\frac{1}{T}\tilde{S}^{-1}\right) = 2N_f\mathrm{Tr}_c\left[\ln\left(\frac{\omega_n^2 + (E_p - \mu - iA_4)^2}{T^2}\right) + \ln\left(\frac{\omega_n^2 + (E_p + \mu + iA_4)^2}{T^2}\right)\right]. \tag{6.54}$$

Using the relation

$$T\sum_{n=-\infty}^{\infty}\ln\left(\frac{\omega_n^2 + \lambda^2}{T^2}\right) = \lambda + 2T\ln\left(1 + e^{-\lambda/T}\right), \tag{6.55}$$

we finally obtain

$$\begin{aligned}\Omega = {} & \mathcal{U}\left(\Phi,\Phi^*;T\right) + \frac{\sigma^2}{2G} && (6.56)\\ & - 2N_f\,T\int\frac{\mathrm{d}^3p}{(2\pi)^3}\left\{\mathrm{Tr}_c\ln\left[1 + L\,e^{-(E_p-\mu)/T}\right] + \mathrm{Tr}_c\ln\left[1 + L^\dagger\,e^{-(E_p+\mu)/T}\right]\right\} \\ & - 6N_f\int\frac{\mathrm{d}^3p}{(2\pi)^3}\,E_p\theta(\Lambda^2 - \boldsymbol{p}^2), && (6.57)\end{aligned}$$

where an irrelevant constant has again been dropped. The last term involves the NJL three-momentum cutoff Λ. The remaining color trace is performed using the explicit representation (6.45) of L:

$$\begin{aligned}& \ln\det\left[1 + L\,e^{-(E_p-\mu)/T}\right] + \ln\det\left[1 + L^\dagger\,e^{-(E_p-\mu)/T}\right] \\ & = \ln\left[1 + 3\left(\Phi + \Phi^* e^{-(E_p-\mu)/T}\right)e^{-(E_p-\mu)/T} + e^{-3(E_p-\mu)/T}\right] \\ & + \ln\left[1 + 3\left(\Phi^* + \Phi e^{-(E_p+\mu)/T}\right)e^{-(E_p+\mu)/T} + e^{-3(E_p+\mu)/T}\right],\end{aligned} \tag{6.58}$$

where we have used $\Phi = \left(e^{i\phi} + e^{i\phi'} + e^{-i\phi-i\phi'}\right)/3$ and $\Phi^* = \left(e^{-i\phi} + e^{-i\phi'} + e^{i\phi+i\phi'}\right)/3$ in intermediate steps. From the thermodynamic potential (6.57) the equations of motion for the mean fields σ, Φ and Φ^* are derived through

$$\frac{\partial\Omega}{\partial\sigma} = 0 \ , \qquad \frac{\partial\Omega}{\partial\Phi} = 0 \ , \qquad \frac{\partial\Omega}{\partial\Phi^*} = 0 \ . \tag{6.59}$$

This set of coupled equations is then solved for the fields as functions of temperature T and quark chemical potential μ. Throughout this procedure we treat Φ and Φ^* as independent, classical fields.

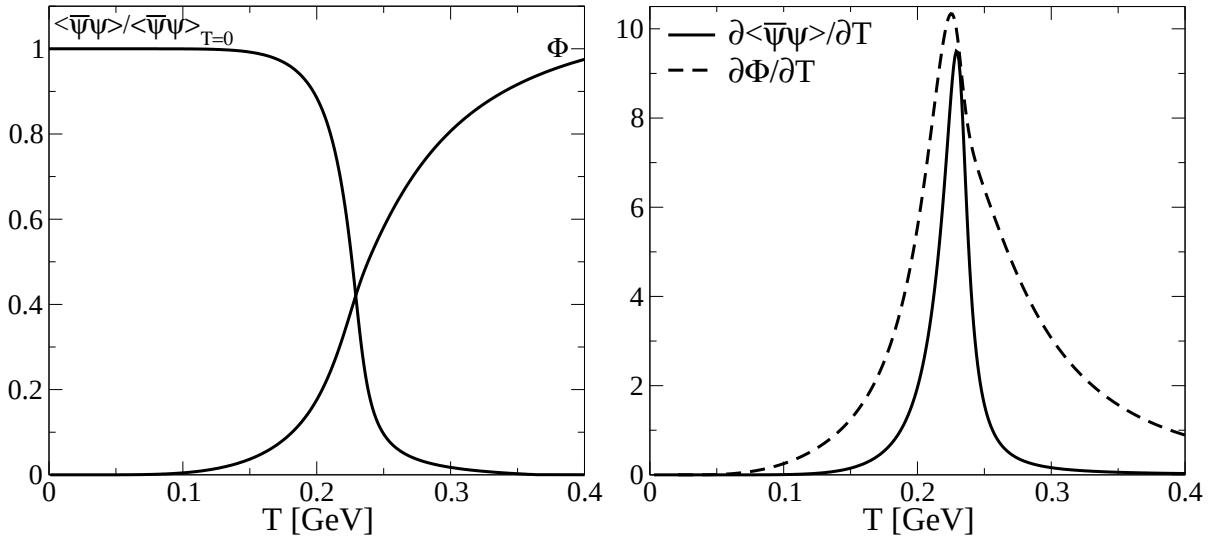

Figure 6.8: Left panel: Scaled chiral condensate and Polyakov loop $\Phi(T)$ as functions of temperature at zero quark chemical potential. Right panel: Plots of $\partial\langle\bar{\psi}\psi\rangle/\partial T$ and $\partial\Phi/\partial T$. Note that $\partial\langle\bar{\psi}\psi\rangle/\partial T$ has dimension [GeV^2], while $\partial\Phi/\partial T$ has dimension [GeV^{-1}].

Fig. 6.8 shows the chiral condensate together with the Polyakov loop Φ as functions of temperature at $\mu = 0$ where we find that $\Phi = \Phi^*$. One observes that the introduction of quarks coupled to the σ, Φ and Φ^* fields turns the first-order transition seen in pure-gauge lattice QCD into a continuous crossover. The original first order transition in the pure-gauge system appears at a critical temperature $T_0 = 270$ MeV. With the introduction of quarks, the crossover transitions for the chiral condensate $\langle\bar{\psi}\psi\rangle$ and for the Polyakov loop perfectly coincide at a lower critical temperature $T_c \simeq 220$ MeV. We point out that this feature is obtained without changing a single parameter with respect to the pure gauge case. The value of the critical temperature that we obtain is a little high if compared to the available data for two-flavor lattice QCD (see Table 1.1) which gives $T_c = (173 \pm 8)$ MeV. On the other hand, it is presently being discussed that detailed continuum extrapolation of these data can increase this temperature up to 210 MeV [Fod]. For quantitative comparison with existing lattice results we choose to reduce T_c by rescaling the parameter T_0 from 270 to 190 MeV. In this case we loose the perfect

coincidence of the chiral and deconfinement transitions, but they are shifted relative to each other by less than 20 MeV. When defining T_c in this case as the average of the two transition temperatures we find $T_c = 180$ MeV. This is also consistent with the observations reported in [DLS01]. As we turn to non-zero chemical potential, we find that Φ and Φ^* are different from each other, even though they are both real. They will finally coincide again at high temperatures, as can be seen in Fig. 6.9. This feature was already observed in [DPZ05]. With increasing chemical potential, the crossover pattern evolves to lower transition temperatures (see Fig. 6.10) until it turns to a first order transition around $\mu \sim 0.3$ GeV. At this point Cooper pairing of quarks presumably sets in. A more detailed discussion of the critical point and its neighborhood therefore requires the additional incorporation of explicit diquark degrees of freedom in the PNJL model.

6.6.2 Detailed comparison with lattice QCD

In this section we test the predictions of our PNJL model with lattice data available for full QCD thermodynamics at zero and finite μ. Consider first the pressure of a quark-gluon system at zero quark chemical potential:

$$p\left(T, \mu = 0\right) = -\Omega\left(T, \mu = 0; \sigma(T,0), \Phi(T,0), \Phi^*(T,0)\right), \tag{6.60}$$

where $\sigma\left(T,0\right)$, $\Phi\left(T,0\right)$ and $\Phi^*\left(T,0\right)$ are the solutions of the field equations at finite temperature and zero quark chemical potential. Our results are presented in Fig. 6.11 and Fig. 6.12 in comparison with corresponding lattice data. We point out that the input parameters of the PNJL model have been fixed independently in the pure gauge and hadronic sectors, so that our calculated pressure is a prediction of the model, without any further tuning of parameters. With this in mind, the agreement with lattice results is quite satisfactory. One must note that the lattice data are grouped in different sets obtained on lattices with temporal extent $N_t = 4$ and $N_t = 6$, both of which are not continuum extrapolated. In contrast, our calculation should, strictly speaking, be compared to the continuum limit. In order to perform meaningful comparisons, the pressure and the energy density are divided by its asymptotic high-temperature (Stefan-Boltzmann) limit for each given case. At high temperatures our predicted curves should be located closer to the $N_t = 6$ sets than to the ones with $N_t = 4$. This is indeed the case. Fig. 6.12 also shows the interaction measure, $(\varepsilon - 3p)/T^4$ and the pressure as a function of the energy density. One should of course note that the lattice results have been produced using relatively large quark masses, with pseudoscalar-to-vector mass ratios $m_{\rm PS}/m_{\rm V}$ around 0.7, whereas our calculation is performed with light quark masses corresponding to the physical pion mass. This will be investigated further in the next section.

At non-zero chemical potential, quantities of interest that have become accessible in lattice QCD are the "pressure difference" and the quark number density. The (scaled) pressure difference is defined as:

$$\frac{\Delta p\left(T,\mu\right)}{T^4} = \frac{p\left(T,\mu\right) - p\left(T,\mu=0\right)}{T^4}. \tag{6.61}$$

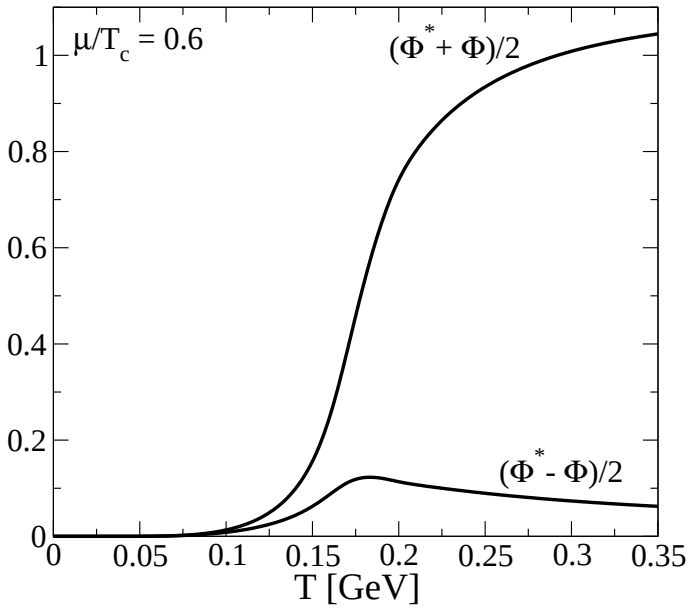

Figure 6.9: Averaged sum and difference of Φ and Φ^* as functions of temperature at a finite quark chemical potential $\mu = 0.6\,T_c$.

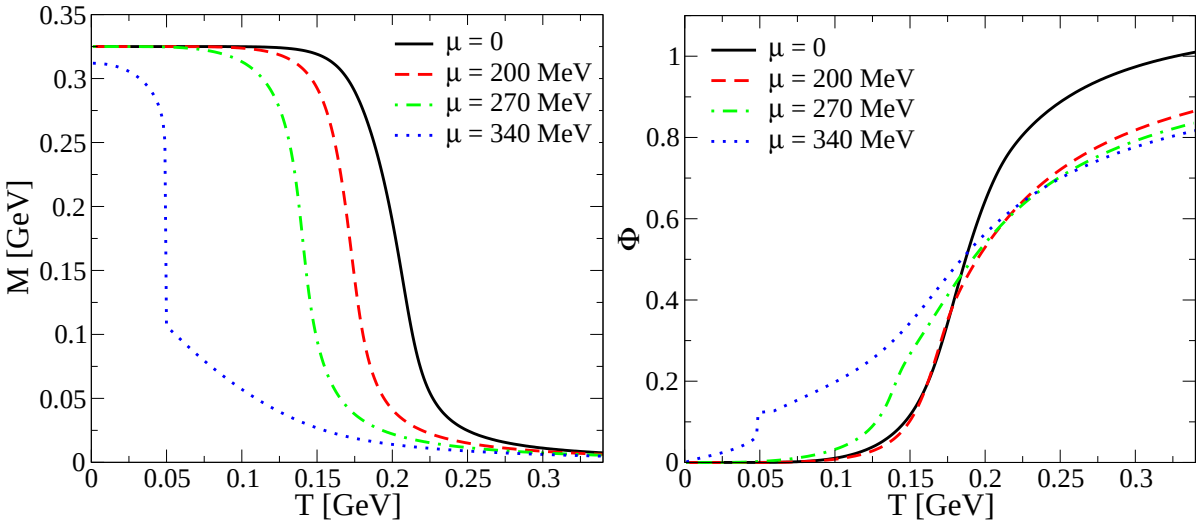

Figure 6.10: Constituent quark mass M and Polyakov loop Φ as functions of temperature for various values of the quark chemical potential μ.

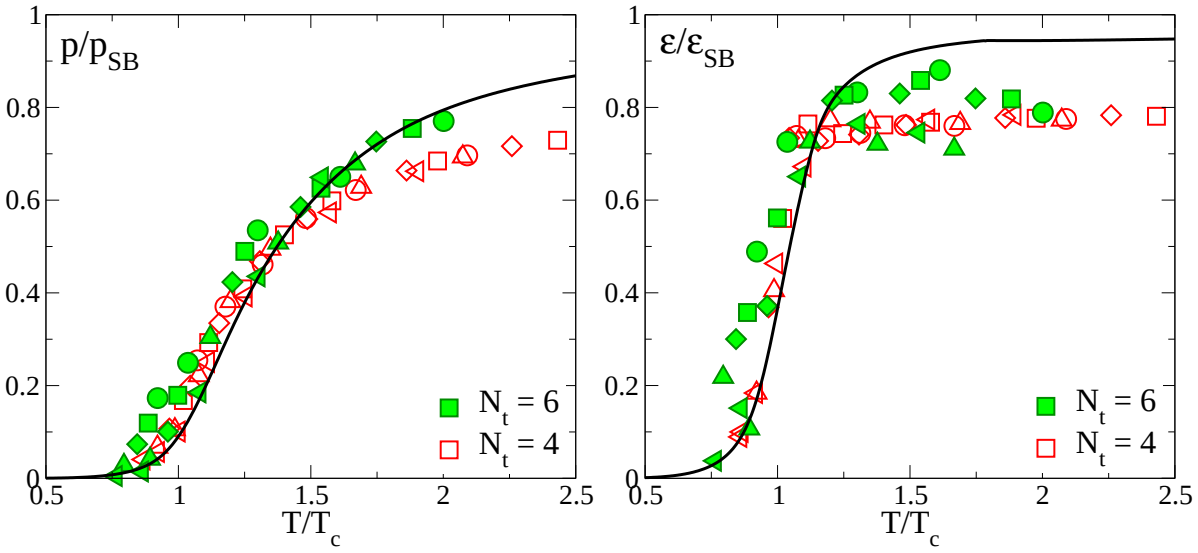

Figure 6.11: The pressure p/p_{SB} (left panel) and the energy density $\epsilon/\epsilon_{\mathrm{SB}}$ (right panel), divided by their respective Stefan-Boltzmann values from our model (solid lines) compared to lattice data from $16^3 \times 4$ and $16^3 \times 6$ lattices (symbols) [AK$^+$01a]. Different values of $m_{\mathrm{PS}}/m_{\mathrm{V}}$ used in the lattice calculations are denoted by different shapes of the symbols (see Fig. 1.2 or [AK$^+$01a]).

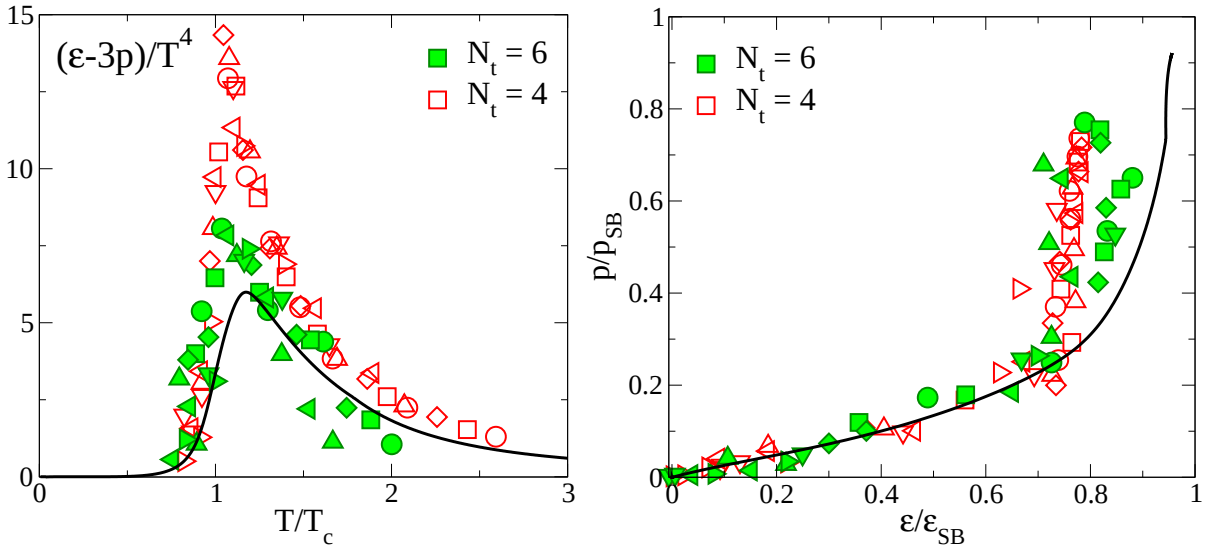

Figure 6.12: The scaled interaction measure $(\epsilon - 3p)/T^4$ (left panel) and the pressure as a function of the energy density (right panel) from our model (solid lines) compared to lattice data from a $16^3 \times 4$ and $16^3 \times 6$ lattice (symbols) [AK$^+$01a]. Different values of $m_{\mathrm{PS}}/m_{\mathrm{V}}$ used in the lattice calculations are denoted by different shapes of the symbols (see Fig. 1.2 or [AK$^+$01a]).

A comparison of Δp, calculated in the PNJL model, with lattice results is presented in Fig. 6.13. This figure shows the scaled pressure difference as a function of the temperature for a series of chemical potentials, with values ranging between $\mu = 0.2\,T_c$ and $\mu \simeq T_c$. The agreement between our results and the lattice data is quite satisfactory.
A related quantity for which lattice results at finite μ exist, is the scaled quark number density, defined as:

$$\frac{n_q\,(T,\mu)}{T^3} = -\frac{1}{T^3}\frac{\partial\Omega\,(T,\mu)}{\partial\mu}. \tag{6.62}$$

Our results for n_q as a function of temperature, for different values of the quark chemical potential, are shown in Fig. 6.14 in comparison with corresponding lattice data [A$^+$03]. Also in this case, the agreement between our PNJL model and the corresponding lattice data is surprisingly good.

It is instructive to study the effect of the Polyakov loop dynamics on the behavior of the quark density n_q. The coupling of the quark quasiparticles to the fields Φ and Φ^* reduces their weight as thermodynamically active degrees of freedom when the critical temperature T_c is approached from above. At T_c the values of Φ and Φ^* tend to zero and the quasiparticle exponentials $\exp[-(E_p \pm \mu)/T]$ are progressively suppressed in the thermodynamic potential as $T \to T_c$. This is what can be interpreted as the impact of confinement in the context of the PNJL model. In contrast, the standard NJL model without coupling to the Polyakov loop does not have this important feature, so that the quark density leaks strongly into the "forbidden" domain $T < T_c \simeq 170$ MeV, as demonstrated in Fig. 6.15.

It is a remarkable feature that the quark densities and the pressure difference at finite μ are so well reproduced even though the lattice "data" have been obtained by a Taylor expansion up to fourth order in μ, whereas our thermodynamical potential is used with its full functional dependence on μ. We have examined the convergence in powers of μ by expanding Eqn. (6.57). It turns out that the Taylor expansion to order μ^2 deviates from the full result by less than 10 % even when the chemical potential reaches values as large as $\mu \sim T_c$, as seen in Figs. 6.13 and 6.14. When expanded to $\mathcal{O}(\mu^4)$, there is no visible difference left between the approximate and full calculations for all cases shown in Figs. 6.13 and 6.14.

6.6.3 Quark mass dependence

In the following we briefly investigate the dependence of the pressure and the energy density on the current quark mass in our model. To this end we have calculated the pressure and the energy density for various current quark masses m_0. The results are shown in Fig. 6.16. Results for $m_0 = 5.5$ MeV, which corresponds to the physical pion mass, are denoted by solid lines. Dashed lines are the pressure and the energy density for a quark mass of 50 MeV ($m_\pi \simeq 430$ MeV), while the dashed-dotted lines correspond to 100 MeV ($m_\pi \simeq 600$ MeV). The critical temperature scales approximately as $T_c \simeq T_c(m_\pi = 0) + 0.04\,m_\pi$, in agreement with the behavior found in [KLP01a].

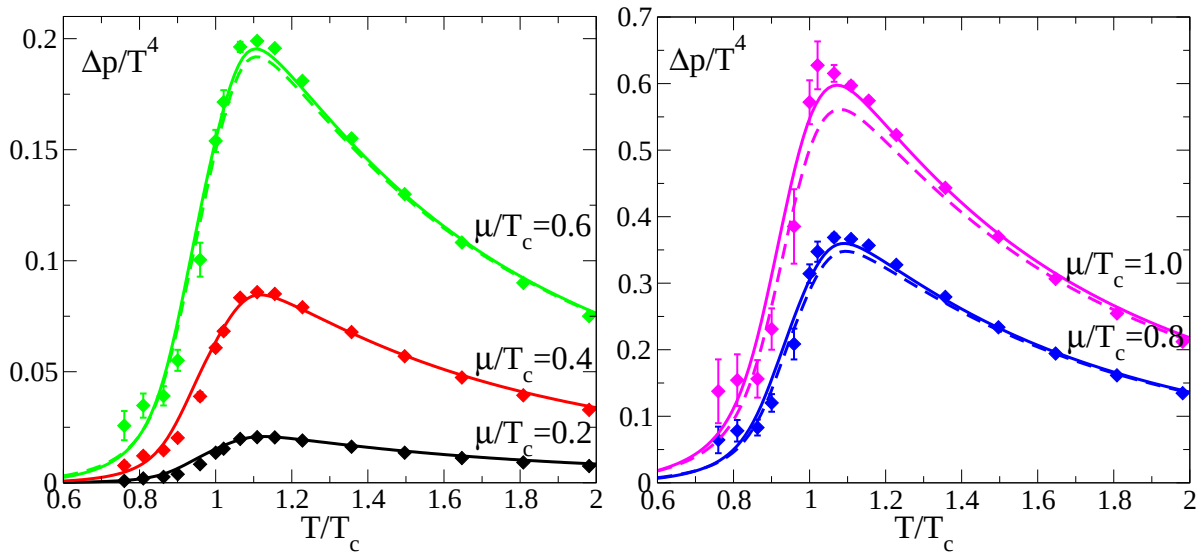

Figure 6.13: Scaled pressure difference as a function of temperature at different values of the quark chemical potential, compared to corresponding lattice data taken from Ref. [A+03]. Dashed lines denote the results from a Taylor expansion to order μ^2 (see text).

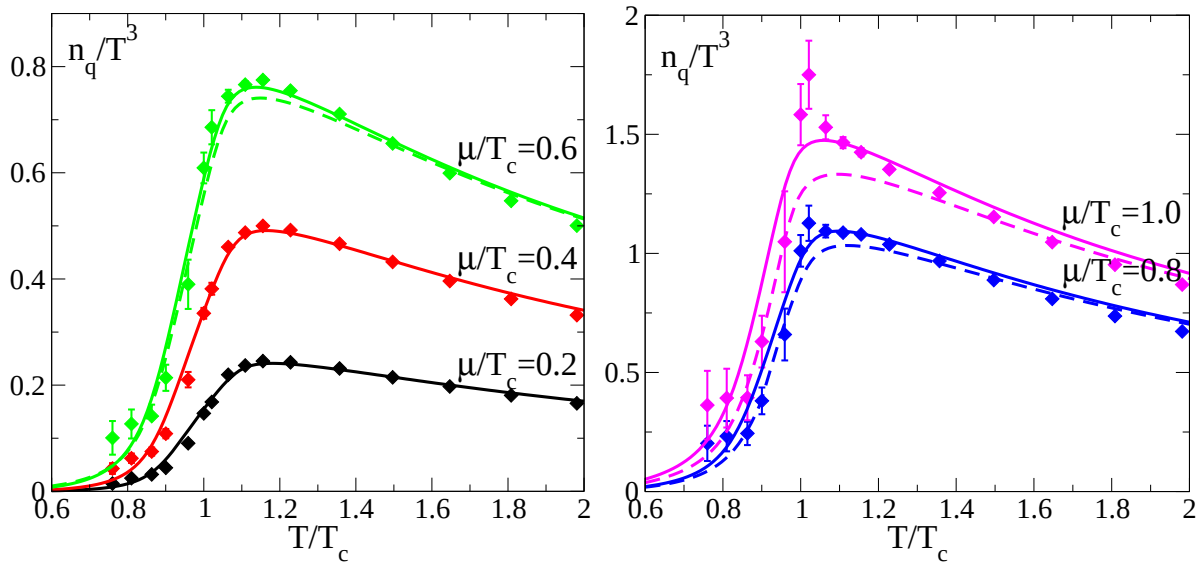

Figure 6.14: Scaled quark number density as a function of temperature at different values of the quark chemical potential, compared to corresponding lattice data taken from Ref. [A+03]. Dashed lines denote the results from a Taylor expansion to order μ^2 (see text).

6.7 Summary

The aim of this chapter was to develop a general model that is suitable to study confinement and chiral symmetry breaking in a unified framework. Our starting point was the heavy-quark limit, where the confined and the deconfined phases are characterized by distinct symmetry properties: the $Z(3)$ center symmetry of the $SU(3)$ gauge group is spontaneously broken in the confined phase, while it is restored in the deconfined phase. The associated order parameter is the Polyakov loop, a Wilson line closed around the Euclidean time direction. Subsequently, we have constructed an effective theory for the Polyakov loop and tested it at finite temperature against results from $SU(3)$ lattice gauge theory. The lattice data are reproduced extremely well by our ansatz. If quarks are added, the center symmetry gets explicitly broken and no order parameter can be established, but the Polyakov loop still changes rapidly close to T_c and serves as an indicator of a rapid crossover towards deconfinement. To include chiral symmetry breaking, we have introduced a generalized NJL Lagrangian with quarks coupled to a (spatially constant) temporal background $SU(3)$ gauge field A_0, representing Polyakov loop dynamics. This Polyakov loop extended (PNJL) model represents a minimal synthesis of the two basic principles that govern QCD at low temperatures: spontaneous chiral symmetry breaking and confinement. The respective order parameters (the chiral quark condensate and the Polyakov loop) are given the meaning of collective degrees of freedom. Quarks couple to these collective fields according to the symmetry rules dictated by QCD itself.

Once a limited set of input parameters is fitted to lattice QCD in the pure gauge sector and to pion properties in the hadron sector, the quark-gluon thermodynamics above T_c up to about 2-3 times the critical temperature is well reproduced, including quark densities up to chemical potentials of about 0.2 GeV. In particular, the PNJL model correctly describes the step from the first-order deconfinement transition observed in pure-gauge lattice QCD (with $T_c \simeq 270$ MeV) to the crossover transition (with T_c less than 200 MeV) when $N_f = 2$ light quark flavors are added. The non-trivial result is that the crossovers for chiral symmetry restoration and deconfinement almost coincide, as found in lattice simulations. The model also reproduces the quark number densities at various chemical potentials remarkably well when confronted with corresponding lattice data. The conclusion that can be drawn at this point is promising: it appears that a relatively straightforward quasiparticle approach, with its dynamics rooted in spontaneous chiral symmetry breaking and confinement and with parameters controlled by a few known properties of the gluonic and hadronic sectors of the QCD phase diagram, can account for essential observations from two-flavor $N_c = 3$ lattice QCD thermodynamics.

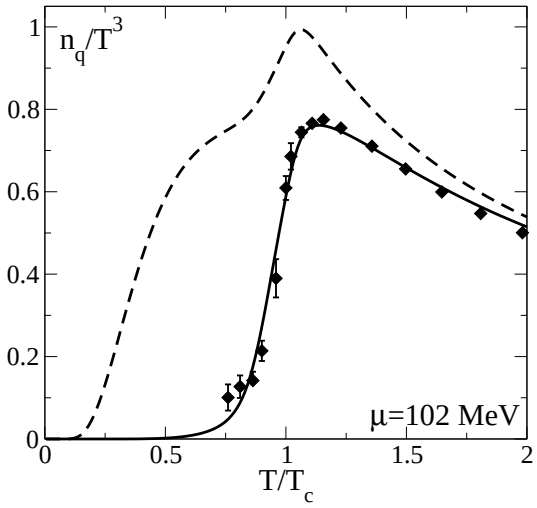

Figure 6.15: Comparison between the results in the PNJL model (solid line) and in the standard NJL model (dashed line) for the quark number density at $\mu = 102$ MeV. The effect of the missing of confinement is evident in the standard NJL model.

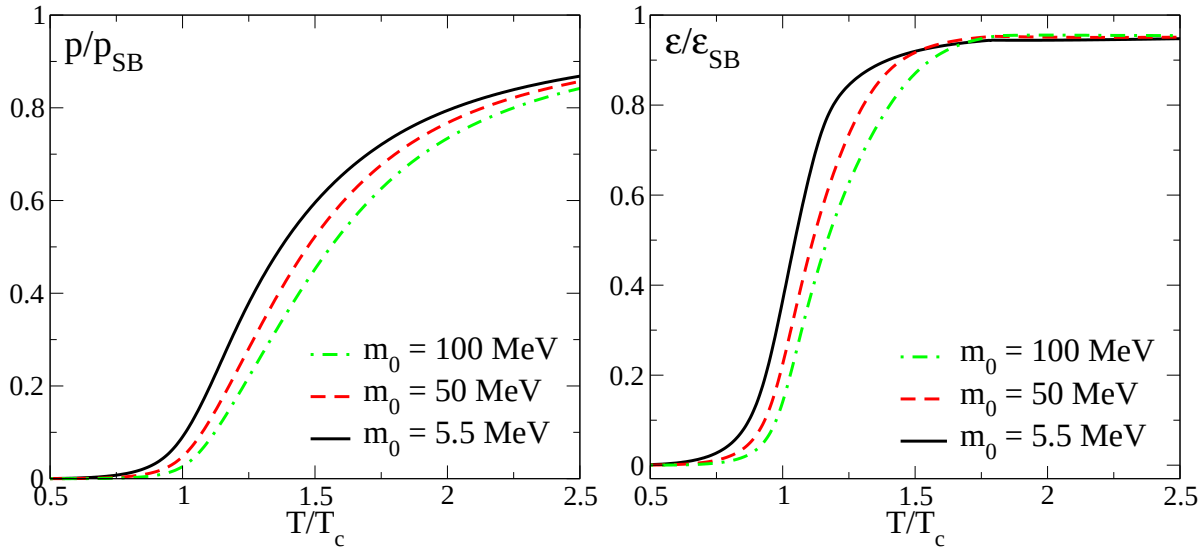

Figure 6.16: The pressure p/p_{SB} (left panel) and the energy density $\epsilon/\epsilon_{\mathrm{SB}}$ (right panel), divided by their respective Stefan-Boltzmann values from our model for various current quark masses. Solid lines are the results for $m_0 = 5.5$ MeV, dashed lines for $m_0 = 50$ MeV and dashed-dotted lines for $m_0 = 100$ MeV.

Chapter 7

Three-Flavor Systems

In the previous chapter we have discussed a generalized Nambu–Jona-Lasinio model in which quarks couple simultaneously to the chiral condensate and to a background temporal gauge field representing Polyakov loop dynamics. This so-called PNJL model includes features of both deconfinement and chiral symmetry restoration. In this chapter we extend our analysis to three quark flavors. The main difference between the two-flavor case and the three-flavor case comes about the fact that the mass of the strange quark is different from the masses of the non-strange quarks. This means that we have to deal with an explicitly broken $SU(3)$ symmetry, and thus $\langle \bar{s}s \rangle \neq \langle \bar{u}u \rangle$, even for equal quark chemical potentials. We extend the PNJL model to three flavors and study how the quark condensate depends on the current quark masses and how the subtle interplay between the chiral condensate and the Polyakov loop dynamics is affected by the larger strange quark mass. As an application, various thermodynamical quantities are calculated and confronted with recent lattice QCD results.

7.1 Vacuum properties

The generalization of the NJL model to three quark flavors is not straight-forward. If the number of flavors is greater than two, any four-fermion interaction which preserves $SU(N_f)_L \otimes SU(N_f)_R$ flavor symmetry also has a $U(1)_A$ symmetry which is not present in nature. The simplest multi-fermion interaction that breaks this unwanted symmetry is the 't Hooft determinant [tH76]. This term is phenomenologically important to get the correct mass splitting of the η and η' mesons. In the chiral limit ($m_u = m_d = m_s = 0$), the η' mass is lifted to a finite value by the 't Hooft determinant, while the other pseudoscalar mesons, including the η, remain massless.

Our starting point is again the color-current interaction (4.2). The color currents $J^a_\mu = \bar{\psi}\gamma_\mu t^a \psi$ now involve the quark fields $\bar{\psi} = (\bar{\psi}_u, \bar{\psi}_d, \bar{\psi}_s)$. The three-flavor current quark mass matrix is $\hat{m}_0 = \mathrm{diag}(m_u, m_d, m_s)$ and we shall work in the isospin symmetric limit with $m_u = m_d \equiv m_0$, whereas m_s will in general be different, thus explicitly breaking the $SU(3)$ flavor symmetry. Again, matrix elements for the interaction $G_c \sum_{a=1}^{8} J^a_\mu J^\mu_a$ involve both direct and exchange terms. To deal with the exchange terms, it is convenient to introduce the Fierz transform of $G_c \sum_{a=1}^{8} (\bar{\psi}\gamma_\mu t^a \psi)^2$ and add it to the original interaction. The Fierz transform gives both color-singlet and color-octet terms (see Appendix C). The

color-singlet part reads

$$\mathcal{L}_{\rm int}^{\rm cs} = \frac{G}{2}\sum_{b=0}^{8}\Big[(\bar\psi\lambda_b\psi)^2 + (\bar\psi i\gamma_5\lambda_b\psi)^2 - \frac{1}{2}(\bar\psi\gamma^\mu\lambda_b\psi)^2 - \frac{1}{2}(\bar\psi\gamma^\mu\gamma_5\lambda_b\psi)^2\Big], \tag{7.1}$$

where $G = \frac{16}{9}G_c$ is the effective coupling strength between quarks and anti-quarks and λ_j, $j = 1\ldots8$ are the Gell-Mann matrices in flavor space and $\lambda_0 = \sqrt{2/3}\,\mathbf{1}_f$. The local interaction between color-currents is again transformed into scalar-pseudoscalar and vector-axialvector interactions which operate in color-singlet channels with quantum numbers (flavor and spin) of the various mesons. The remaining color-octet part which includes the original color-current interaction and the color-octet terms of the Fierz transform, is

$$\begin{aligned}\mathcal{L}_{\rm int}^{\rm co} = &-\frac{3}{16}\frac{G}{2}\sum_{a=1}^{8}\sum_{b=0}^{8}\Big[(\bar\psi t_a\lambda_b\psi)^2 + (\bar\psi i\gamma_5 t_a\lambda_b\psi)^2 - \frac{1}{2}(\bar\psi\gamma^\mu t_a\lambda_b\psi)^2 - \frac{1}{2}(\bar\psi\gamma^\mu\gamma_5 t_a\lambda_b\psi)^2\Big]\\ &-\frac{9}{8}\frac{G}{2}\sum_{a=1}^{8}(\bar\psi\gamma^\mu t_a\tau_b\psi)^2.\end{aligned} \tag{7.2}$$

In this chapter we will restrict ourselves to the discussion of the color-singlet part (7.1) of the interaction and for simplicity we will only consider the scalar and pseudoscalar channels:

$$\mathcal{L}_{\rm sym} = \bar\psi(i\partial\!\!\!/ - \hat m_0)\psi + \frac{G}{2}\sum_{b=0}^{8}\Big[(\bar\psi\lambda_b\psi)^2 + (\bar\psi i\gamma_5\lambda_b\psi)^2\Big]. \tag{7.3}$$

The $U(1)_A$ breaking 't Hooft determinant is given by

$$\mathcal{L}_{\rm det} = -K\left\{\det{}_f[\bar\psi(1+\gamma_5)\psi] + \det{}_f[\bar\psi(1-\gamma_5)\psi]\right\}. \tag{7.4}$$

It is a determinant in flavor space, which means that it is a maximally flavor-mixing $2N_f$-point interaction, involving an incoming and an outgoing quark of each flavor. The flavor structure is illustrated in Fig. 7.1.

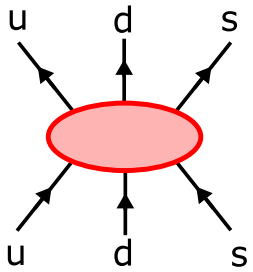

Figure 7.1: Flavor structure of the $U(1)_A$-breaking effective interaction.

The complete three-flavor NJL Lagrangian then reads

$$\mathcal{L} = \mathcal{L}_{\rm sym} + \mathcal{L}_{\rm det}. \tag{7.5}$$

7.1.1 Constituent quarks and mesons

Compared to the two-flavor case there is an additional term in the gap equation involving two quark loops, which arises from the 't Hooft interaction. In Hartree approximation the self-energy is local and thus, only gives rise to a constant shift in the quark masses:

$$M_u = m_u - 2G\langle\bar{u}u\rangle + K\langle\bar{d}d\rangle\langle\bar{s}s\rangle, \tag{7.6}$$
$$M_d = m_d - 2G\langle\bar{d}d\rangle + K\langle\bar{u}u\rangle\langle\bar{s}s\rangle, \tag{7.7}$$
$$M_s = m_s - 2G\langle\bar{s}s\rangle + K\langle\bar{u}u\rangle\langle\bar{d}d\rangle. \tag{7.8}$$

Terms of the form $2G\langle\bar{u}u\rangle$ are already familiar from the two-flavor case. Terms of the form $K\langle\bar{d}d\rangle\langle\bar{s}s\rangle$ only appear in the three flavor case. They represent the t' Hooft interaction illustrated in Fig. 7.1. Linearizing this interaction is equivalent to closing two quark loops. The flavor mixture of the determinant (7.4) then implies that the u quark mass receives contributions from the product $\langle\bar{d}d\rangle\langle\bar{s}s\rangle$ of the condensates of the other two flavors and so forth. For each flavor $q = u, d, s$ the quark condensate is given by

$$\langle\bar{q}q\rangle = -4iN_c \int^{\Lambda} \frac{\mathrm{d}^4p}{(2\pi)^4} \frac{M_q}{p^2 - M_q^2}. \tag{7.9}$$

If we apply a three-momentum cutoff, Eqn. (7.9) becomes

$$\langle\bar{q}q\rangle = 4N_cM \int^{\Lambda} \frac{\mathrm{d}^3p}{(2\pi)^3} \frac{1}{2E_p} = N_c\frac{M_q}{\pi^2} \int_0^{\Lambda} \mathrm{d}p\, \frac{p^2}{E_p}, \tag{7.10}$$

where $E_p = \sqrt{\boldsymbol{p}^2 + M_q^2}$. The three-flavor NJL Lagrangian (7.5) can also be employed to study the properties of mesonic states. One first needs to reduce the six-point interaction $\mathcal{L}_{\mathrm{det}}$ to an effective four point interaction by closing one quark loop, as illustrated in Fig. 7.2. The general procedure to study meson properties is then the same as in the two-flavor NJL model, although it is technically more involved because of the unequal strange and non-strange quark masses. It will not be presented here, for further details see e. g. Refs. [KLVW90, RKH96].

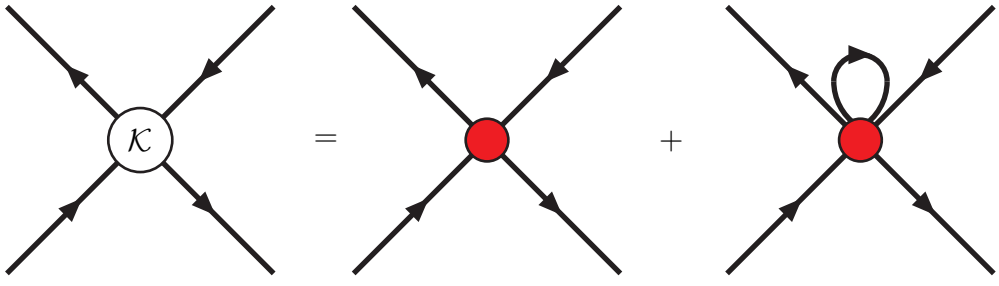

Figure 7.2: The two-body Bethe-Salpeter kernel generated by the three-flavor NJL interaction.

7.1.2 Model parameters

The three-flavor NJL model has five model parameters: the coupling constants G and K, the cutoff parameter Λ and the bare quark masses $m_u = m_d$ and m_s. Thus, compared to the two-flavor NJL model defined by (4.8) we have two additional parameters: m_s and the six-point coupling strength K. However, now there are three additional physical quantities to fix these parameters, namely the masses of the pseudoscalar mesons K, η and η'. Therefore, in the three-flavor NJL model we do not have to rely on the poorly known quark condensate for fixing the parameters. Instead we can use the five well-known observables f_π, m_π, m_K, m_η and m'_η. We will employ the parameters from [RKH96] in the following. They are listed in Table 7.1, together with the corresponding physical quantities in the quark and meson sector.

Λ [MeV]	G [GeV^{-2}]	K [GeV^{-5}]	$m_{u,d}$ [MeV]	m_s [MeV]
602.3	10.1167	311.878	5.5	140.7
f_π [MeV]	m_π [MeV]	m_K [MeV]	m_η [MeV]	$m_{\eta'}$ [MeV]
92.4	135	479.7	514.8	957.8
$M_{u,d}$ [MeV]	M_s [MeV]	$\lvert\langle\bar\psi_u\psi_u\rangle\rvert^{1/3}$ [MeV]	$\lvert\langle\bar\psi_s\psi_s\rangle\rvert^{1/3}$ [MeV]	
367.7	549.5	241.9	257.7	

Table 7.1: Parameter set used in this work for the three-flavor NJL model, and the resulting physical quantities.

7.2 The three-flavor PNJL model

It is straight-forward to generalize the formalism of Sec. 6.6 to the three-flavor case. First we introduce a generalized $N_f = 3$ Nambu–Jona-Lasinio Lagrangian with quarks coupled to a (spatially constant) temporal background $SU(3)$ gauge field A_0, representing Polyakov loop dynamics:

$$\begin{aligned}\mathcal{L}_{\mathrm{PNJL}} = {}& \bar\psi\left(i\not{D} - \hat m_0\right)\psi + \frac{G}{2}\left[\left(\bar\psi\psi\right)^2 + \left(\bar\psi i\gamma_5\lambda_b\psi\right)^2\right] \\ & - K\left\{\det{}_f[\bar\psi(1+\gamma_5)\psi] + \det{}_f[\bar\psi(1-\gamma_5)\psi]\right\} - \mathcal{U}\left(\Phi[A],\Phi^*[A];T\right), \end{aligned} \tag{7.11}$$

where

$$D_\mu = \partial_\mu + iA_\mu \qquad \text{and} \qquad A_\mu = \delta_{\mu 0}A_0, \tag{7.12}$$

and we take the sum over b ($b = 1\ldots 8$). Note that in the chiral limit ($\hat m_0 \to 0$), this Lagrangian is invariant under the chiral flavor group, $SU(3)_L \times SU(3)_R \times U(1)_V$, whereas

the $U_A(1)$ symmetry is broken by the 't Hooft interaction.

The bosonization technique from chapter 4 cannot directly be used to rewrite the Lagrangian (7.11) in terms of the auxiliary field variables σ and $\vec{\pi}$ because of the t' Hooft interaction. Again one first needs to reduce the six-point interaction to an effective four point interaction by closing one quark loop. After this the formalism of sections 4.3 and 6.6 is straightforwardly generalized to the three-flavor case. In the isopsin symmetric case $m_u = m_d \neq m_s$ with two independent chemical potentials $\mu_u = \mu_d \neq \mu_s$, the mean-field thermodynamic potential reads

$$\begin{aligned}\Omega =& \mathcal{U}\left(\Phi, \Phi^*; T\right) + \frac{\sigma_u^2}{2G} + \frac{\sigma_s^2}{4G} - \frac{K}{4G^3}\sigma_u^2\sigma_s \qquad (7.13)\\ &-4\,T\int\frac{\mathrm{d}^3p}{(2\pi)^3}\left\{\mathrm{Tr}_c\ln\left[1 + L\,\mathrm{e}^{-(E_{p,u}-\mu_u)/T}\right] + \mathrm{Tr}_c\ln\left[1 + L^\dagger\,\mathrm{e}^{-(E_{p,u}+\mu_u)/T}\right]\right\}\\ &-2\,T\int\frac{\mathrm{d}^3p}{(2\pi)^3}\left\{\mathrm{Tr}_c\ln\left[1 + L\,\mathrm{e}^{-(E_{p,s}-\mu_s)/T}\right] + \mathrm{Tr}_c\ln\left[1 + L^\dagger\,\mathrm{e}^{-(E_{p,s}+\mu_s)/T}\right]\right\}\\ &-12\int\frac{\mathrm{d}^3p}{(2\pi)^3}E_{p,u}\,\theta(\Lambda^2 - \boldsymbol{p}^2) - 6\int\frac{\mathrm{d}^3p}{(2\pi)^3}E_{p,s}\,\theta(\Lambda^2 - \boldsymbol{p}^2). \qquad (7.14)\end{aligned}$$

The quasiparticle energies are given by

$$E_{p,u} = \sqrt{p^2 + \left(m_{u0} - \sigma_u + \frac{K}{4G^2}\sigma_u\sigma_s\right)^2}, \qquad (7.15)$$

and

$$E_{p,s} = \sqrt{p^2 + \left(m_{s0} - \sigma_s + \frac{K}{4G^2}\sigma_u\sigma_u\right)^2}. \qquad (7.16)$$

The remaining color trace is performed using the explicit representation (6.45) of L. From the thermodynamic potential (7.14) the equations of motion for the mean fields σ_u, σ_s, Φ and Φ^* are derived through

$$\frac{\partial\Omega}{\partial\sigma_u} = 0\ , \qquad \frac{\partial\Omega}{\partial\sigma_s} = 0\ , \qquad \frac{\partial\Omega}{\partial\Phi} = 0\ , \qquad \frac{\partial\Omega}{\partial\Phi^*} = 0\ . \qquad (7.17)$$

This set of coupled equations is then solved for the fields as functions of temperature T and quark chemical potentials μ_u and μ_s. The parameters a_i and b_i are taken to be the same as in the pure gauge case and are listed in Table 6.1. The critical temperature for deconfinement $T_0 = 176$ MeV appearing in Eqn.(6.30) is close to the value $T_c \sim 170$ MeV found in $2+1$ flavor lattice QCD simulations [FKS03]. The parameters of the NJL part remain unchanged and are given in Table 7.1.

Fig. 7.3 shows the constituent quark masses

$$M_u = m_{u0} - \langle\sigma_u\rangle + \frac{K}{4G^2}\langle\sigma_u\rangle\langle\sigma_s\rangle \quad \text{and} \quad M_s = m_{s0} - \langle\sigma_s\rangle + \frac{K}{4G^2}\langle\sigma_u\rangle^2, \qquad (7.18)$$

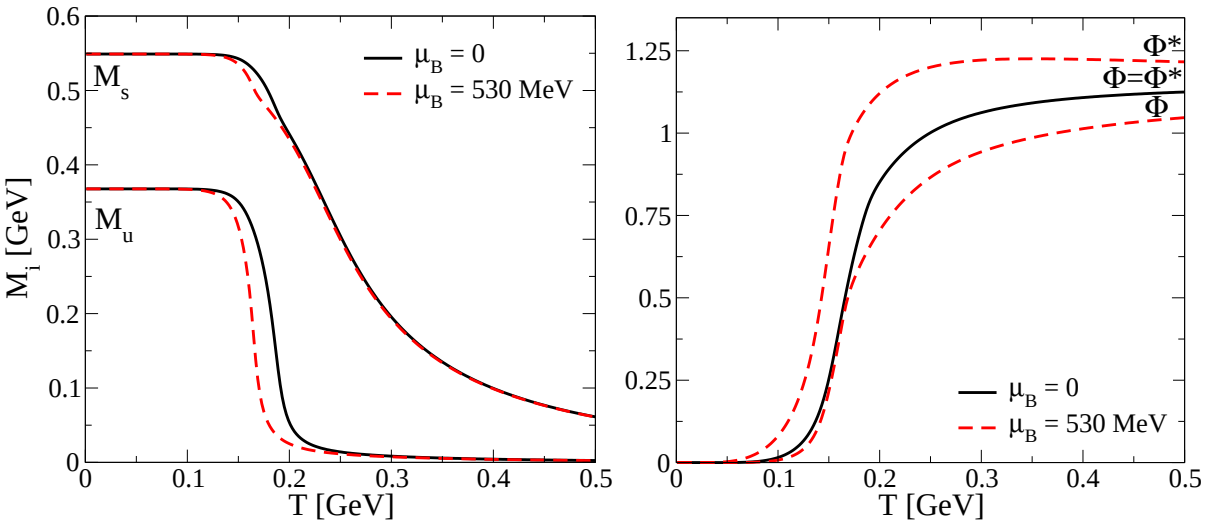

Figure 7.3: Left panel: Constituent quark masses M_u and M_s as functions of the temperature at $\mu_B = 0$ and $\mu_B = 530$. Right panel: Polyakov loop Φ and its charge conjugate Φ^* as functions of temperature at $\mu_B = 0$ and $\mu_B = 530$ MeV.

and the Polyakov loop Φ and its charge conjugate Φ^* as functions of temperature at $\mu_B = 0$ and $\mu_B = 530$ MeV. Note that the constituent quark masses approach zero at high temperature because we did not employ a momentum cutoff on the integrals involving Fermi-Dirac distribution functions in (7.14). This is necessary to preserve the correct behavior of thermodynamical quantities in the high temperature limit.

7.3 Comparison with lattice QCD

In this section we test the predictions of our three-flavor PNJL model with lattice data available for full QCD thermodynamics at finite μ. The scaled pressure difference $\Delta p(T,\mu)/T^4 = (p(T,\mu) - p(T,0))/T^4$ and the scaled baryon number density $n_B(T,\mu)/T^3$ were calculated for $2+1$ flavors of dynamical staggered quarks on $N_t = 4$ lattices using an overlap improved reweighting technique [FKS03]. Only μ-values for the light quarks have been considered in these simulations. A comparison of Δp, calculated in the PNJL model, with corresponding lattice results is presented in Fig. 7.4. This figure shows the scaled pressure difference as a function of temperature for a series of chemical potentials, with values ranging between $\mu_B = 100$ MeV and $\mu_B = 530$ MeV.

A related quantity for which lattice results at finite μ exist is the scaled baryon number density n_B. Our results for n_B compared to corresponding lattice data [FKS03] are shown in Fig. 7.5. Also in this case, the agreement between our PNJL model and the corresponding lattice data is excellent.

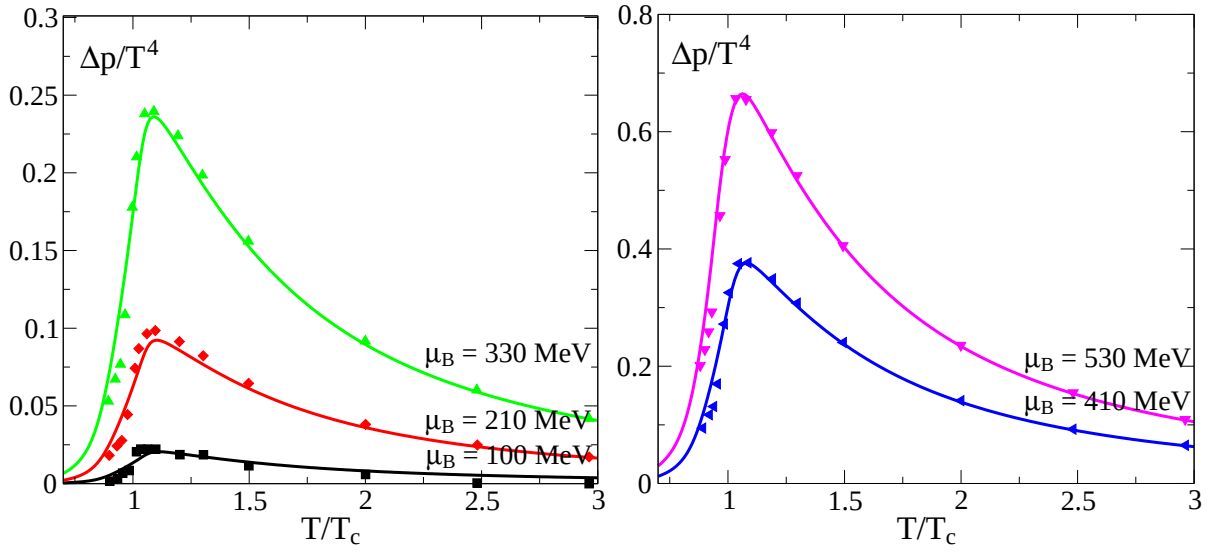

Figure 7.4: Scaled pressure difference as a function of temperature at different values of the baryon chemical potential, compared to corresponding lattice data taken from Ref. [FKS03].

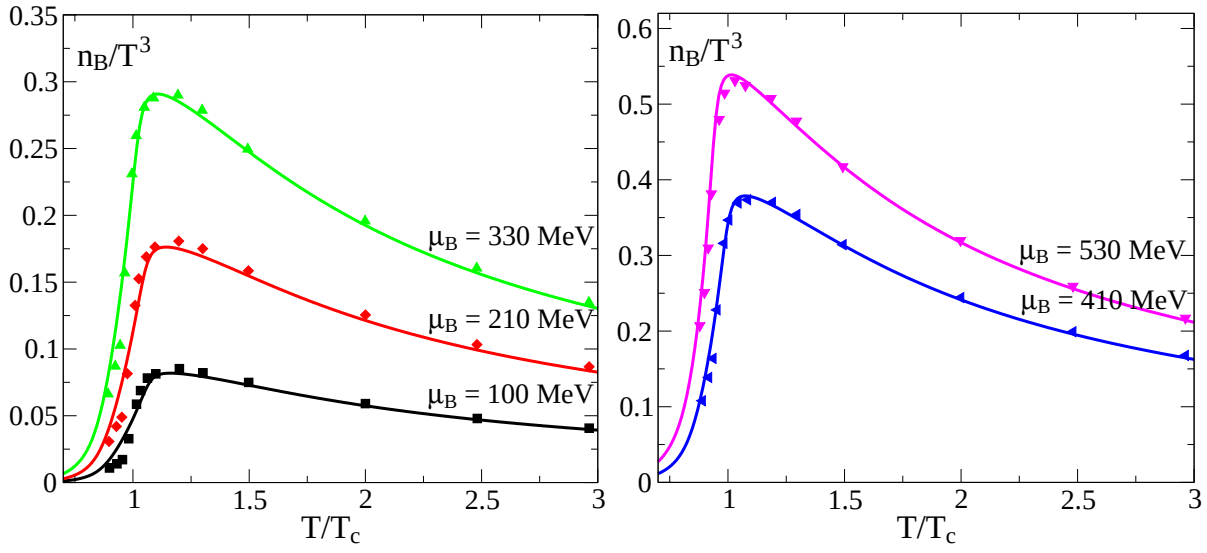

Figure 7.5: Scaled baryon number density as a function of temperature at different values of the baryon chemical potential, compared to corresponding lattice data taken from Ref. [FKS03].

7.4 Summary

In this chapter we have studied a three-flavor Polyakov-loop-extended Nambu–Jona-Lasinio (PNJL) model. The non-trivial result is that the crossovers for chiral symmetry restoration and deconfinement still almost coincide if the strange quark is added. The subtle interplay between the chiral condensate and the Polyakov loop is not altered qualitatively by the additional heavier quark. The model reproduces the pressure difference and the baryon number density at various chemical potentials extremely well when confronted with corresponding lattice data.

Conclusions and Outlook

In this work we have studied the thermodynamics of QCD at high temperatures and finite quark chemical potential using QCD inspired phenomenological and field theoretical models. There are several motivations to study QCD under extreme conditions, such as high temperatures. First, QCD is expected to undergo a phase transition from a confined hadronic phase to a deconfined partonic phase, the so-called *Quark-Gluon Plasma* (QGP), at a temperature roughly equal to the QCD scale $\Lambda_{\mathrm{QCD}} \sim 200$ MeV. In this deconfined phase, quarks and gluons are no longer bound into hadrons, but can move over larger distances. At the same time, the chiral symmetry which is spontaneously broken in the hadronic phase, is restored. Studying these transitions is interesting in itself, but it may also help us to understand the structure of hadrons and their interactions. Second, QCD simplifies under extreme conditions: At scales relevant to hadrons, the QCD coupling constant is large and perturbative calculations are bound to fail. We have to rely on numerical simulations in order to test predictions of QCD. However, at very high temperatures the coupling constant becomes small and perturbative calculations should become feasible. Third, the QGP may be created in earth-bound experiments, the ultra-relativistic heavy-ion collisions. It is expected that the colliding nuclei deposit so much energy in the collision region that a thermalized system of particles forms which subsequently expands and cools off. If the initial energy density is above the critical energy density $\epsilon_c \sim 1$ GeV/fm^3, a QGP should form. First dedicated experiments started at CERN at SPS, followed by AGS and RHIC at BNL. Such extreme conditions also existed in the early universe: About 10^{-5} seconds after the big bang the temperature in the universe was of order $\mathcal{O}(200$ MeV) and the universe was filled with a QGP.

However, there are several obstacles that considerably complicate studies of the phase transition and the QGP. To begin with, the QGP might very well have been produced in ultra-relativistic heavy-ion collisions, but for us to study its properties, we require it to leave distinct traces in the detectors. Any signature of the QGP is folded with the time evolution (and consequently the evolution of volume, temperature, and baryon density) of the fireball created in the collision. Furthermore, this evolution continues after the system runs through the phase transition and thus, any information is mixed with signals from the conventional hadronic phase. On the theoretical side, even at temperatures several orders of magnitude higher than the critical temperature, where the formation of the QGP is expected, perturbative calculations are not feasible due to the bad convergence of the perturbative expansion. One has to rely on numerical simulations or phenomenological models for all but astronomically high temperatures that are clearly

beyond any practical importance. As a consequence, previous work has mainly focused on interpreting one piece of data within a specific approach and with a certain number of fit parameters. The main goal of this thesis was to develop a novel field-theoretical model based on two key properties of QCD, confinement and chiral symmetry breaking, with parameters controlled by a few properties of the gluonic and hadronic sectors of the QCD phase diagram. Since the dynamics of this model is rooted in symmetries dictated by QCD itself, it does not merely parametrize QCD thermodynamical quantities, but rather predicts them, which is a significant improvement over previous approaches.

To set the stage we have given an up-to-date review of QCD thermodynamics in chapter 1, referring mainly to the latest data from lattice QCD simulations. In chapter 2 we demonstrated that basic features of lattice QCD thermodynamics can be understood using the MIT bag model, a simple phenomenological model that implements two of the key properties of QCD, asymptotic freedom and confinement. This model is the most widely used equation of state (EoS) in astrophysics to study the properties of deconfined quark matter. The aim of this chapter was twofold: First we wanted to explain some of the key features of the lattice QCD phase diagram and the EoS exemplarily in terms of a clear and simple physical model and set the stage for the more refined models which were discussed in subsequent chapters of this work. The second purpose was to demonstrate that the MIT bag model is clearly not apt to describe quark matter at finite densities: it fails to reproduce the non-trivial behavior of lattice thermodynamical quantities at finite quark chemical potential. Thus, while the bag model is quite attractive due to its simplicity, it is clearly not adequate to perform precise numerical calculations of quark matter properties at finite temperature and finite quark chemical potential.

The aim of chapter 3 was to construct a more realistic EoS that could be used to interpret lattice results at high temperatures and finite quark chemical potential. To this end we have generalized a novel quasiparticle description of the QCD EoS to finite quark chemical potential. This model schematically includes confinement by a modification of the particle distribution functions and achieves a simple, thermodynamically consistent and economic parametrization of lattice data for the QCD EoS. To extend this model to finite quark chemical potential, we derived partial differential flow equations for the confinement function $C(T,\mu)$ and the effective coupling $G(T,\mu)$ of the model and solved them numerically. These flow equations follow directly from the Maxwell relations of thermodynamics which assure thermodynamic self-consistency. Such an extension is important for a number of reasons: First, for current heavy ion collision experiments at SPS and RHIC the chemical freeze-out occurs at $\mu_{f.o.} \simeq 100$ MeV, (baryon chemical potential $\mu_B \simeq 300$ MeV) [BMHS99] and $\mu_{f.o.} \simeq 15$ MeV, ($\mu_B \simeq 45$ MeV) [BMMRS01], respectively. Thus, a finite quark chemical potential should be introduced to describe the deconfined quark matter created in these experiments. Second, first lattice QCD simulations at finite quark chemical potential are now available and it is of great theoretical interest to interpret these lattice results. Third, the introduction of an additional external control parameter helps to test the reliability of the quasiparticle approach. We used this model to calculate the phase boundary line $T_c(\mu)$, the scaled pressure difference

$\Delta p(T,\mu) = (p(T,\mu) - p(T,\mu=0))/T^4$ and the scaled quark number density $n_q(T,\mu)/T^3$. We compared our results to recent lattice calculations and found remarkably good agreement even for large quark chemical potentials $\mu \sim T_c$. Finally, we have dropped the assumption that the confinement factor only depends on temperature and constructed a model with momentum dependent confinement, following Ref. [EFR+89]. We applied this model to pure $SU(3)$ gauge theory and full QCD and found good agreement with lattice results for the pressure, the energy density, and the interaction measure. All in all, the confinement quasiparticle model successfully describes and predicts a variety of lattice data at vanishing and finite quark chemical potential and seems to be a reasonable and useful representation of the QGP equation of state.

Strong interactions also lead to another important phenomenon, the spontaneous breaking of chiral symmetry, which is essential to understand the lightest hadrons and the generation of mass in QCD. Thus, we devoted chapter 4 to the Nambu–Jona-Lasinio (NJL) model, which is particularly well suited to study and exemplify the mechanisms of chiral symmetry breaking and restoration. The NJL model is an effective Lagrangian of relativistic quarks interacting through local fermion-fermion couplings. In principle it can be obtained from QCD by "integrating out" the gluonic degrees of freedom, replacing them by a four-point color-current interaction. Starting from this QCD motivated interaction we investigated the vacuum properties of the theory and outlined how the NJL model can be employed to study quark and meson properties at finite temperature and finite quark chemical potential. As an application we calculated the constituent quark mass, the pion mass and the sigma mass as functions of temperature and quark chemical potential. The NJL model emphasizes symmetries and ignores confinement. However, one of the key properties of QCD is color confinement, which requires that quarks at low energies have to be part of bound color-singlet states. Colored quark-antiquark pairs have never been observed in nature. In chapter 5 we have studied the color-octet sector of the NJL model and calculated the masses of various color-octet bound states. Poles of the respective Bethe-Salpeter amplitudes appear at mass scales several times the NJL cutoff scale and are far removed from the low-energy spectrum. Finally we showed that this also holds at finite temperature and finite quark chemical potential.

We have studied confinement and chiral symmetry breaking in two very successful, but rather different theoretical frameworks: the confinement quasiparticle model and the NJL model. The aim of chapter 6 was to develop a more general model that is suitable to study confinement and chiral symmetry breaking in a unified framework. Our starting point was the heavy quark limit, where the confined and deconfined phases are characterized by distinct symmetry properties: the $Z(3)$ center symmetry of the $SU(3)$ gauge group is spontaneously broken in the confined phase, while it is restored in the deconfined phase. The associated order parameter is the Polyakov loop, a Wilson line closed around the Euclidean time direction. Subsequently, we have constructed an effective theory for the Polyakov loop and tested it at finite temperature against results from $SU(3)$ lattice gauge theory. The lattice data are reproduced extremely well by our ansatz. If quarks are added, the center symmetry gets explicitly broken and no order parameter can be estab-

lished, but the Polyakov loop still changes rapidly close to T_c and serves as an indicator of a rapid crossover towards deconfinement. To include chiral symmetry breaking and its restoration at high temperatures, we have introduced a generalized NJL Lagrangian with quarks coupled to a (spatially constant) temporal background $SU(3)$ gauge field A_0, representing Polyakov loop dynamics. This Polyakov-loop extended (PNJL) model represents a minimal synthesis of the two basic principles that govern QCD at low temperatures: spontaneous chiral symmetry breaking and confinement. The respective order parameters (the chiral quark condensate and the Polyakov loop) are given the meaning of collective degrees of freedom. Quarks couple to these collective fields according to the symmetry rules dictated by QCD itself. Once a limited set of input parameters is fitted to lattice QCD in the pure gauge sector and to pion properties in the hadron sector, the quark-gluon thermodynamics above T_c up to about twice the critical temperature is well reproduced, including quark densities up to chemical potentials of about 0.2 GeV. In particular, the PNJL model correctly describes the step from the first-order deconfinement transition observed in pure-gauge lattice QCD (with $T_c \simeq 270$ MeV) to the crossover transition (with T_c less than 200 MeV) when $N_f = 2$ light quark flavors are added. The non-trivial result is that the crossovers for chiral symmetry restoration and deconfinement almost coincide, as found in lattice simulations. The model also reproduces the scaled pressure differences and the quark number densities at various chemical potentials remarkably well when confronted with corresponding lattice data. In chapter 7 we have extended the PNJL model to the physical relevant three-flavor case. The crossovers for chiral symmetry restoration and deconfinement still almost coincide if the strange quark is added. The subtle interplay between the chiral condensate and the Polyakov loop is not altered qualitatively by the additional heavier quark. Lattice QCD results for the pressure difference and the baryon number density for baryon chemical potentials up to $\mu_B = 530$ MeV are reproduced extremely well by this model.

Further developments should be directed towards improvements to overcome some obvious limitations. First, the NJL model operates with constant four-point coupling strengths which presumably average the relevant running couplings over a limited low-energy kinematic domain, corresponding to temperatures $T \lesssim 2\,T_c$ and quark chemical potentials $\mu_q \lesssim 0.3$ GeV. Contacts with the high-temperature limit of QCD and the HTL approaches need to be established. Second, in order to proceed into the range of larger chemical potentials, diquark degrees of freedom need to be explicitly involved. Also, the effective potential for the Polyakov loop field, determined so far entirely as a function of temperature by investigating the pure gauge sector, must be examined with respect to its dependence on the chemical potential.

Nevertheless, the conclusion that can be drawn at this point is promising: it appears that a relatively straightforward quasiparticle approach, with its dynamics rooted in spontaneous chiral symmetry breaking and confinement and with parameters controlled by a few known properties of the gluonic and hadronic sectors of the QCD phase diagram, can account for essential observations from two-flavor and three-flavor lattice QCD thermodynamics.

Appendix A

Calculation of $B(T, \mu)$

The "background field" quantity $B(T, \mu)$ appearing in Eqn. (3.21) can be obtained from the Gibbs-Duhem relation

$$\epsilon + p = Ts + \mu n = T\frac{\partial p}{\partial T} + \mu\frac{\partial p}{\partial \mu}. \tag{A.1}$$

The left hand side reads:

$$\epsilon + p = \frac{N_c N_f}{3\pi^2}\int_0^\infty \mathrm{d}k\,[f_D^+ + f_D^-]C(T,\mu)k^2\left(\frac{4k^2+3m_q^2}{E_k}\right). \tag{A.2}$$

To evaluate the right-hand side, derivatives of $f_D^\pm(E_k^q)$ with respect to T and μ are rewritten as derivatives with respect to k. After an integration by parts, the first term on the right-hand side reads

$$\begin{aligned} T\frac{\partial p}{\partial T} =& T\frac{N_c N_f}{3\pi^2}\int_0^\infty \mathrm{d}k f_D^+\left(\frac{\partial C}{\partial T}\frac{k^4}{E_k} - C(T,\mu)\frac{3k^2}{2E_k}\frac{\partial m_q^2}{\partial T} + C(T,\mu)(E_k+\mu) + C(T,\mu)\frac{k^4}{TE_k}\right) \\ &+ T\frac{N_c N_f}{3\pi^2}\int_0^\infty \mathrm{d}k f_D^-\left(\frac{\partial C}{\partial T}\frac{k^4}{E_k} - C(T,\mu)\frac{3k^2}{2E_k}\frac{\partial m_q^2}{\partial T} + C(T,\mu)(E_k-\mu) + C(T,\mu)\frac{k^4}{TE_k}\right) \\ &- T\frac{\partial B(T,\mu)}{\partial T}, \end{aligned} \tag{A.3}$$

and the second term is given by

$$\begin{aligned} \mu\frac{\partial p}{\partial \mu} =& \mu\frac{N_c N_f}{3\pi^2}\int_0^\infty \mathrm{d}k f_D^+\left(\frac{\partial C(T,\mu)}{\partial \mu}\frac{k^4}{E_k} - C(T,\mu)\frac{\partial m_q^2}{\partial \mu}\frac{3k^2}{2E_k} - C(T,\mu)3k^2\right) \\ &+ \mu\frac{N_c N_f}{3\pi^2}\int_0^\infty \mathrm{d}k f_D^-\left(\frac{\partial C(T,\mu)}{\partial \mu}\frac{k^4}{E_k} - C(T,\mu)\frac{\partial m_q^2}{\partial \mu}\frac{3k^2}{2E_k} + C(T,\mu)3k^2\right) - \mu\frac{\partial B(T,\mu)}{\partial \mu}. \end{aligned} \tag{A.4}$$

Substituting (A.2), (A.3) and (A.4) in the Gibbs-Duhem relation yields a partial differential equation of the type

$$x\frac{\partial f(x,y)}{\partial x} + y\frac{\partial f(x,y)}{\partial y} = \mathcal{I}(x,y). \tag{A.5}$$

It has the general solution

$$f(x,y) = \int^x \mathrm{d}t\, \mathcal{I}(t, \frac{y}{x}t) + \mathcal{H}\left(\frac{y}{x}\right). \tag{A.6}$$

Here, $\mathcal{H}(y/x)$ is a solution of the homogeneous equation. Returning to our case, $\mathcal{H}(\mu/T)$ becomes an arbitrary function of the ratio μ/T to be fixed by boundary conditions. For $\mu \to 0$, $\mathcal{H}(\mu/T)$ does not depend on T anymore and therefore has to be identified with an integration constant B_0. Provided that $\mathcal{H}(\mu/T)$ is a continuous function it must be close to B_0 for small μ/T. The first term in a Taylor expansion of $\mathcal{H}(\mu/T)$ vanishes and the series starts only at order $(\mu/T)^2$. Therefore we identify $\mathcal{H}(\mu/T)$ with the constant B_0 for all μ under consideration. Assembling all pieces, the final result reads

$$\begin{aligned}
B(T,\mu) &= B_1(T,\mu) + B_2(T,\mu) + B_0, \\
B_1(T,\mu) &= \frac{N_c N_f}{3\pi^2}\int_0^\infty \mathrm{d}k \int_{T_c}^T \mathrm{d}\tau \left[f_D^+(E_k^q) + f_D^-(E_k^q)\right] \left(\frac{\partial C}{\partial \tau} + \frac{\mu}{T}\frac{\partial C}{\partial\left(\frac{\mu}{T}\tau\right)}\right) \frac{k^4}{E_k^q}, \\
B_2(T,\mu) &= -\frac{N_c N_f}{2\pi^2}\int_0^\infty \mathrm{d}k \int_{T_c}^T \mathrm{d}\tau\, C \left[f_D^+(E_k^q) + f_D^-(E_k^q)\right] \left(\frac{\partial m_q^2}{\partial \tau} + \frac{\mu}{T}\frac{\partial m_q^2}{\partial\left(\frac{\mu}{T}\tau\right)}\right) \frac{k^2}{E_k^q},
\end{aligned} \tag{A.7}$$

where the explicit τ-dependence in $C(\tau, \mu/T\,\tau)$, $m_q(\tau, \mu/T\,\tau)$ and $E_k^q(\tau, \mu/T\,\tau)$ has been suppressed for the sake of lucidity.

Appendix B

Method of Characteristics

Equations (3.24) and (3.25) are a set of coupled quasilinear first order partial differential equations for the effective coupling constant $G^2(T,\mu)$ and the confinement factor $C(T,\mu)$. Equation (3.24) does not depend on $C(T,\mu)$. Thus we can first solve this equation for $G^2(T,\mu)$ and insert the result in equation (3.25).

The usual method found in textbooks is to reduce a quasilinear partial differential equation of the form

$$a_T(T,\mu;X)\frac{\partial X}{\partial T} + a_\mu(T,\mu;X)\frac{\partial X}{\partial \mu} = c(T,\mu;X) \tag{B.1}$$

to a system of coupled ordinary differential equations,

$$\frac{\mathrm{d}T(s)}{\mathrm{d}s} = a_T, \quad \frac{\mathrm{d}\mu(s)}{\mathrm{d}s} = a_\mu, \quad \frac{\mathrm{d}X(s)}{\mathrm{d}s} = c. \tag{B.2}$$

This determines the characteristic curves $T(s)$, $\mu(s)$, and the evolution of X along such a curve, given an initial value. However, this method is not well suited for numerical use which is necessary for non-trivial a_T, a_μ and c. Rewriting equation (B.1) as

$$a_T\left(\frac{\mathrm{d}X}{\mathrm{d}T} - \frac{\partial X}{\partial \mu}\frac{\mathrm{d}\mu}{\mathrm{d}T}\right) + a_\mu\frac{\partial X}{\partial \mu} = c \Longrightarrow \frac{\partial X}{\partial \mu}\left(\frac{a_\mu}{a_T}\mathrm{d}T - \mathrm{d}\mu\right) = \frac{c}{a_T}\mathrm{d}T - \mathrm{d}X, \tag{B.3}$$

we find the equation $a_\mu\,\mathrm{d}T - a_T\,\mathrm{d}\mu = 0$ for the characteristics and $c\,\mathrm{d}T - a_T\,\mathrm{d}X = 0$ for the evolution of X. These equations can easily be solved numerically.

Appendix C

Fierz Transformations

In this appendix we derive the color-singlet interaction (4.3) and the color-octet interaction (4.4) from the simple color-current interaction (4.2).

C.1 General aim

Consider a local four-point interaction of the form

$$\mathcal{L}_{\rm int} = g_K \left(\bar{\psi}\Gamma^{(K)}\psi\right)^2 = g_K \Gamma^{(K)}_{ab}\Gamma^{(K)}_{cd}\bar{\psi}_a\psi_b\bar{\psi}_c\psi_d, \tag{C.1}$$

where $\Gamma^{(K)}_{ab}$ is a matrix in Dirac-, color- and flavor space, with $a = (\alpha, c, f)$ combining indices in these three spaces. The superscript K spans the space of matrices in the three spaces given. Permuting two of the fields and taking into account the anti-commutation relation for fermions, we obtain the identity

$$\mathcal{L}_{\rm int} = -g_K \left(\bar{\psi}\Gamma^{(K)}\psi\right)^2 = g_K \Gamma^{(K)}_{ab}\Gamma^{(K)}_{cd}\bar{\psi}_a\psi_d\bar{\psi}_c\psi_b \equiv \mathcal{L}_{\rm ex}. \tag{C.2}$$

If we restrict ourselves to Hartree-type approximations where the first field is contracted with the second, and the third one with the forth, $\mathcal{L}_{\rm ex}$ yields the exchange diagrams (Fock terms) of $\mathcal{L}_{\rm int}$. For this purpose it is useful to rewrite the operators as

$$\sum_K \Gamma^{(K)}_{ab}\Gamma^{(K)}_{cd} = \sum_M c_{KM}\Gamma^{(M)}_{ad}\Gamma^{(M)}_{cb}, \tag{C.3}$$

to get

$$\mathcal{L}_{\rm ex} = -g_K \sum_M c_{KM}\left(\bar{\psi}\Gamma^{(M)}\psi\right)^2. \tag{C.4}$$

Combining (C.3) with the original interaction (C.1) we obtain

$$\mathcal{L}_{\bar{q}q} = \mathcal{L}_{\rm int} + \mathcal{L}_{\rm ex} = \sum_M G_M \left(\bar{\psi}\Gamma^{(M)}\psi\right)^2, \tag{C.5}$$

with $G_M = c_{KM}g_M$ for $M \neq K$ and $G_K = (1 - c_{KK})g_K$. By construction, $\mathcal{L}_{\bar{q}q}$ is to be used in Hartree approximation only, to avoid double counting.

C.2 Fierz identities for local four-point operators

In the following we will list the crossing matrices in Dirac-, color- and flavor-space. In Dirac space, we find the following relations in the quark-antiquark channel,

$$\begin{pmatrix} (I)_{ij}(I)_{kl} \\ (i\gamma_5)_{ij}(i\gamma_5)_{kl} \\ (\gamma^\mu)_{ij}(\gamma_\mu)_{kl} \\ (\gamma^\mu\gamma_5)_{ij}(\gamma_\mu\gamma_5)_{kl} \\ (\sigma^{\mu\nu})_{ij}(\sigma_{\mu\nu})_{kl} \end{pmatrix} = \begin{pmatrix} \frac{1}{4} & -\frac{1}{4} & \frac{1}{4} & -\frac{1}{4} & \frac{1}{8} \\ -\frac{1}{4} & \frac{1}{4} & \frac{1}{4} & -\frac{1}{4} & -\frac{1}{8} \\ 1 & 1 & -\frac{1}{2} & -\frac{1}{2} & 0 \\ -1 & -1 & -\frac{1}{2} & -\frac{1}{2} & 0 \\ 3 & -3 & 0 & 0 & -\frac{1}{2} \end{pmatrix} \begin{pmatrix} (I)_{il}(I)_{kj} \\ (i\gamma_5)_{il}(i\gamma_5)_{kj} \\ (\gamma^\mu)_{il}(\gamma_\mu)_{kj} \\ (\gamma^\mu\gamma_5)_{il}(\gamma_\mu\gamma_5)_{kj} \\ (\sigma^{\mu\nu})_{il}(\sigma_{\mu\nu})_{kj} \end{pmatrix}, \quad \text{(C.6)}$$

while for the generators of $U(N)$ we find

$$\begin{pmatrix} (I)_{ij}(I)_{kl} \\ (\lambda_a)_{ij}(\lambda_a)_{kl} \end{pmatrix} = \begin{pmatrix} \frac{1}{N} & \frac{1}{2} \\ 2\frac{N^2-1}{N^2} & -\frac{1}{N} \end{pmatrix} \begin{pmatrix} (I)_{il}(I)_{kj} \\ (\lambda_a)_{il}(\lambda_a)_{kj} \end{pmatrix}, \quad \text{(C.7)}$$

where $\lambda_a, a = 1, \ldots, N^2-1$ are the generators of $SU(N)$, normalized as $\mathrm{tr}[\lambda_a, \lambda_b] = 2\delta_{ab}$ and I is the $N \times N$ unit matrix.

C.3 Color-current interaction

Next we demonstrate in detail how the color-singlet interaction (4.3) and the color-octet interaction (4.4) are obtained from the color-current interaction (4.2) by Fierz-transformations in Dirac-, color- and flavor-space. Explicitly writing out color, flavor and Dirac indices Eqn. (4.2) reads:

$$\mathcal{L}^c_{\mathrm{int}} = -G_c \sum_{a=1}^{3} \left[\bar\psi_{i,p,\mu}\psi_{j,q,\nu}\bar\psi_{k,r,\rho}\psi_{l,s,\sigma}(\gamma_\alpha)_{\mu\nu}(\gamma^\alpha)_{\rho\sigma}(t_a)_{ij}(t_a)_{kl}(I)_{pq}(I)_{rs}\right]. \quad \text{(C.8)}$$

The indices are:

$$\begin{aligned} i,j,k,l \quad &\rightarrow \quad \text{color indices,} \\ p,q,r,s \quad &\rightarrow \quad \text{flavor indices,} \\ \mu,\nu,\rho,\sigma \quad &\rightarrow \quad \text{Dirac indices.} \end{aligned} \quad \text{(C.9)}$$

In order to Fierz-transform the flavor indices we use the identity

$$(I)_{pq}(I)_{rs} = \frac{1}{2}\sum_{b=0}^{4}(\tau_b)_{ps}(\tau_b)_{rq}, \quad \text{(C.10)}$$

which is given by the first line of (C.7) for two flavors. τ_1, τ_2 and τ_3 are the usual Pauli matrices and τ_0 is the 2×2 identity matrix. Eqn. (C.8) then becomes

$$\mathcal{L}^c_{\mathrm{int}} = -\frac{1}{2}G_c \sum_{a=1}^{8}\sum_{b=0}^{3}\left[\bar\psi_{i,p,\mu}\psi_{j,q,\nu}\bar\psi_{k,r,\rho}\psi_{l,s,\sigma}(\gamma_\alpha)_{\mu\nu}(\gamma^\alpha)_{\rho\sigma}(t_a)_{ij}(t_a)_{kl}(\tau_b)_{ps}(\tau_b)_{rq}\right]. \quad \text{(C.11)}$$

To Fierz-transform the color indices we employ the identity

$$\sum_{a=1}^{8}(t_a)_{ij}(t_a)_{kl} = \left(\frac{16}{9}(I)_{il}(I)_{kj} - \frac{1}{3}\sum_{a=1}^{8}(t_a)_{il}(t_a)_{kj}\right), \tag{C.12}$$

which is the second line of (C.7) for three colors. The result reads

$$\mathcal{L}^c_{\text{int}} = -\frac{1}{2}G_c\sum_{b=0}^{3}\Bigg[\bar\psi_{i,p,\mu}\psi_{j,q,\nu}\bar\psi_{k,r,\rho}\psi_{l,s,\sigma}(\gamma_\alpha)_{\mu\nu}(\gamma^\alpha)_{\rho\sigma} \times\left(\frac{16}{9}(I)_{il}(I)_{kj} - \frac{1}{3}\sum_{a=1}^{8}(t_a)_{il}(t_a)_{kj}\right)(\tau_b)_{ps}(\tau_b)_{rq}\Bigg]. \tag{C.13}$$

Finally, we use the relation

$$(\gamma^\alpha)_{\mu\nu}(\gamma_\alpha)_{\rho\sigma} = \frac{1}{4}\Big[4(I)_{\mu\sigma}(I)_{\rho\nu} - 2(\gamma^\alpha)_{\mu\sigma}(\gamma_\alpha)_{\rho\nu} - 2(\gamma^\alpha\gamma^5)_{\mu\sigma}(\gamma_\alpha\gamma_5)_{\rho\nu} + 4(i\gamma^5)_{\mu\sigma}(i\gamma_5)_{\rho\nu}\Big], \tag{C.14}$$

which is given by the third line of (C.6). We obtain

$$\mathcal{L}^c_{\text{int}} = -\frac{1}{2}G_c\sum_{b=0}^{3}\Bigg[\bar\psi_{i,p,\mu}\psi_{j,q,\nu}\bar\psi_{k,r,\rho}\psi_{l,s,\sigma}\Bigg((I)_{\mu\sigma}(I)_{\rho\nu} - \frac{1}{2}(\gamma^\alpha)_{\mu\sigma}(\gamma_\alpha)_{\rho\nu} - \frac{1}{2}(\gamma_\alpha\gamma_5)_{\mu\sigma}(\gamma^\alpha\gamma^5)_{\rho\nu} + (i\gamma_5)_{\mu\sigma}(i\gamma^5)_{\rho\nu}\Bigg)\left(\frac{16}{9}(I)_{il}(I)_{kj} - \frac{1}{3}\sum_{a=1}^{8}(t_a)_{il}(t_a)_{kj}\right)(\tau_b)_{ps}(\tau_b)_{rq}\Bigg]. \tag{C.15}$$

Permuting the fermion field operators and omitting the Dirac, color and flavor indices this can be written as

$$\begin{aligned}\mathcal{L}^c_{\text{int}} = {}& \frac{8}{9}G_c\sum_{b=0}^{3}\left[(\bar\psi\tau_b\psi)^2 + (\bar\psi i\gamma_5\tau_b\psi)^2 - \frac{1}{2}(\bar\psi\gamma_\alpha\tau_b\psi)^2 - \frac{1}{2}(\bar\psi\gamma_\alpha\gamma_5\tau_b\psi)^2\right] \\ & - \frac{1}{6}G_c\sum_{a=1}^{8}\sum_{b=0}^{3}\left[(\bar\psi t_a\tau_b\psi)^2 + (\bar\psi i\gamma_5 t_a\tau_b\psi)^2 - \frac{1}{2}(\bar\psi\gamma_\alpha t_a\tau_b\psi)^2 - \frac{1}{2}(\bar\psi\gamma_\alpha\gamma_5 t_a\tau_b\psi)^2\right],\end{aligned} \tag{C.16}$$

from which we can easily read

$$\frac{G}{2} = \frac{8}{9}G_c. \tag{C.17}$$

A similar calculation for three quark flavors leads to

$$\begin{aligned}\mathcal{L}^c_{\text{int}} = {}& \frac{8}{9}G_c\sum_{b=0}^{8}\left[(\bar\psi\lambda_b\psi)^2 + (\bar\psi i\gamma_5\lambda_b\psi)^2 - \frac{1}{2}(\bar\psi\gamma_\alpha\lambda_b\psi)^2 - \frac{1}{2}(\bar\psi\gamma_\alpha\gamma_5\lambda_b\psi)^2\right] \\ & - \frac{1}{6}G_c\sum_{a=1}^{8}\sum_{b=0}^{8}\left[(\bar\psi t_a\lambda_b\psi)^2 + (\bar\psi i\gamma_5 t_a\lambda_b\psi)^2 - \frac{1}{2}(\bar\psi\gamma_\alpha t_a\lambda_b\psi)^2 - \frac{1}{2}(\bar\psi\gamma_\alpha\gamma_5 t_a\lambda_b\psi)^2\right],\end{aligned} \tag{C.18}$$

where λ_b are now the Gell-Mann matrices in flavor space. The coefficients of (C.16) and (C.18) are the same.

Appendix D

Loop Integrals

In this appendix we derive the expressions for the finite temperature loop integrals that are used in this work. We start from the vacuum expressions and use the Matsubara formalism to obtain the loop integrals at finite temperature and non-zero quark chemical potential. We perform the frequency sums and obtain explicit expressions involving only an integration in momentum space.

D.1 One fermion line

Loop integrals with a single fermion line are used e.g. to evaluate the gap equation at finite temperature and non-zero quark chemical potential. The vacuum expression for the one fermion line integral reads

$$A(m) = \int \frac{\mathrm{d}^4 p}{(2\pi)^4} \frac{1}{p^2 - m^2 + i\epsilon}, \tag{D.1}$$

where m denotes the mass of the particle. In the imaginary time formalism, which we have introduced in chapter 1, the only modifications of the usual Feynman rules at $T = 0$ arise from the (anti)periodic boundary conditions of the fields. As a consequence, integrals have to be replaced by

$$\int \frac{\mathrm{d}^4 p}{(2\pi)^4} \;\rightarrow\; iT \sum_{n=-\infty}^{+\infty} \int \frac{\mathrm{d}^3 p}{(2\pi)^3}, \tag{D.2}$$

where the sum is understood to be taken over the discrete set of Matsubara frequencies ω_n. Energy-momentum conserving delta functions become

$$(2\pi)^4 \delta^{(4)}(p) \;\rightarrow\; \frac{(2\pi)^3}{iT} \delta_{n,0} \delta^{(3)}(\boldsymbol{p}). \tag{D.3}$$

The Matsubara frequencies appear as

$$p_0 \;\rightarrow\; i\omega_n + \mu = \frac{2\pi i}{\beta}(n + \zeta) + \mu, \quad n \in \mathbb{Z} \text{ and } \zeta = \begin{cases} 0 & \text{for bosons,} \\ \frac{1}{2} & \text{for fermions.} \end{cases} \tag{D.4}$$

Thus, at finite temperature and non-zero quark chemical potential Eqn. (D.1) is given by

$$A(m) \overset{T\geq 0}{=} -iT \sum_n \int \frac{\mathrm{d}^3 p}{(2\pi)^3} \frac{1}{(\omega_n - i\mu)^2 + E_p^2}, \tag{D.5}$$

where $E_p = \sqrt{\boldsymbol{p}^2 + m^2}$. To evaluate the Matsubara frequencies in (D.5) it is useful to decompose it into partial fractions. Employing the identity

$$\frac{1}{u^2 + v^2} = \sum_{s=\pm 1} \frac{s}{2v} \frac{1}{iu + sv}, \tag{D.6}$$

we obtain

$$A(m) = -iT \sum_n \sum_{s=\pm 1} \int \frac{\mathrm{d}^3 p}{(2\pi)^3} \frac{s}{2E_p} \frac{1}{i(\omega_n - i\mu) + sE_p}. \tag{D.7}$$

Next we can make use of the identity

$$T \sum_{n \in Z} \frac{1}{2\pi i T n + x} = b(x) + \frac{1}{2}, \quad \text{with} \quad b(x) \equiv \frac{1}{e^{x/T} - 1}, \tag{D.8}$$

to calculate the sum in (D.7):

$$A(m) = -i \sum_{s=\pm 1} \int \frac{\mathrm{d}^3 p}{(2\pi)^3} \frac{s}{2E_p} \left[b(i\pi T + \mu + sE_p) + \frac{1}{2} \right]. \tag{D.9}$$

To further simplify (D.9) we use the identity

$$b(x + i\pi T) = -f(x), \quad \text{with} \quad b(x) \equiv \frac{1}{e^{x/T} + 1}, \tag{D.10}$$

and perform the sum over s. Dropping the vacuum part (the factor 1/2), we find

$$A(m) = -i \int \frac{\mathrm{d}^3 p}{(2\pi)^3} \frac{-f(\mu + E_p) + f(\mu - E_p)}{2E_p}. \tag{D.11}$$

Next, we use the relation

$$f(-x) = 1 - f(x), \tag{D.12}$$

to bring (D.11) to the usual form:

$$A(m) = -i \frac{1}{4\pi^2} \int_0^\Lambda \mathrm{d}p \, \frac{p^2 [1 - f(E_p + \mu) - f(E_p - \mu)]}{E_p}. \tag{D.13}$$

We can simplify this expressions further by transforming the variable of integration from p to E and finally obtain

$$A(m) = -i \frac{1}{4\pi^2} \int_m^{\Lambda_E} \mathrm{d}E \, \sqrt{E^2 - m^2} [1 - f(E + \mu) - f(E - \mu)], \tag{D.14}$$

where $\Lambda_E = \sqrt{\Lambda^2 + m^2}$.

D.2 Two fermion lines

Loop integrals with two fermion lines were used e.g. to evaluate meson masses at finite temperature and non-zero quark chemical potential. The vacuum expression for the two fermion line integral reads

$$B(m_1, m_2) = \int \frac{\mathrm{d}^4 p}{(2\pi)^4} \frac{1}{p^2 - m_1^2 + i\epsilon} \frac{1}{(p-q)^2 - m_2^2 + i\epsilon}, \tag{D.15}$$

where m_1 and m_2 denote the particle masses and q the external momentum. We can again employ the Matsubara formalism defined by (D.2), (D.3) and (D.4) to obtain the finite temperature expression

$$B(m_1, m_2) \overset{T>0}{=} iT \sum_n \int \frac{\mathrm{d}^3 p}{(2\pi)^3} \frac{1}{(\omega_n - i\mu)^2 + E_1^2} \frac{1}{(\omega_n - i\mu - \nu_m)^2 + E_2^2}, \tag{D.16}$$

where $E_1 = \sqrt{\boldsymbol{p}^2 + m_1^2}$, $E_2 = \sqrt{(\boldsymbol{p} - \boldsymbol{p})^2 + m_2^2}$ and $\nu_m = 2\pi T m$ are the bosonic Matsubara frequencies. In order to evaluate the sum over the Matsubara frequencies, it is again useful to decompose (D.16) into partial fractions.

$$\begin{aligned}
B(m_1, m_2) &\overset{\text{(D.6)}}{=} iT \sum_n \sum_{s_1, s_2 = \pm 1} \int \frac{\mathrm{d}^3 p}{(2\pi)^3} \frac{s_1 s_2}{4 E_1 E_2} \frac{1}{i\omega_n + \mu + s_1 E_1} \frac{1}{i\omega_n + \mu - i\nu_m + s_2 E_2} \\
&= iT \sum_n \sum_{s_1, s_2 = \pm 1} \int \frac{\mathrm{d}^3 p}{(2\pi)^3} \frac{s_1 s_2}{4 E_1 E_2} \frac{1}{-i\nu_m - s_1 E_1 + s_2 E_2} \\
&\quad \times \left(\frac{1}{i\omega_n + \mu + s_1 E_1} + \frac{1}{i\omega_n + \mu - i\nu_m + s_2 E_2} \right) \\
&\overset{\text{(D.8)}}{=} i \sum_{s_1, s_2 = \pm 1} \int \frac{\mathrm{d}^3 p}{(2\pi)^3} \frac{s_1 s_2}{4 E_1 E_2} \frac{b(i\pi T + \mu + s_1 E_1) - b(i\pi T + \mu - i\nu_m + s_2 E_2)}{-i\nu_m - s_1 E_1 + s_2 E_2}.
\end{aligned} \tag{D.17}$$

In the second line we used the identity

$$\frac{1}{ab} = \frac{1}{b-a} \left(\frac{1}{a} - \frac{1}{b} \right). \tag{D.18}$$

Using $b(i2\pi T m + x) = b(x)$ and $b(x + i\pi T) = -f(x)$ and replacing $i\nu_m \to q_0$ we can write (D.17) as

$$B(m_1, m_2) = -i \sum_{s_1, s_2 = \pm 1} \int \frac{\mathrm{d}^3 p}{(2\pi)^3} \frac{s_1 s_2}{4 E_1 E_2} \frac{-f(\mu + s_1 E_1) + f(\mu + s_2 E_2)}{q_0 + s_1 E_1 - s_2 E_2}. \tag{D.19}$$

Performing the sum over s_1 and s_2, rearranging the terms and using the relation $f(-x) = 1 - f(x)$ we obtain

$$\begin{aligned}
B(m_1, m_2) = -i \int \frac{\mathrm{d}^3 p}{(2\pi)^3} \Bigg[&\frac{-f(E_1 + \mu)}{2E_1[(q_0 + E_1)^2 - E_2^2]} + \frac{1 - f(E_1 - \mu)}{2E_1[(q_0 - E_1)^2 - E_2^2]} \\
&+ \frac{-f(E_2 + \mu)}{2E_2[(q_0 - E_2)^2 - E_1^2]} + \frac{1 - f(E_2 - \mu)}{2E_2[(q_0 + E_2)^2 - E_1^2]} \Bigg].
\end{aligned} \tag{D.20}$$

In the frame $q = (q_0, \mathbf{0})$ Eqn. (D.20) does not depend on θ and ϕ and consequently the $\theta-$ and $\phi-$integrals can be evaluated trivially. Using $E_2^2 = E_1^2 - m_1^2 + m_2^2$ and $E_1^2 = E_2^2 + m_1^2 - m_2^2$ we find

$$\begin{aligned} &B(m_1, m_2) = \\ &-\frac{i}{2\pi^2}\int_0^\Lambda \mathrm{d}p\, p^2\Bigg[\frac{-f(E_1+\mu)}{2E_1(q_0^2+2q_0E_1+m_1^2-m_2^2)} + \frac{1-f(E_1-\mu)}{2E_1(q_0^2-2q_0E_1+m_1^2-m_2^2)} \\ &\qquad + \frac{-f(E_2+\mu)}{2E_2(q_0^2-2q_0E_2-m_1^2+m_2^2)} + \frac{1-f(E_2-\mu)}{2E_2(q_0^2+2q_0E_2-m_1^2+m_2^2]}\Bigg]. \end{aligned} \tag{D.21}$$

Next we change the variable of integration to $E_1 = \sqrt{p^2+m_1^2}$ and $E_2 = \sqrt{p^2+m_2^2}$:

$$\begin{aligned} &B(m_1, m_2) = \\ &-\frac{i}{2\pi^2}\int_{m_1}^{\sqrt{\Lambda^2+m_1^2}} \mathrm{d}E_1\left[\frac{\sqrt{E_1^2-m_1^2}(-f(E_1+\mu))}{2(q_0^2+2q_0E_1+m_1^2-m_2^2)} + \frac{\sqrt{E_1^2-m_1^2}(1-f(E_1-\mu))}{2(q_0^2-2q_0E_1+m_1^2-m_2^2)}\right] \\ &-\frac{i}{2\pi^2}\int_{m_2}^{\sqrt{\Lambda^2+m_2^2}} \mathrm{d}E_2\left[\frac{\sqrt{E_2^2-m_2^2}(-f(E_2+\mu))}{2(q_0^2-2q_0E_2-m_1^2+m_2^2)} + \frac{\sqrt{E_2^2-m_2^2}(1-f(E_2-\mu))}{2(q_0^2+2q_0E_2-m_1^2+m_2^2)}\right]. \end{aligned} \tag{D.22}$$

The integrand of the first term in the first line of (D.22) has a pole at

$$E_{1,0} = -\frac{q_0^2+m_1^2-m_2^2}{2q_0}, \tag{D.23}$$

if $m_1 \le E_{1,0} \le \sqrt{\Lambda^2+m_1^2}$. To calculate the integral in this case, we recall that the particle masses are complex, $m_1^2 \to m_1^2 - i\epsilon$, $m_2^2 \to m_2^2 - i\epsilon$, and apply the formula

$$\lim_{\epsilon\to 0}\frac{1}{x-i\epsilon} = \mathcal{P} + i\pi\delta(x), \tag{D.24}$$

where $\mathcal{P}$ denotes the Cauchy principal value. From this, we find

$$\begin{aligned} &\lim_{\epsilon\to 0}\frac{-i}{2\pi^2}\int_{m_1}^{\sqrt{\Lambda^2+m_1^2}} \mathrm{d}E_1 \frac{\sqrt{E_1^2-m_1^2}(-f(E_1+\mu))}{2(q_0^2+2q_0E_1+m_1^2-m_2^2-i\epsilon\,\mathrm{sgn}(q_0))} \\ =&\mathcal{P}\frac{-i}{2\pi^2}\int_{m_1}^{\sqrt{\Lambda^2+m_1^2}} \mathrm{d}E_1 \frac{\sqrt{E_1^2-m_1^2}(-f(E_1+\mu))}{2(q_0^2+2q_0E_1+m_1^2-m_2^2)} \\ &-\frac{1}{4\pi q_0}\sqrt{\left(\frac{q_0^2+m_1^2-m_2^2}{2q_0}\right)^2 - m_1^2}\left(-f\left(-\frac{q_0^2+m_1^2-m_2^2}{2q_0}+\mu\right)\right) \\ &\times\theta\left(\left(\sqrt{\Lambda^2+m_1^2}+\frac{q_0^2+m_1^2-m_2^2}{2q_0}\right)\left(-\frac{q_0^2+m_1^2-m_2^2}{2q_0}-m_1\right)\right). \end{aligned} \tag{D.25}$$

The integrand of the second term in the first line has a pole at

$$E_{1,0} = \frac{q_0^2 + m_1^2 - m_2^2}{2q_0}, \tag{D.26}$$

if $m_1 \leq E_{1,0} \leq \sqrt{\Lambda^2 + m_1^2}$. We obtain

$$\begin{aligned}
&\lim_{\epsilon \to 0} \frac{-i}{2\pi^2} \int_{m_1}^{\sqrt{\Lambda^2+m_1^2}} \mathrm{d}E_1 \frac{\sqrt{E_1^2 - m_1^2}(1 - f(E_1 - \mu))}{2(q_0^2 - 2q_0 E_1 + m_1^2 - m_2^2 - i\epsilon\,\mathrm{sgn}(q_0))} \\
=&\mathcal{P}\frac{-i}{2\pi^2} \int_{m_1}^{\sqrt{\Lambda^2+m_1^2}} \mathrm{d}E_1 \frac{\sqrt{E_1^2 - m_1^2}(1 - f(E_1 - \mu))}{2(q_0^2 - 2q_0 E_1 + m_1^2 - m_2^2)} \\
&- \frac{1}{4\pi q_0} \sqrt{\left(\frac{q_0^2 + m_1^2 - m_2^2}{2q_0}\right)^2 - m_1^2} \left(1 - f\left(\frac{q_0^2 + m_1^2 - m_2^2}{2q_0} - \mu\right)\right) \\
&\times \theta\left(\left(\sqrt{\Lambda^2 + m_1^2} - \frac{q_0^2 + m_1^2 - m_2^2}{2q_0}\right)\left(\frac{q_0^2 + m_1^2 - m_2^2}{2q_0} - m_1\right)\right).
\end{aligned} \tag{D.27}$$

The integrand of the first term in the second line has a pole at

$$E_{2,0} = \frac{q_0^2 - m_1^2 + m_2^2}{2q_0}, \tag{D.28}$$

if $m_2 \leq E_{2,0} \leq \sqrt{\Lambda^2 + m_2^2}$. We find

$$\begin{aligned}
&\lim_{\epsilon \to 0} \frac{-i}{2\pi^2} \int_{m_2}^{\sqrt{\Lambda^2+m_2^2}} \mathrm{d}E_2 \frac{\sqrt{E_2^2 - m_2^2}(-f(E_2 + \mu))}{2(q_0^2 - 2q_0 E_1 - m_1^2 + m_2^2 - i\epsilon\,\mathrm{sgn}(q_0))} \\
=&\mathcal{P}\frac{-i}{2\pi^2} \int_{m_2}^{\sqrt{\Lambda^2+m_2^2}} \mathrm{d}E_2 \frac{\sqrt{E_2^2 - m_2^2}(-f(E_2 + \mu))}{2(q_0^2 - 2q_0 E_2 - m_1^2 + m_2^2)} \\
&- \frac{1}{4\pi q_0} \sqrt{\left(\frac{q_0^2 - m_1^2 + m_2^2}{2q_0}\right)^2 - m_2^2} \left(-f\left(\frac{q_0^2 - m_1^2 + m_2^2}{2q_0} + \mu\right)\right) \\
&\times \theta\left(\left(\sqrt{\Lambda^2 + m_2^2} - \frac{q_0^2 - m_1^2 + m_2^2}{2q_0}\right)\left(\frac{q_0^2 - m_1^2 + m_2^2}{2q_0} - m_2\right)\right).
\end{aligned} \tag{D.29}$$

The integrand of the second term in the second line has a pole at

$$E_{2,0} = -\frac{q_0^2 - m_1^2 + m_2^2}{2q_0}, \tag{D.30}$$

if $m_2 \leq E_{2,0} \leq \sqrt{\Lambda^2 + m_2^2}$. We find

$$\begin{aligned}
&\lim_{\epsilon\to 0} \frac{-i}{2\pi^2} \int_{m_2}^{\sqrt{\Lambda^2+m_2^2}} \mathrm{d}E_2 \frac{\sqrt{E_2^2 - m_2^2}(1 - f(E_2 - \mu))}{2(q_0^2 + 2q_0 E_1 - m_1^2 + m_2^2 - i\epsilon\,\mathrm{sgn}(q_0))} \\
=&\mathcal{P}\frac{-i}{2\pi^2} \int_{m_2}^{\sqrt{\Lambda^2+m_2^2}} \mathrm{d}E_2 \frac{\sqrt{E_2^2 - m_2^2}(1 - f(E_2 - \mu))}{2(q_0^2 + 2q_0 E_2 - m_1^2 + m_2^2)} \\
&-\frac{1}{4\pi q_0}\sqrt{\left(\frac{q_0^2 - m_1^2 + m_2^2}{2q_0}\right)^2 - m_1^2}\left(1 - f\left(-\frac{q_0^2 - m_1^2 + m_2^2}{2q_0} - \mu\right)\right) \\
&\times\theta\left(\left(\sqrt{\Lambda^2 + m_2^2} + \frac{q_0^2 - m_1^2 + m_2^2}{2q_0}\right)\left(-\frac{q_0^2 - m_1^2 + m_2^2}{2q_0} - m_2\right)\right).
\end{aligned} \tag{D.31}$$

In the limit $m_1 = m_2 \equiv m$ we obtain

$$\begin{aligned}
B(m,m) = &\mathcal{P}\frac{-i}{2\pi^2} \int_{m}^{\sqrt{\Lambda^2+m^2}} \mathrm{d}E \frac{\sqrt{E^2 - m^2}(1 - f(E - \mu) - f(E + \mu))}{q_0^2 - 4E^2} \\
&- \frac{1}{16\pi q_0}\sqrt{q_0^2 - 4m^2}\left[1 - f\left(\frac{q_0}{2} - \mu\right) - f\left(\frac{q_0}{2} + \mu\right)\right]\theta\left[\left(2\sqrt{\Lambda^2 + m^2} - q_0\right)(q_0 - 2m)\right].
\end{aligned} \tag{D.32}$$

List of figures

Bibliography

[A+02] C. R. Allton et al. The qcd thermal phase transition in the presence of a small chemical potential. *Phys. Rev.*, D66:074507, 2002.

[A+03] C. R. Allton et al. The equation of state for two flavor qcd at non-zero chemical potential. *Phys. Rev.*, D68:014507, 2003.

[ABPS02] Jens O. Andersen, Eric Braaten, Emmanuel Petitgirard, and Michael Strickland. Htl perturbation theory to two loops. *Phys. Rev.*, D66:085016, 2002.

[ABS99] Jens O. Andersen, Eric Braaten, and Michael Strickland. Hard-thermal-loop resummation of the free energy of a hot gluon plasma. *Phys. Rev. Lett.*, 83:2139–2142, 1999.

[AK+01a] A. Ali Khan et al. Equation of state in finite-temperature qcd with two flavors of improved wilson quarks. *Phys. Rev.*, D64:074510, 2001.

[AK+01b] A. Ali Khan et al. Phase structure and critical temperature of two flavor qcd with renormalization group improved gauge action and clover improved wilson quark action. *Phys. Rev.*, D63:034502, 2001.

[B+95a] G. Boyd et al. Equation of state for the su(3) gauge theory. *Phys. Rev. Lett.*, 75:4169–4172, 1995.

[B+95b] G. Boyd et al. Hadron properties just before deconfinement. *Phys. Lett.*, B349:170–176, 1995.

[B+96] G. Boyd et al. Thermodynamics of su(3) lattice gauge theory. *Nucl. Phys.*, B469:419–444, 1996.

[B+97] Claude W. Bernard et al. The equation of state for two flavor qcd at n(t) = 6. *Phys. Rev.*, D55:6861–6869, 1997.

[Bel96] M. Le Bellac. *Thermal Field Theory.* Cambridge University Press, Cambridge, 1996.

[BI94] Jean Paul Blaizot and Edmond Iancu. Soft collective excitations in hot gauge theories. *Nucl. Phys.*, B417:608–673, 1994.

[BI02] Jean-Paul Blaizot and Edmond Iancu. The quark-gluon plasma: Collective dynamics and hard thermal loops. *Phys. Rept.*, 359:355–528, 2002.

[BIR99a] J. P. Blaizot, Edmond Iancu, and A. Rebhan. The entropy of the qcd plasma. *Phys. Rev. Lett.*, 83:2906–2909, 1999.

[BIR99b] J. P. Blaizot, Edmond Iancu, and A. Rebhan. Self-consistent hard-thermal-loop thermodynamics for the quark-gluon plasma. *Phys. Lett.*, B470:181–188, 1999.

[BIR01] J. P. Blaizot, Edmond Iancu, and A. Rebhan. Approximately self-consistent resummations for the thermodynamics of the quark-gluon plasma. i: Entropy and density. *Phys. Rev.*, D63:065003, 2001.

[BIR03] J. P. Blaizot, E. Iancu, and A. Rebhan. On the apparent convergence of perturbative qcd at high temperature. *Phys. Rev.*, D68:025011, 2003.

[BKLP99] B. Beinlich, F. Karsch, E. Laermann, and A. Peikert. String tension and thermodynamics with tree level and tadpole improved actions. *Eur. Phys. J.*, C6:133–140, 1999.

[BKS05] Marcus Bluhm, Burkhard Kampfer, and Gerhard Soff. Quasi-particle model of strongly interacting matter. *J. Phys.*, G31:S1151–S1154, 2005.

[BMHS99] P. Braun-Munzinger, I. Heppe, and J. Stachel. Chemical equilibration in pb + pb collisions at the sps. *Phys. Lett.*, B465:15–20, 1999.

[BMMRS01] P. Braun-Munzinger, D. Magestro, K. Redlich, and J. Stachel. Hadron production in au au collisions at rhic. *Phys. Lett.*, B518:41–46, 2001.

[BP92] Eric Braaten and Robert D. Pisarski. Simple effective lagrangian for hard thermal loops. *Phys. Rev.*, D45:1827–1830, 1992.

[CJJ+74] A. Chodos, R. L. Jaffe, K. Johnson, Charles B. Thorn, and V. F. Weisskopf. A new extended model of hadrons. *Phys. Rev.*, D9:3471–3495, 1974.

[CJJT74] A. Chodos, R. L. Jaffe, K. Johnson, and Charles B. Thorn. Baryon structure in the bag theory. *Phys. Rev.*, D10:2599, 1974.

[Cre83] M. Creutz. *Quarks, Gluons and Lattices*. Cambridge University Press, Cambridge, 1983.

[dFP02] Philippe de Forcrand and Owe Philipsen. The qcd phase diagram for small densities from imaginary chemical potential. *Nucl. Phys.*, B642:290–306, 2002.

[dFP03] Philippe de Forcrand and Owe Philipsen. The qcd phase diagram for three degenerate flavors and small baryon density. *Nucl. Phys.*, B673:170–186, 2003.

[DGDSS02] A. Di Giacomo, H. G. Dosch, V. I. Shevchenko, and Yu. A. Simonov. Field correlators in qcd: Theory and applications. *Phys. Rept.*, 372:319–368, 2002.

[DGP92] A. Di Giacomo and H. Panagopoulos. Field strength correlations in the qcd vacuum. *Phys. Lett.*, B285:133–136, 1992.

[DGR04] Alessandro Drago, Marina Gibilisco, and Claudia Ratti. Evaporation of the gluon condensate: A model for pure gauge su(3)c phase transition. *Nucl. Phys.*, A742:165–181, 2004.

[DJJK75] T. DeGrand, R. L. Jaffe, K. Johnson, and J. E. Kiskis. Masses and other parameters of the light hadrons. *Phys. Rev.*, D12:2060, 1975.

[DL03] Massimo D'Elia and Maria-Paola Lombardo. Finite density qcd via imaginary chemical potential. *Phys. Rev.*, D67:014505, 2003.

[DLS01] S. Digal, E. Laermann, and H. Satz. Deconfinement through chiral symmetry restoration in two- flavour qcd. *Eur. Phys. J.*, C18:583–586, 2001.

[DN98] H. G. Dosch and Stephan Narison. Direct extraction of the chiral quark condensate and bounds on the light quark masses. *Phys. Lett.*, B417:173–176, 1998.

[DPZ05] Adrian Dumitru, Robert D. Pisarski, and Detlef Zschiesche. Dense quarks, and the fermion sign problem, in a su(n) matrix model. *Phys. Rev.*, D72:065008, 2005.

[E+04] S. Eidelman et al. Review of particle physics. *Phys. Lett.*, B592:1, 2004.

[EFK+90] J. Engels, J. Fingberg, F. Karsch, D. Miller, and M. Weber. Nonperturbative thermodynamics of su(n) gauge theories. *Phys. Lett.*, B252:625–630, 1990.

[EFR+89] J. Engels, J. Fingberg, K. Redlich, H. Satz, and M. Weber. The onset of deconfinement in su(2) lattice gauge theory. *Z. Phys.*, C42:341, 1989.

[EHK98] R. G. Edwards, Urs M. Heller, and T. R. Klassen. Accurate scale determinations for the wilson gauge action. *Nucl. Phys.*, B517:377–392, 1998.

[EKS82] J. Engels, F. Karsch, and H. Satz. The high temperature behavior of lattice qcd with fermions. *Phys. Lett.*, B113:398, 1982.

[Eve80] H. Eves. *Elementary Matrix Theory*. Dover publications, New York, 1980.

[FK02a] Z. Fodor and S. D. Katz. Lattice determination of the critical point of qcd at finite t and mu. *JHEP*, 03:014, 2002.

[FK02b] Z. Fodor and S. D. Katz. A new method to study lattice qcd at finite temperature and chemical potential. *Phys. Lett.*, B534:87–92, 2002.

[FKS03] Z. Fodor, S. D. Katz, and K. K. Szabo. The qcd equation of state at nonzero densities: Lattice result. *Phys. Lett.*, B568:73–77, 2003.

[Fod] Z. Fodor. *Private communication.*

[FT92] J. Frenkel and J. C. Taylor. Hard terminal qcd, forward scattering and effective actions. *Nucl. Phys.*, B374:156–168, 1992.

[Fuk04] Kenji Fukushima. Chiral effective model with the polyakov loop. *Phys. Lett.*, B591:277–284, 2004.

[GMOR68] Murray Gell-Mann, R. J. Oakes, and B. Renner. Behavior of current divergences under su(3) x su(3). *Phys. Rev.*, 175:2195–2199, 1968.

[GRTV99] L. Giusti, F. Rapuano, M. Talevi, and A. Vladikas. The qcd chiral condensate from the lattice. *Nucl. Phys.*, B538:249–277, 1999.

[GW73] D. J. Gross and Frank Wilczek. Ultraviolet behavior of non-abelian gauge theories. *Phys. Rev. Lett.*, 30:1343–1346, 1973.

[GY95] M. I. Gorenstein and Shin-Nan Yang. Gluon plasma with a medium dependent dispersion relation. *Phys. Rev.*, D52:5206–5212, 1995.

[Han01] Simon Hands. The phase diagram of qcd. *Contemp. Phys.*, 42:209–225, 2001.

[Hei01] Ulrich W. Heinz. The little bang: Searching for quark-gluon matter in relativistic heavy-ion collisions. *Nucl. Phys.*, A685:414–431, 2001.

[HK84] T. Hatsuda and T. Kunihiro. Possible critical phenomena associated with the chiral symmetry breaking. *Phys. Lett.*, B145:7–10, 1984.

[HK94] Tetsuo Hatsuda and Teiji Kunihiro. Qcd phenomenology based on a chiral effective lagrangian. *Phys. Rept.*, 247:221–367, 1994.

[Hol90] Barry R. Holstein. How large is f(pi)? *Phys. Lett.*, B244:83–87, 1990.

[HW00] Kieran Holland and Uwe-Jens Wiese. The center symmetry and its spontaneous breakdown at high temperatures. 2000. Published in *At the Frontier of Particle Physics: Handbook of QCD, Vol. 3*, edited by M. Shifman, World Scientific.

[IRV04] A. Ipp, A. Rebhan, and A. Vuorinen. Perturbative qcd at non-zero chemical potential: Comparison with the large-n(f) limit and apparent convergence. *Phys. Rev.*, D69:077901, 2004.

[IST05] Yu. B. Ivanov, V. V. Skokov, and V. D. Toneev. Equation of state of deconfined matter within dynamical quasiparticle description. *Phys. Rev.*, D71:014005, 2005.

[Kap89] J. Kapusta. *Finite-temperature Field Theory.* Cambridge University Press, Cambridge, 1989.

[KKPZ02] O. Kaczmarek, F. Karsch, P. Petreczky, and F. Zantow. Heavy quark anti-quark free energy and the renormalized polyakov loop. *Phys. Lett.*, B543:41–47, 2002.

[Kle] Hagen Kleinert. On the hadronization of quark theories. Lectures presented at Erice Summer School of Subnuclear Physics, Erice, Italy, Jul 23 - Aug 8, 1976.

[Kle92] S. P. Klevansky. The nambu-jona-lasinio model of quantum chromodynamics. *Rev. Mod. Phys.*, 64:649–708, 1992.

[KLP00] F. Karsch, E. Laermann, and A. Peikert. The pressure in 2, 2+1 and 3 flavour qcd. *Phys. Lett.*, B478:447–455, 2000.

[KLP01a] F. Karsch, E. Laermann, and A. Peikert. Quark mass and flavor dependence of the qcd phase transition. *Nucl. Phys.*, B605:579–599, 2001.

[KLP$^+$01b] F. Karsch, E. Laermann, A. Peikert, C. Schmidt, and S. Stickan. Flavor and quark mass dependence of qcd thermodynamics. *Nucl. Phys. Proc. Suppl.*, 94:411–414, 2001.

[KLRS03] K. Kajantie, M. Laine, K. Rummukainen, and Y. Schroder. The pressure of hot qcd up to g**6 ln(1/g). *Phys. Rev.*, D67:105008, 2003.

[KLVW90] S. Klimt, M. Lutz, U. Vogl, and W. Weise. Generalized su(3) nambu-jona-lasinio model. part. 1. mesonic modes. *Nucl. Phys.*, A516:429–468, 1990.

[LH98] Peter Levai and Ulrich W. Heinz. Massive gluons and quarks and the equation of state obtained from su(3) lattice qcd. *Phys. Rev.*, C57:1879–1890, 1998.

[LKW92] M. Lutz, S. Klimt, and W. Weise. Meson properties at finite temperature and baryon density. *Nucl. Phys.*, A542:521–558, 1992.

[LP03] Edwin Laermann and Owe Philipsen. Status of lattice qcd at finite temperature. *Ann. Rev. Nucl. Part. Sci.*, 53:163, 2003.

[MNNT03] Shin Muroya, Atsushi Nakamura, Chiho Nonaka, and Tetsuya Takaishi. Lattice qcd at finite density: An introductory review. *Prog. Theor. Phys.*, 110:615–668, 2003.

[MO96] Peter N. Meisinger and Michael C. Ogilvie. Coupling the deconfining and chiral transitions. *Nucl. Phys. Proc. Suppl.*, 47:519–522, 1996.

[MOM04] Peter N. Meisinger, Michael C. Ogilvie, and Travis R. Miller. Gluon quasiparticles and the polyakov loop. *Phys. Lett.*, B585:149–154, 2004.

[MP99] Colin J. Morningstar and Mike J. Peardon. The glueball spectrum from an anisotropic lattice study. *Phys. Rev.*, D60:034509, 1999.

[MRST01] P. Maris, Craig D. Roberts, S. M. Schmidt, and P. C. Tandy. T-dependence of pseudoscalar and scalar correlations. *Phys. Rev.*, C63:025202, 2001.

[NJL61a] Yoichiro Nambu and G. Jona-Lasinio. Dynamical model of elementary particles based on an analogy with superconductivity. i. *Phys. Rev.*, 122:345–358, 1961.

[NJL61b] Yoichiro Nambu and G. Jona-Lasinio. Dynamical model of elementary particles based on an analogy with superconductivity. ii. *Phys. Rev.*, 124:246–254, 1961.

[O+99] M. Okamoto et al. Equation of state for pure su(3) gauge theory with renormalization group improved action. *Phys. Rev.*, D60:094510, 1999.

[Pis00] Robert D. Pisarski. Quark-gluon plasma as a condensate of su(3) wilson lines. *Phys. Rev.*, D62:111501, 2000.

[PKPS96] A. Peshier, B. Kampfer, O. P. Pavlenko, and G. Soff. A massive quasiparticle model of the su(3) gluon plasma. *Phys. Rev.*, D54:2399–2402, 1996.

[PKS00] A. Peshier, B. Kampfer, and G. Soff. The equation of state of deconfined matter at finite chemical potential in a quasiparticle description. *Phys. Rev.*, C61:045203, 2000.

[Pol73] H. David Politzer. Reliable perturbative results for strong interactions? *Phys. Rev. Lett.*, 30:1346–1349, 1973.

[Pol78] Alexander M. Polyakov. Thermal properties of gauge fields and quark liberation. *Phys. Lett.*, B72:477–480, 1978.

[RA88] H. Reinhardt and R. Alkofer. Instanton induced flavor mixing in mesons. *Phys. Lett.*, B207:482–488, 1988.

[Raj99] Krishna Rajagopal. Mapping the qcd phase diagram. *Nucl. Phys.*, A661:150–161, 1999.

[Rip97] G. Ripka. *Quarks bound by Chiral Fields.* Oxford University Press, Oxford, 1997.

[Ris04] Dirk H. Rischke. The quark-gluon plasma in equilibrium. *Prog. Part. Nucl. Phys.*, 52:197–296, 2004.

[RKH96] P. Rehberg, S. P. Klevansky, and J. Hufner. Hadronization in the su(3) nambu-jona-lasinio model. *Phys. Rev.*, C53:410–429, 1996.

[RR03] A. Rebhan and P. Romatschke. Htl quasiparticle models of deconfined qcd at finite chemical potential. *Phys. Rev.*, D68:025022, 2003.

[RTW05] Claudia Ratti, Michael A. Thaler, and Wolfram Weise. Phases of qcd: Lattice thermodynamics and a field theoretical model. 2005.

[Sch00] P. Schmidt. *Hadronic properties in the vicinity of the critical temperature - A lattice investigation with improved Wilson quarks*. PhD thesis, University Bielefeld, Germany, 2000.

[Sch02] R. Schneider. *QCD Phenomenology at high Temperatures*. PhD thesis, Technical University Munich, Germany, 2002.

[Shu88] E. Shuryak. *The QCD Vacuum, Hadrons and Superdense Matter*. World Scientific, Singapur, 1988.

[ST99] Andreas Schaefer and Markus H. Thoma. Quark propagation in a quark-gluon plasma with gluon condensate. *Phys. Lett.*, B451:195–200, 1999.

[ST03] K. K. Szabo and A. I. Toth. Quasiparticle description of the qcd plasma, comparison with lattice results at finite t and mu. *JHEP*, 06:008, 2003.

[Sus79] Leonard Susskind. Lattice models of quark confinement at high temperature. *Phys. Rev.*, D20:2610–2618, 1979.

[Sve86] Benjamin Svetitsky. Symmetry aspects of finite temperature confinement transitions. *Phys. Rept.*, 132:1–53, 1986.

[SW01] R. A. Schneider and W. Weise. On the quasiparticle description of lattice qcd thermodynamics. *Phys. Rev.*, C64:055201, 2001.

[tH76] Gerard 't Hooft. Symmetry breaking through bell-jackiw anomalies. *Phys. Rev. Lett.*, 37:8–11, 1976.

[tH78] Gerard 't Hooft. On the phase transition towards permanent quark confinement. *Nucl. Phys.*, B138:1, 1978.

[TSW04] M. A. Thaler, R. A. Schneider, and W. Weise. Quasiparticle description of hot qcd at finite quark chemical potential. *Phys. Rev.*, C69:035210, 2004.

[Vol84] M. K. Volkov. Meson lagrangians in a superconductor quark model. *Annals Phys.*, 157:282–303, 1984.

[VW91] U. Vogl and W. Weise. The nambu and jona lasinio model: Its implications for hadrons and nuclei. *Prog. Part. Nucl. Phys.*, 27:195–272, 1991.

[Wei81] Nathan Weiss. The effective potential for the order parameter of gauge theories at finite temperature. *Phys. Rev.*, D24:475, 1981.

[Wei82] Nathan Weiss. The wilson line in finite temperature gauge theories. *Phys. Rev.*, D25:2667, 1982.

[Wil74] Kenneth G. Wilson. Confinement of quarks. *Phys. Rev.*, D10:2445–2459, 1974.

[Won94] C.-Y. Wong. *Introduction to High-Energy Heavy-Ion Collisions*. World Scientific, Singapore, 1994.

[Zic] A. Zichichi. Understanding the fundamental constituents of matter. proceedings of the 1976 international school of subnuclear physics (nato-mpi-mrst advanced study institute) held in erice, trapani, sicily, july 23 - august 8, 1976. New York, Usa: Plenum Pr.(1978) 915 P.(The Subnuclear Series, 14).

[ZK95] Cheng-xing Zhai and Boris M. Kastening. The free energy of hot gauge theories with fermions through g**5. *Phys. Rev.*, D52:7232–7246, 1995.

Acknowledgments

There are many people who have - in one way or another - contributed to the success of this work. I would like to thank all of them, especially...

- Prof. Dr. Wolfram Weise, for his support and interest, for many insightful and motivating discussions, and for making my stay at the QGP summer school in Turin possible.
- Claudia Ratti, my collaborator, for many stimulating and helpful discussions, and for showing me around in Turin.
- all members of T39, for the pleasant working climate.
- Markus Bleuel, Martin Brückel, Stefan Christlmeier, Stefan Fritsch, Alex & Roland Kuhn, Markus Müller and Stephan Trumm, for mountain hikes, barbecues and for making Garching appear not quite that isolated.
- Jörn Kersten, Thorten Renk and Roland Schneider, for many nice evenings with games and movies.
- Peter Hank, Sabine & Helmut Maier and Thorsten Winter, for the regular Friday evening D&D games.
- Steffen Dietz, for many years of friendship and for always finding the right words to cheer me up.
- my parents, for arousing my early interest in physics and for supporting me all these years.